The Development of Carbon Nanostructured Sensors

by
Pieter Christo Kritzinger

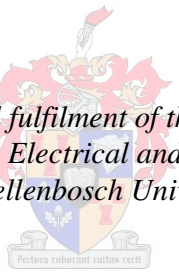

Thesis presented in partial fulfilment of the requirements for the degree of Master of Science in Electrical and Electronic Engineering at Stellenbosch University

Supervisor: Prof Willem Jacobus Perold
Department of Electrical and Electronic Engineering

December 2010

Declaration

By submitting this thesis electronically, I declare that the entirety of the work contained therein is my own, original work, and that I have not previously in its entirety or in part submitted it for obtaining any qualification.

December 2010

Abstract

The Development of Carbon Nanostructured Sensors

P.C. Kritzinger

Department of Electrical and Electronic Engineering
University of Stellenbosch
Private Bag X1, 7602 Matieland, South Africa

Thesis: MScEng (E and E)

December 2010

During this research the possibility of using carbon nanostructures in sensors were investigated. Graphene and carbon nanotubes (CNTs) are the nanostructures that were used in the developed sensors. Graphene is a single atomic layer of carbon and a carbon nanotube (CNT) is a rolled up sheet of graphene that forms a tube. The unique structure and incredible properties of both these materials make them ideal to be used in sensory applications. A graphene sensor was developed and experiments were performed to determine whether graphene is a viable candidate to be used in a wide range of sensory applications. The graphene sensor operated successfully as a humidity sensor and this led to the discovery that humidity can be used to control the bandgap in graphene. The absorption of CO_2 in graphene was successfully measured using surface acoustic waves. As a result, any gas that graphene absorbs can be detected using this method. The use of graphene in three liquid applications was tested. The graphene showed no potential to be used as a pH sensor or as a flow sensor. An experiment was undertaken to determine whether graphene can increase the efficiency of a water electrolysis process, but it was established that the graphene does not make a significant difference. A CNT gas sensor that identifies a gas based on its ionization characteristics was studied and designed. Due to the insufficient height of the grown CNTs, it was decided to focus on the creation of a model of the sensor that can be used to design it optimally. The results of the experiments confirmed that carbon nanostructures such as graphene and CNTs have potential to be used in future sensing applications.

Opsomming

Die Ontwikkelling van Koolstof-nanogestruktueerde Sensors

("The Development of Carbon Nanostructured Sensors")

P.C. Kritzinger

Departement Elektriese en Elektroniese Ingenieurswese
Universiteit van Stellenbosch
Privaatsak X1, 7602 Matieland, Suid Afrika

Tesis: MScIng (E en E)

Desember 2010

Hierdie navorsing ondersoek die moontlikheid om koolstof-nanostrukture in sensor-apparate te gebruik. Grafeen en koolstof-nanobuisies (KNB) is die nanostrukture wat in die ontwikkelde sensors gebruik is. Grafeen is 'n enkel atomiese koolstoflagie en KNBs is 'n opgerolde grafeenlagie wat 'n buisie vorm. Die unieke struktuur en ongelooflike eienskappe van beide hierdie materiale, maak hulle uiters geskik om in sensor-toepassings gebruik te word. 'n Grafeensensor is ontwikkel en eksperimente is uitgevoer om te bepaal of grafeen 'n goeie kanidaat is om in 'n wye verskeidenheid van toepassings gebruik te word. Die grafeensensor is suksesvol aangewend as 'n humiditeitsensor en dit het gelei tot die uitvindsel dat humiditeit gebruik kan word om die energiegaping in grafeen te varieer. Die absorpsie van CO_2 in grafeen is suksesvol gemeet deur oppervlak akoestiese golwe te gebruik. Gevolglik kan enige gas wat grafeen absorbeer op hierdie manier gemeet word. Die gebruik van grafeen is in drie vloeistof-toepassings getoets. Die grafeen het geen potensiaal getoon om as 'n pH-sensor of as 'n vloei-sensor aangewend te word nie. 'n Eksperiment is ook uitgevoer om te toets of grafeen die effektiwiteit van 'n water-elektroliese proses kan verhoog, maar die resultate het gewys dat dit nie 'n wesenlike verskil maak nie. 'n KNB-gassensor, wat 'n gas identifiseer uit die ioniseerings eienskappe van die gas, is bestudeer en ontwikkel. Die lengte van die KNBs wat gegroei is, was onvoldoende en daar is gefokus op die ontwerp van 'n model van die sensor wat gebruik kan word om dit optimaal te ontwerp. Die resultate van die eksperimente het bevestig dat koolstof-nanostrukture soos grafeen en KNB baie potentiaal het om in toekomstige sensor-toepassings gebruik te word.

Acknowledgements

I would like to express my sincere gratitude to the following people and organisations: My study leader, Professor Willie Perold, for his guidance and motivation throughout this study. Also, the *Sentrale Elektroniese Dienste* at Stellenbosch University, especially Ulrich Buttner. Sasol, for agreeing to postpone my work obligations for two years in order to complete this degree. I also want to thank the National Research Foundation, the International Office and Bursary Department of Stellenbosch University for their financial assistance during this study.

A special word of thanks to Samantha Walbrugh-Parsadh of the International Office of Stellenbosch University and Karen Dvorak of the International Office of Rensselaer Polytechnic Institute (RPI) who facilitated the exchange from Stellenbosch University to RPI. Furthermore, a word of thanks to Professor Nikhil Koratkar and Professor Theo Borca-Tasciuc of RPI, who welcomed me to their laboratories and guided me while conducting research at RPI. I would also like to thank my fellow students at RPI who showed me around the laboratories and assisted me on countless occasions.

Finally, my mother, Sandra, sisters, Irene-marie and Sanet, as well as Deline, Daniel and Tjaart who supported me throughout this research project. None of this would have been possible without God's grace and blessing.

Dedications

Hierdie tesis word opgedra aan my ma, Sandra.

Contents

List of Figures

List of Tables

Nomenclature

Abbreviations

AFM	:	Atomic Force Microscopy
CNT	:	Carbon Nanotube
CVD	:	Chemical Vapour Deposition
IDT	:	Interdigitated Transducer
MWCNT	:	Multiwalled Carbon Nanotube
PCB	:	Printed Circuit Board
SAW	:	Surface Acoustic Wave
SCCM	:	Standard Cubic Centimeters per Minute
SEM	:	Scanning Electron Microscopy
SWCNT	:	Single-walled Carbon Nanotube
TEM	:	Transmission Electron Microscopy

Chapter 1

Introduction

1.1 Motivation of this work

Sensors are part of our daily lives and involved in most of the processes that manufacture the products around us. Advances in sensor technology are continuously needed as there will always be a demand for an improved sensor, either through a faster response time, higher accuracy, increased sensitivity or any other improvement to a certain characteristic of the sensor. It is estimated that the chemical sensor market will be worth more than 40 billion dollars worldwide in less than 10 years, with sensors utilised over a large range of applications such as environmental monitoring, process and quality control in industrial processes, medical applications and detection of security threats. In all these applications there is a demand for improved sensors compared to those currently commercially available [1].

Recently, nanotechnology related products have shown potential to lead the way towards the next generation of sensors [2], [3]. Nanotechnology refers to the ability to work with matter at the molecular level. It is specifically concerned with devices that have novel and significantly improved properties because of its nanoscale size. This holds the key to building smaller and more sensitive sensors. Due to the fact that the nanostructures are at the same scale as atoms and molecules, it enables the nanodevices to operate at sensitivities and accuracies that would not be possible with conventional techniques. Carbon nanostructure materials such as graphene and carbon nanotubes (CNT) are likely candidates to be used in this next generation of sensors and as such, both these materials have been receiving much attention due to their unique and extraordinary properties [4], [5]. These materials were also the subject of this study for their potential use in sensors.

1.2 Background

Graphene is a single atomic layer of sp^2-bonded carbon atoms, which is tightly packed into a two dimensional honeycomb lattice. It is the basic building block of graphite, as graphite consists of millions of these graphene layers stacked on top of each other [6]. Graphene was discovered in 2004 and this once thought to be theoretical material has recently been the subject of large scale international research efforts. It has been stated that it is the thinnest material in the universe [5], the strongest ever measured [7] and the material with the lowest resistance [8], [9]. Various studies have shown that graphene has excellent capabilities as a sensing material [2], [10], [11].

A carbon nanotube (CNT) can be thought of as a graphene sheet that is rolled up with the sides joining, forming a seamless tube instead of a spiral structure. The tube's diameter is typically a few nanometres and this unique structure results in extraordinary electrical and mechanical properties [12]. CNTs have also been successfully used in various sensing applications [3], [4], [13], [14].

1.3 Objectives of this study

The aim of this study was to investigate the feasibility of using a nanostructure in a sensor device. The main objectives are summarised as follows:

- Study suitable nanostructured materials that can be used as a sensor.
- Fabricate a device using the studied nanostructured material.
- Investigate the feasibility of using the device as a sensor.

Two materials were identified that have shown potential to be used as sensors, namely graphene and carbon nanotubes.

To study the feasibility of using graphene as a sensor, it was decided to test it in a wide range of possible application areas:

- **Humidity and temperature sensing:** Measure resistive changes of the graphene sample when it is exposed to different levels of humidity and temperature.
- **Gas and pressure sensing**: Measure resistive changes of the graphene sample at varying levels of pressure and exposure to various gases. Investigate whether the amount of gas absorbed by the graphene can be detected using a surface acoustic wave (SAW) device.
- **pH level sensing**: Measure resistive changes of the graphene sample when it is exposed to different pH levels.

- **Flow speed sensing**: Determine whether a voltage appears over the graphene sheet's surface when water flows over it.
- **Water electrolysis**: Investigate whether graphene can improve the efficiency of a water electrolysis process.

The goal of studying all of these applications was to determine the effect that they might have on one another. For instance, when graphene is used as a humidity sensor, it is important to know if pressure has an influence on the sensor. It would not be desirable for the graphene to respond to every test performed in the same manner as that would make the sensor unusable. Although the focus of the experiments was on sensory applications, the results obtained were also used to study the properties of graphene.

The objective of the research was solely to investigate whether graphene shows any *potential* to be used as a sensor in a specific application. All sensors have certain parameters that define the performance of the sensor such as its transfer function, sensitivity, span or dynamic range, accuracy or uncertainty, hysteresis or repeatability, non-linearity, noise and bandwidth [15]. Attempting to develop a single sensor that is superior in all these aspects compared to currently available commercial sensors would be an unrealistic task and was outside the scope of this research.

The primary use of CNTs were in a gas ionization sensor with the following objectives:

- Grow vertically aligned carbon nanotubes. Investigate the available methods to synthesize CNTs and use the method most appropriate for this application.
- Construct the sensor.
- Fabricate a testing environment and test the sensor.
- Create a model of the sensor. The model should show the electric field around the tips of the nanotubes. This can be used to find the optimal size and distribution of the nanotubes.

1.4 Contributions to the field

The most interesting result of the research proved to be the detection of CO_2 absorption in graphene using surface acoustic waves (SAW). Initial experiments showed that graphene absorbs CO_2 and this caused a small resistance change to the graphene film, but was not large enough to be of significance. The graphene was then used in conjunction with a SAW device that is able to measure small quantities of absorbed gas by the graphene. The sensor operates by measuring phase changes of a surface acoustic wave

that travels on the surface of a crystal. Graphene is deposited on the crystal, and changes to the graphene's properties directly influence the phase of the travelling wave. One test showed that the deposited graphene can increase the phase change from 0.7° to over 4°, when compared to the a blank SAW device. The graphene SAW sensor was especially sensitive to small changes in concentration at low pressures.

The significance of the tests performed was that it showed the SAW device operates as an amplifier of the amount of gas absorbed by the graphene. Furthermore, it was found that this process is completely reversible. It is consequently not only applicable to CO_2, but to other gases absorbed by the graphene. The detection of CO_2 using this method is so far unreported and it has the potential to be used to detect various gases. The SAW measurements were done with a doctoral electrical engineering student from Rensselaer Polytechnic Institute (RPI), Venkata S. Chivukula. The results obtained are being presented by V. Chivukula at the 2010 IEEE Ultrasonics symposium in San Diego, California, USA.

The humidity sensing experiments also provided very intriguing results. The first set of experiments clearly showed that the graphene has potential to be used as a humidity sensor. This was confirmed with two different types of graphene. Additional testing showed that a CNT sensor fabricated in a similar process is unable to sense humidity. Subsequent temperature tests revealed another very interesting application for graphene and humidity. The temperature tests performed revealed that the graphene used in this project possesses a certain bandgap. This led to additional experiments that investigated the value of the bandgap at certain humidity levels. Due to time constraints, the tests had to be completed by Fazel Yavari, a graduate student at Rensselaer Polytechnic Institute. The tests found that it is possible to vary the value of the bandgap by exposing the graphene to different humidity levels. Pristine graphene is a semi-metal with zero bandgap and conduction can only occur by the thermal excitation of electrons. This lack of bandgap is a major obstacle in the use of graphene in nano-electronic and nano-photonic devices such as p-n junctions, transistors, photo-diodes and lasers. The ability to control the bandgap in graphene is very desirable as it could lead to the development of these types of nano-electronic devices. The results of the bandgap experiments have been published in the nanotechnology journal, *Small* [16].

Various liquid based experiments were performed to determine whether graphene can be used as a pH sensor, a flow sensor and whether it is able to improve the efficiency of a water electrolysis process. From the tests no evidence was found that the graphene used in this project has potential to be used in any of these three applications.

A model of the gas ionization sensor was developed to calculate the electric field around the sharp tips of the CNTs. The model was created in COMSOL Multiphysics and it clearly showed that a decreasing diameter of the CNTs

caused the electric field to increase. Through the use of the model, the optimal size and distribution of the nanotubes can be determined. It also facilitates the explanation of the operating principles of the sensor.

1.5 Overview of this work

This section provides a summary of the work completed and also points out some of the main results. Each of these findings is later discussed in detail, where each chapter corresponds to a specific application area that was tested.

As stated previously, the main objective of the project was to investigate the use of nanostructures in sensing applications. More specifically the nanostructures used as the detection mechanism are graphene and carbon nanotubes (CNT). Supplementary information about nanotechnology, graphene, CNTs and some of the equipment used during this research is given in Chapter 2 on page 10.

1.5.1 Sensors used in this project

The graphene used in this project was created using the method of Askay and co-workers [17], [18]. With this method, graphite is completely oxidized using a strong acidic treatment. The graphite oxide is then exposed to a thermal shock by placing it in a furnace heated at 1050 °C for 30 seconds. This thermal shock causes CO_2 trapped in the graphite oxide to expand rapidly and break the bonds between the individual graphene layers that make up the bulk graphite. This results in the formation of few layered graphene sheets.

The graphene flakes that formed were mixed with distilled water using a sonication process. This made the deposition of graphene in specific areas easier. The graphene sensor was fabricated by spraying this mixture onto a glass substrate, which produced a graphene film that consisted of millions of graphene flakes overlapping each other. Chapter 3 on page 23 contains the exact steps that were followed to create the graphene and the sensor as well as various images of the graphene. After the graphene dried, four electrical contacts were connected to the corners of the sample using silver paste. Four connections were established as this made it possible to use the van der Pauw method when performing resistive measurements. The van der Pauw method was used as it eliminates contact resistance. Section 3.4 on page 38 elaborates on the van der Pauw method.

A CNT sensor that was only used for humidity testing was fabricated in a similar process as the graphene sensor. Single-walled carbon nanotubes (SWCNT) were mixed with distilled water using the sonication process and afterwards sprayed onto a glass substrate. Contacts were also attached to the corners of the sample using silver paste. With the naked eye, the two sensors looked identical.

1.5.2 Humidity and temperature sensing

The graphene film sensor was exposed to varying levels of relative humidity and the resistance was recorded. The sensor showed a linear increase in resistance as the relative humidity level increased. A SWCNT sensor was fabricated to determine if this effect is unique to graphene or if CNTs also display this behaviour. The SWCNT sample's resistance did not change when the relative humidity level changed. A third humidity test consisted of another graphene sample, but this graphene was fabricated using chemical vapour deposition. This method produced a single graphene sheet as opposed to the graphene film sensor that consisted of millions of graphene sheets overlapping each other. This test was done to determine whether the change in resistance is observable in individual sheets as well. The single graphene sheet sensor did indeed respond to changes in humidity. The additional results as well as discussions about the mechanism for the change can be found in Chapter 4 on page 41. Section 3.3 on page 34 contains the details of the SWCNT film sample as well as the graphene sheet sensor.

The temperature tests showed that the graphene has a certain bandgap. This led to further tests that showed the bandgap can be varied by exposing the graphene to different humidity levels. This is significant, because a lack of bandgap in graphene is a major obstacle to the creation of graphene based electronic devices. This simple method of tuning the bandgap with an exposure to humidity could assist in the development of graphene related electronics.

1.5.3 Gas sensing and pressure sensing

Gas and pressure tests were subsequently performed on the graphene film sensor. These tests were completed to investigate the gas sensing possibilities of the graphene used in this project. In the first test, the resistance change of the sample at various pressures was measured. Through the use of argon it was shown that the sensor is unaffected by a change in pressure.

With the second test it was shown that exposure of the sensor to CO_2 can slightly increase the resistance of the sample (0.145%). This was not enough to justify the use of graphene to detect CO_2. The graphene was subsequently used in conjunction with a surface acoustic wave (SAW) device. Refer to Section 5.2 on page 58 for more information on SAW devices. The graphene was deposited between the receiving and transmitting interdigitated transducers (IDT) of the SAW device. This made it possible to detect very small resistance changes of the graphene sheet caused by the absorption of CO_2. The graphene-SAW sensor underwent a phase change of 4° when it was exposed to 0.43 mg/cm^3 CO_2 for 50 minutes. The CO_2 was subsequently extracted from the testing chamber and the sensor recovered to its initial value within 35 minutes. When the SAW sensor was used without any graphene, a

phase change of 0.7° was observed, which was caused by a change in pressure.

The last test performed demonstrated that the graphene-SAW sensor also has some potential to detect concentrations of CO_2 in air. The changes were not as pronounced as the pure CO_2 experiments, but still showed that the sensors undergoes a 1° phase change when exposed to a CO_2 concentration of 0 to 20%. All of these results are discussed in detail in Chapter 5 on page 54.

1.5.4 pH sensing

The use of the graphene film sensor in liquid applications was also investigated. In the first test the graphene film sensor was used in an attempt to find a relationship between the resistance of the sensor and a pH level. Although the resistance changed at different pH levels, it was not repeatable and was caused by a change in the conductance of the liquid instead of the pH level. Interestingly, the sensor generated a relatively large voltage when it was placed in the solution and it was attempted to find a relationship between this voltage and the pH level. Unfortunately, no relationship could be found. After various tests the graphene film sample did not show any potential to be used as a pH sensor. Refer to Section 6.1 on page 66 for a full discussion of the experiments and results.

1.5.5 Water electrolysis

This is the one experiment in this research where the graphene was not used in a sensory application. In this experiment, the graphene was used in an attempt to increase the efficiency of a water electrolysis process, which is the process where water is split into hydrogen and oxygen by passing an electrical current through the water. This process is generally not very efficient [19] and it was investigated whether graphene can be used to increase the overall efficiency. To perform the experiment, the same graphene solution that was used to create the sensor was sprayed onto two graphite rods. The rods were placed in an aqueous solution, a voltage was applied to the rods and the corresponding current was measured. A graph was then drawn from the measured values. The test was repeated with two blank graphite rods to determine whether the graphene increases the efficiency of the process. It was found that the graphene slightly improved the efficiency, but not significant enough to justify the use of graphene in water electrolysis processes. Section 6.2 on page 74 contains the detailed results and discussions of the experiments.

1.5.6 Flow speed sensing

The last liquid based experiment was undertaken to determine whether the graphene has potential to be used as a flow sensor. See Section 6.3 on page 78 for a detailed discussion. Similar experiments have been successfully completed with CNTs [14] and this test used a similar approach. The sensor

was placed in a tube and the potential difference over the graphene film at various flow velocities of water was recorded. The effect of different orientation angles of the graphene film to the flow of water on the potential difference was also recorded. The tests unfortunately found no correlation with the flow speed and the potential difference across the film.

The three liquid based experiments were largely unsuccessful and it seems that the graphene used in this research is not well suited to these types of applications. It does not rule out that graphene in general could not be used for one of these applications, but rather that a different method to synthesize the graphene must be used. Other methods of creating the sensor as well as alternative measuring techniques may well produce a sensor that can operate successfully under these circumstances.

1.5.7 Carbon nanotube gas sensor

The CNT gas sensor that was constructed was based on the work done by Modi *et al* entitled *Miniaturized gas ionization sensors using carbon nanotubes* [13]. The sensor consisted of two parallel spaced electrodes, with one electrode covered with vertically aligned multiwalled carbon nanotubes (MWCNT) and the other being a plain aluminium electrode. The two electrodes were separated by a thin insulating material, leaving the electrodes 150 μm apart. The sensor operates by applying a sufficiently high voltage to the electrodes until electrical breakdown occurs. By monitoring this voltage, the gas can be identified, as each gas has a unique breakdown voltage. The MWCNTs significantly lowers the voltage at which this breakdown occurs compared to a traditional ionization sensor. This makes the device more portable and safer to operate. They also found that the current after breakdown is proportional to the concentration of the gas.

The main motivation for following the work done by Modi *et al* was to gain insight into the growth techniques, structure and properties of CNTs. It was also envisioned to investigate possible methods of improving the device such as measuring capacitive changes instead of electrical breakdown, as well as using the sensor with a mixture of various gases instead of one pure gas. Unfortunately, after numerous attempts and seeking the help of experts in the field of CNT growth, the CNT growth attempts remained unsuccessful. The method used to synthesize the CNTs is discussed in Chapter 7 on page 82.

Despite all the difficulties faced, there are positive aspects that can be taken from the attempts to construct the CNT gas sensor. Valuable experience was gained in the use of nanofabrication techniques and equipment such as lithography, film deposition, wire bonding and an atomic force microscope. The most insightful area of the CNT gas sensor research was the creation of a model of the sensor. A model was created in COMSOL Multiphysics, as this powerful simulation and modeling software package was available at Stellenbosch University. The model calculates and plots the electric field

around the tips of the nanotubes. The model clearly shows that the electric field around the nanotubes is significantly higher than the electric field between two smooth electrodes. The model can also be used to study the effect of the size and distribution of the nanotubes on the electric field. For more information regarding the model refer to Section 7.3 on page 91.

1.5.8 Conclusions

The results of the experiments performed showed that graphene has potential to be used in gas absorption applications. This was used to fabricate a humidity sensors as well as a CO_2 sensor. The humidity sensing experiments led to the discovery that the bandgap in graphene can be altered by exposing it to different levels of humidity. The use of graphene in absorption based gas sensing applications can be improved by using the graphene in conjunction with a SAW device. The graphene used in this project is not well suited to liquid applications and different manufacturing techniques should be considered if graphene is to be used in these applications. For a detailed discussion of the conclusions of the project and future recommendations refer to Chapter 8 on page 97.

Chapter 2

Background

This chapter gives an overview of some of the main topics that were used in this project. It starts with a section on nanotechnology, where nanotechnology is defined, and the past and future developments are discussed. The structure, properties and applications of the two main carbon nanostructures that were used in this research, namely, graphene and carbon nanotubes are then reviewed. Lastly, the operating principles of the tools and equipment that were used to observe the nanostructures during this project are explained.

2.1 Nanotechnology

Nanotechnology is an interdisciplinary field of science and technology. Chemists, biologists, physicists and engineers are all involved in nanoscience and nanotechnology. *Nanoscience* involves the fundamental study of structures and molecules where one of the dimensions is at least 100 nm. *Nanotechnology* is the application of these *nanostructures* in useful devices and materials [20]. It is quite apparent from this description that the term *nanotechnology* refers to an extremely wide range of application areas and it is no surprise that so many fields and researchers are involved with nanotechnology. The areas where the most research are being done and have the biggest potential for near future nanotechnology based products include electronic devices, healthcare and composite materials.

2.1.1 The size scale

The minuteness of a nanometre can be difficult to comprehend at times as this example shows: A nanometre is to a metre what a marble is to the size of the earth [21]. Table 2.1 gives the sizes of the very small things around us to put the size of a nanometre in perspective.

Hair	∼100 μm
Complex Cell	∼10 μm
Bacteria	∼1 μm
Virus	∼100 nm
Large molecule	∼1-10 nm
Atom	∼0.1nm

Table 2.1: Size comparisons of various micro-and nanosized objects [22].

One of the very interesting aspects about nanotechnology is that as materials move down the size scale from the macro world to the quantum world, the properties of the material change. Indeed, the behaviour of nanosized materials can be accurately predicted using quantum mechanics [23]. Familiar properties such as conductivity, hardness, melting point and colour can change or lose meaning altogether [24]. For instance, a stable material such as aluminium becomes combustible at the nanoscale [21]. A big branch of nanotechnology is concerned about studying these new properties and how we might be able to take advantage of them in various applications. Most of the properties of materials are formed at this level, so being able to control matter at the nanoscale provides you with the ability to change the properties of materials.

2.1.2 The present and future of nanotechnology

Various organizations and governments around the world are very optimistic about the prospects nanotechnology. This led the US government to allocate more than a billion dollars to nanotechnology research in 2005 and the National Science Foundation in the USA predicts that by 2015, nano related devices could be a trillion dollar market [21]. For obvious reasons, big companies such as HP, NEC and IBM have invested large amounts of money towards research and development of nanodevices. IBM created the world's smallest advertisement by writing the letters *IBM* with 35 individual xenon atoms as shown in Figure 2.1.

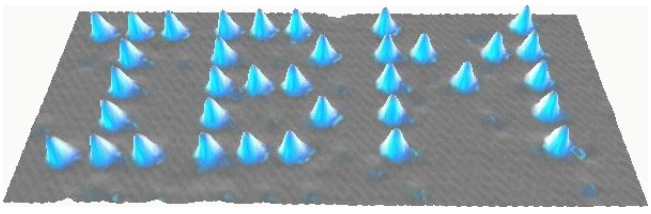

Figure 2.1: The world's smallest advertisement: The IBM logo spelled out in xenon atoms [25].

Over the past few years there has been a steady increase in products that contain some form of nanotechnology. Most of these products were previously available products and nanotechnology was used to improve them. Examples of these products include integrated circuits, sunscreen, stain-proof or static-free clothing, scratch resistance coatings, bandages and sporting equipment such as tennis rackets and balls [26]. Figure 2.2 shows the amount of nanotechnology-based consumer products that are created each year. The trend line shows that the number of products available appears to be increasing linearly. Most of the products (60 %) are used in health and fitness applications [26].

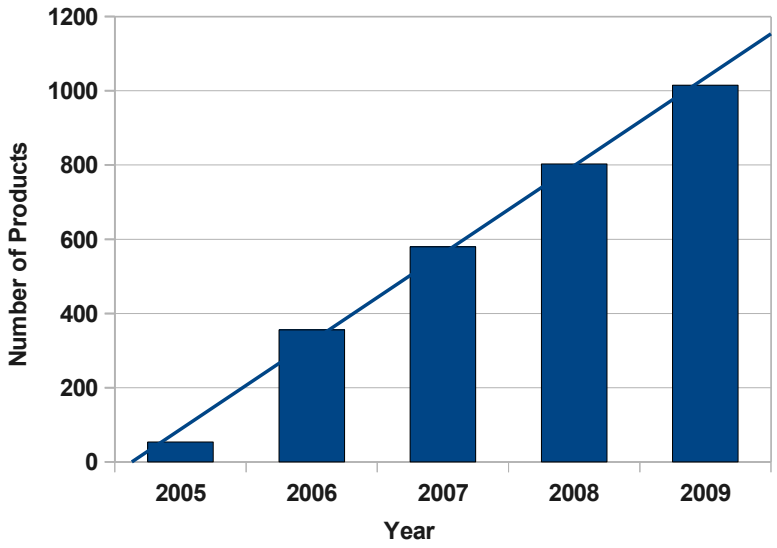

Figure 2.2: Number of total nanotechnology-based consumer products [26].

The exact implications nanotechnology will have on the world is still a heavily debated topic. Many people believe it can have an impact of the same scale as the industrial revolution [27], while others are more sceptical about the immediate future implications of nanotechnology [23]. While only actual revolutionary applications (or lack thereof) would prove either of these parties correct, there still remains enormous amounts of research ahead before a definite answer about the future of nanotechnology will be found. New materials and more importantly uses for these materials are found on a regular basis as nano-related research continues.

Any new technology poses various challenges regarding health risks. There are a number of examples in history where a new technology had serious health risks and people only became aware of these risks years after it has been used. Therefore, it is imperative that while applications are being developed, their associated health risks should also be considered. This necessary process could slow down the development of nano related products.

The potential of nanotechnology products go far beyond what is currently available. Nanotechnology is still in its infancy and nobody can argue that exciting times lie ahead for the route that nanotechnology will follow.

2.2 Graphene

Graphene is a single atomic layer of sp^2-bonded carbon atoms, which is tightly packed into a two dimensional honeycomb lattice. It is the basic building block of other carbon nanostructures such as carbon nanotubes and fullerenes. Graphite consists entirely of millions of graphene layers stacked on top of each other [6]. Figure 2.3 shows how other carbon structures are formed from graphene.

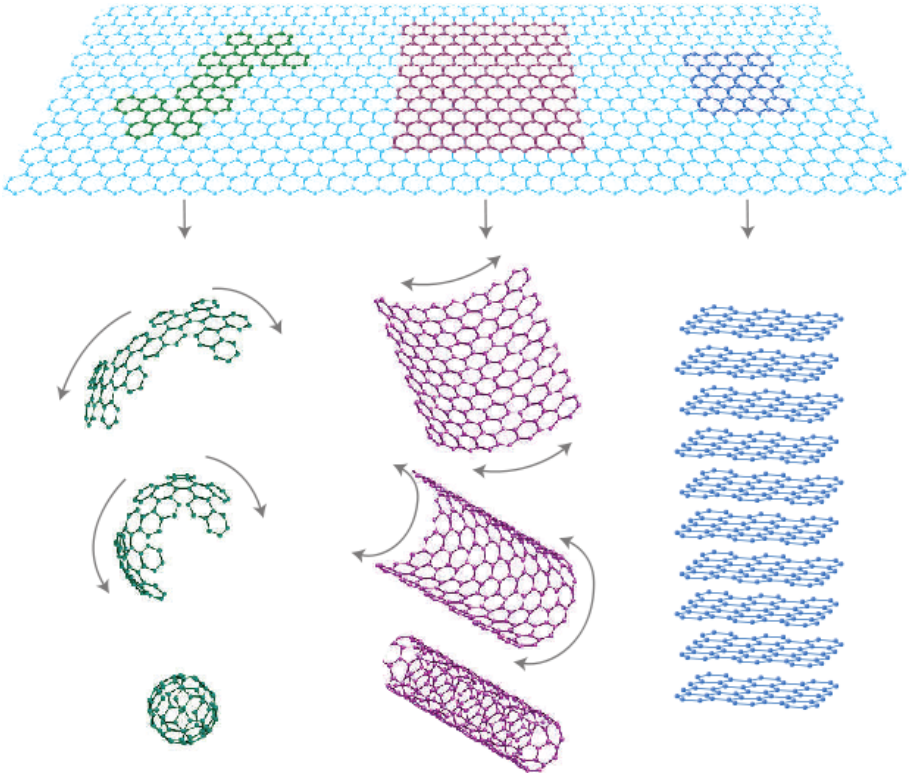

Figure 2.3: Graphene: Basic building block of graphitic materials of all dimensionalities. 0D fullerenes, 1D nanotubes and 3D Graphite [6].

2.2.1 Experimental discovery

Graphene was once thought to be a theoretical material [28], but its discovery in 2004 by Geim and co-workers showed the world some of its fascinating properties [29]. They used a peculiar method to manufacture the graphene:

A piece of graphite is sandwiched between two pieces of scotch tape and ripped apart. This process is repeated numerous times and the piece of tape is then dissolved. A silicon wafer is placed in the solution and the flakes stick to the surface of the substrate. The graphene flakes are then hunted down under a microscope. Between all the graphitic debris they found single layer graphene pieces measuring tens of micrometers in size. Since then various other methods have been developed and they are discussed in Chapter 3. Interestingly enough, the scotch tape method still produces the highest quality graphene sheets [30].

2.2.2 Properties

Geim and co-workers used this method a few years later to fabricate a gas sensor that has the ability to detect individual gas molecules [2]. This sparked the start of intensive graphene related research. Since then graphene has steadily been replacing carbon nanotubes as the poster child of nanotechnology due to its remarkable and at times unbelievable physical and electrical properties, such as:

- Graphene exhibits ultra-high electron mobility [31] and is the material with the lowest resistivity [8], [9].
- Graphene is the strongest material ever tested with a Young's modulus of over 1.0 TPa [7].
- Graphene has an extremely high value of the thermal conductivity of up to 5300 W/mK [32]. This high value outperforms carbon nanotubes, diamond and is ten times more than any metal [33].
- Single layer graphene absorbs only 2.6% of light and reflects less than 0.1% [30]. This absorption and reflection increases linearly with an increase in the number of layers.
- Electrons that travel in graphene behave like massless relativistic particles [34], [35].

From these properties it is clear that graphene has the potential to start a nanotechnology revolution.

2.2.3 Potential applications

These extraordinary and unusual properties of graphene together with its simple structure have led to intense amounts of research into possible applications for graphene. What further fuelled this research interest is that graphene solves various limitations that other materials such as carbon nanotubes have faced [30]. The following paragraphs will give a brief summary of some of the most exciting applications of graphene.

Electronics

Due to graphene's high electron mobility, it has the potential to create transistors that are faster than today's state-of-the-art high electron mobility transistors [36]. Therefore, it is an attractive material to be used in field effect transistors and the possibility of using graphene in molecular-scale electronics has been demonstrated [37]. Lithography techniques that are currently used to fabricate integrated circuits are reaching its limits and graphene is a likely candidate to be used in future electronic devices [38].

Optoelectronic devices

The use of graphene for optically transparent electrodes has also been proposed [39]. Thin, transparent and conductive films are often needed in various optoelectronic devices. Existing technologies are often complicated and expensive. The optical properties of graphene together with its high chemical stability and mechanical strength may well be an excellent alternative to currently used materials such as indium tin oxide (ITO) [39]. The optical properties of graphene have also been exploited by using graphene films as transparent electrodes for solar cells [40]. Graphene photo detectors have also been developed and employed in a 10 Gbit/s optical data link [41].

Composite materials

Similar to most carbon materials, such as diamond, carbon nanotubes and graphite, tests performed on graphene have showed that it is an incredibly strong material [7]. It has been proposed that the strength of graphene as well as some of its other properties can be exploited by using it in a composite material [42]. Moreover, it has also been reported that graphene is far superior to carbon nanotubes and other nanoparticles in transferring its strength to a host material when used as a composite material [43].

Sensors

The two dimensional nature of graphene enables the entire surface of a suspended graphene sheet to be exposed to the environment. This coupled with graphene's electronic properties, mechanical robustness and chemical stability, makes graphene an excellent candidate for sensing applications [30]. As stated earlier, graphene has achieved the ultimate detection sensitivity, when it was showed that graphene responds to a single gas molecule absorbed on its surface [2].

Despite all the remarkable properties of graphene, various challenges still remain that need to be addressed before mass production of graphene related products would be possible. Industrial production of graphene devices requires large-area, wafer scale graphene films [36]. Most of the applications described

above are not yet ready to be implemented economically on a large scale. Continual improvements to manufacturing graphene are being made every day and gradually building the road to enabling revolutionary graphene products [44], [45]. For the short lifespan of graphene so far, its accomplishments are remarkable. Given the relentless pace that graphene related research has progressed, it is only a matter of time before graphene related products can be seen in our daily lives.

2.3 Carbon nanotubes

The discovery of carbon nanotubes (CNTs) is most often attributed to Sumio Iijima who observed multiwalled carbon nanotubes (MWCNTs) in 1991 [46], [47]. However, there was an article in 1952 in the Journal of Physical Chemistry of Russia that contained TEM evidence of a tubular nanosized carbon filament, or otherwise known as a CNT [48]. The fact that the article is in Russian and Western scientists' access to Russian publications were limited during the cold war, resulted in most Western scientists failing to take notice of the discovery. It was however the discovery by Iijima in 1991 that sparked an intense research interest in CNTs and since then numerous papers and articles have been published regarding nanotubes. In 1992 only 9 articles containing the words "carbon nanotube" were published, but this number increased to over 5000 in 2004 [47]. Iijima is however credited for the discovery of single-walled carbon nanotubes (SWCNTs) in 1993 [49]. This section will briefly explore the structure, properties and applications of this nanostructure.

2.3.1 Structure

Despite the incredible properties of CNTs, it has a quite simple structure. A CNT can be thought of as a graphene sheet that is rolled up with the sides joining, forming a seamless tube instead of a spiral structure. This produces a single-walled carbon nanotube (SWCNT). Multiwalled carbon nanotube (MWCNT) can also be formed, which is essentially a set of SWCNTs with increasing diameters that shares a common axis.

Different chiralities of the CNT can be realized by rolling the graphene sheet in different directions. This in turn directly influences the electronic properties of the CNT and is therefore an important characteristic of the nanotube [50]. One of the most interesting properties is its ability to either behave as a conductor, an insulator or a semiconductor depending on its chirality. Figure 2.4 shows the different directions that CNTs can be rolled.

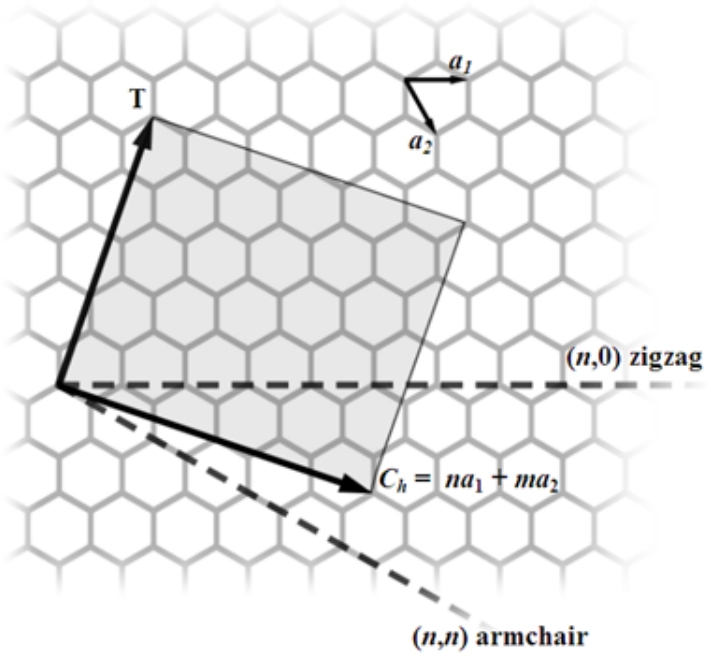

Figure 2.4: The rolling vector used to define the type of nanotube [51].

A CNT is characterized by its rolling vector $\mathbf{C}$, where $\mathbf{C} = n\mathbf{a}_1 + m\mathbf{a}_2$. The special case where m = 0, the CNT is called zigzag tubes and when m=n the CNT is called armchair tubes. In other general cases the CNTs are called chiral tubes [12]. Figure 2.5 shows the different types of CNTs.

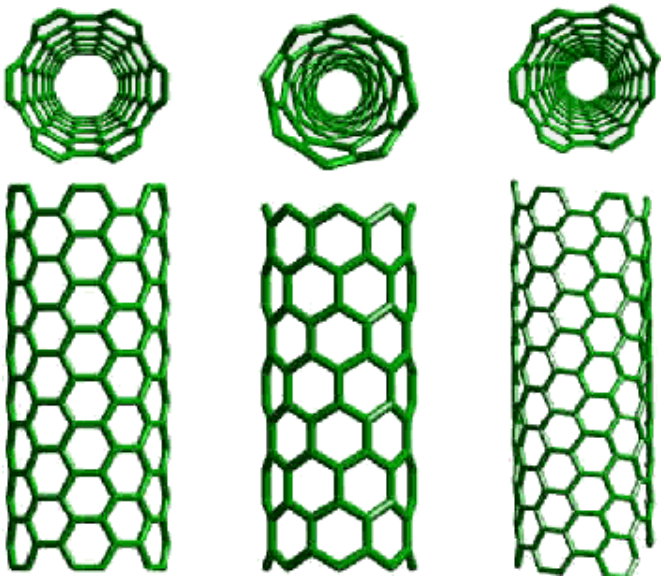

(a) Armchair **(b)** Zigzag **(c)** Chiral

Figure 2.5: Different types of CNTs [52].

Although this method is used to describe the structure of CNTs, in reality, CNTs are not formed in this manner and are almost never a perfect tube. It is currently not possible to selectively control the chirality of the CNT and it is a major challenge today to find a way to manufacture a specific type of CNT [12]. Chapter 7 discusses the various methods available to synthesize CNTs.

2.3.2 Properties and applications

The unique structure and high aspect ratio of CNTs, together with the high strength of carbon-carbon bonds found in CNTs, give them unique and remarkable properties that can be exploited to form new novel materials and devices.

CNTs can handle extremely high current densities, in the order of 10^9 A/cm^2. During tests performed on the CNTs, this current was sustained at temperatures up to 250 °C for two weeks, which suggests CNTs have the potential to be used as interconnects in future integrated circuits [53].

CNTs are the strongest known fibres [4] and have been used as a composite material to fabricate an ultra light and strong bicycle frame [54]. CNTs have been used in other material applications such as hydrogen storage [55] and composites for coatings, filling and structural materials. Possible applications for CNT have been as far reached as using it for a space elevator [56], which will be used to transport materials to and from space.

Various CNT based devices have also been invented such as actuators [57], AFM probe tips [58], nanoelectronic devices such as CNT transistors [59], field emission devices [60] and various sensors including gas sensors [13], [61], [62], flow sensors [14], humidity sensors [63] and pressure sensors [64].

However, similar to graphene, very few CNT based devices currently exist. The main obstacle that has slowed the commercialization of CNT products is manufacturing issues [65]. The devices described above are still in early stages of development and currently few of these products have mass market appeal. The CNT community believes that this will change within ten years [66].

2.4 Nanotechnology equipment

One of the main drivers of nanotechnology related advancements is the development of the tools that are used to view and manipulate matter at the nanoscale. The equipment that has been developed is equally impressive to the nanodevices that have been produced using them.

The maximum resolution of a light microscope is limited to the wave length of light. The wavelength of light is around 500 nm, so objects smaller than that would not be visible with an optical microscope [20], [67]. The maximum magnification of an optical microscope is therefore less than 1500. Other techniques had to be developed to enable scientists to view objects at much higher magnifications levels and even view individual atoms. This section will discuss some of the devices that enable viewing at these high magnification levels.

2.4.1 Scanning Electron Microscope (SEM)

The first work describing the concept of a scanning electron microscope (SEM) was done by Max Knoll in 1935. Since then, the SEM has played a huge part in scientific research. It is capable of magnification levels ranging from 10 times to 500 000 times, showing details up to 1 nm [68].

A SEM uses electrons instead of light to form the image of the sample. Electrons can have more momentum than photons which results in a smaller de Broglie wavelength, which translates directly into a higher viewing resolution compared to a light microscope. A SEM bombards the surface of the sample with a beam of electrons [69]. This electron beam is generated by what is creatively called an electron gun. The electron beam passes through a series of electrostatic and electromagnetic lenses to focus the beam onto a specific area of the sample. The electrons interact with the sample and produces signals that can be detected and analysed to form the image of the sample. Inside the chamber are various detectors for this purpose. A secondary electron detector is used to detect the amount of scattered electrons and the image is formed by the number of electrons that reach the detector. Backscattered electron detectors and X-ray detectors are used to determine the composition of the

sample [70]. This process is performed only on a small part of the sample, so the beam is scanned over the entire surface of the sample to form the image. This is why it is called a *scanning* electron microscope. The magnification can be increased by scanning a smaller area. The resolution can be increased by giving the fired electrons more energy, which would result in a shorter wavelength. SEM analysis has to be performed in high vacuum because gas particles would interfere with the electron beam [71]. Figure 2.6 shows a schematic of how a SEM operates.

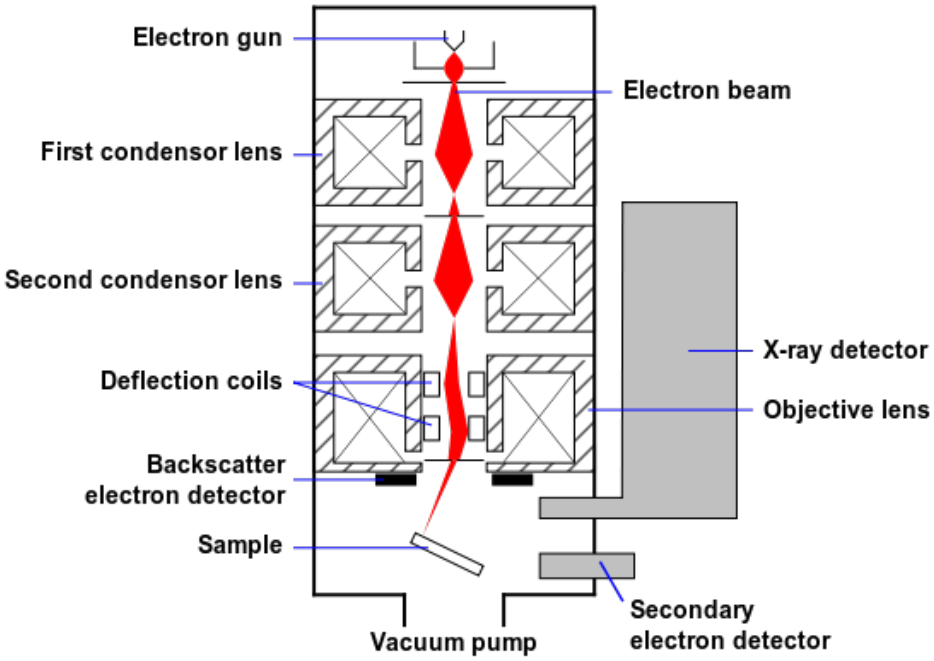

Figure 2.6: Schematic of how a SEM operates [72].

2.4.2 Transmission Electron Microscope (TEM)

The transmission electron microscope (TEM) works on a similar principle as the SEM, but instead of reflecting the electrons from the surface of the sample, the electrons pass through the sample. Consequently, the sample has to be very thin to be able to use this technique, typically less than 100 nm. The electrons interact with the sample as it passes through and this interaction is used to form the image of the sample. Under the correct conditions, it is possible to view individual atoms using a TEM [20]. A TEM also features an electron gun with a series of lenses that is fired in a vacuum column. The electrons that pass through the sample hit a fluorescent screen forming a type of shadow image, where different parts of the image are different levels of

brightness, corresponding to the density of the sample [73]. The image can be studied directly or photographed with a camera.

2.4.3 Atomic Force Microscope (AFM)

The atomic force microscope (AFM) was invented by Gerd Binnig and Heinrich Rohrer in the early 1980s at IBM Research - Zurich, and they both later received a Nobel Prize for physics for this invention [20]. The AFM represents an atomic scale gramophone. A nanosized tip ($\sim$ 10 nm) is connected to a cantilever that scans across the surface of a material [69]. A laser beam is reflected off the cantilever onto a position sensitive detector. The AFM effectively measures extremely small forces ($<$ 1 nN) between the tip of the cantilever and the sample [27]. Figure 2.7 shows a schematic of how an AFM operates.

There are several mode of operation used by the AFM to form the image of the surface. One of the most widely used methods is *contact mode* operation, and this was the method used during AFM scans in this project. In this mode, the tip is adjusted to maintain a constant force (or deflection of the cantilever) between it and the sample [27]. This adjustment then represents the surface topology of the sample. The quality of the image is therefore highly dependent on a proper feedback circuit and its ability to track the surface [74].

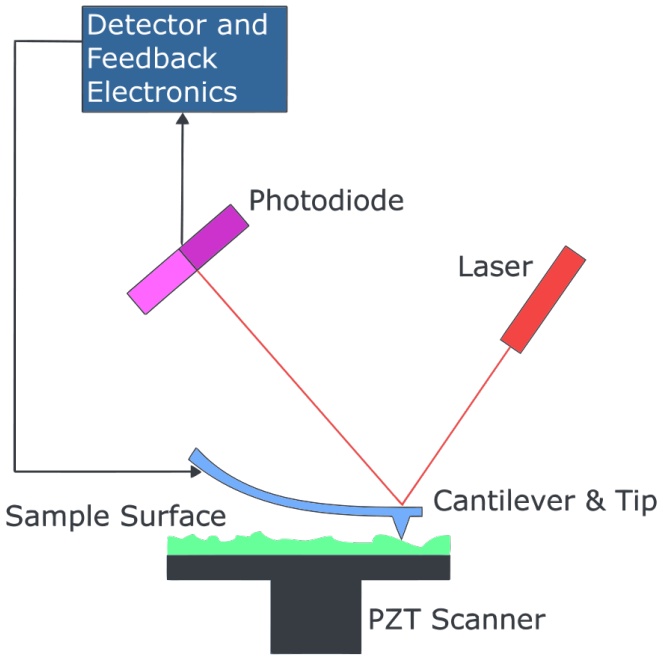

Figure 2.7: Schematic of how an AFM operates [75].

This chapter gave a brief overview of the carbon nanostructures that were used in this project, as well as the equipment that was used to view them. The rest of this report is concerned with the details of how sensors were constructed using these nanostructures, and subsequent investigations into the feasibility of using these nanostructures for various sensing applications.

Chapter 3

Sensors Used In This Project

This chapter briefly reviews some of the available methods to synthesize graphene. The method used to create graphene in this research is then given in detail. It follows with an explanation of how the sample that was used for testing was fabricated from this graphene. The manufacturing process of a different type of graphene sample and a SWCNT sample is then given. The chapter ends with an explanation of the van der Pauw method that was used to measure the sheet resistance of the sensors.

3.1 Graphene synthesis

The existence of graphene was a much debated topic before its discovery in 2004 and there has been numerous attempts to manufacture graphene since the 1960s [30]. Since its discovery, various other methods has been invented to synthesize graphene, each one with its own advantages. This section will briefly explore some of the most commonly used methods as well as others that were only recently invented.

3.1.1 Exfoliated graphene

Exfoliated Graphene, also known as the scotch tape method or micromechanical cleavage, was the first technique used to synthesize graphene [29]. Geim and co-workers [2] used this method in their ground breaking paper, *Detection of Individual Gas Molecules Adsorbed on Graphene*, which led to the graphene gold rush. With this crude method, a graphite flake is sandwiched in scotch tape and peeled apart. This process is repeated numerous times after which the tape is placed on a layer of oxidized silicon. The tape is pressed firmly against the substrate for a few minutes, after which it is slowly peeled off. The sample is then examined with a microscope to search for graphene sheets among mostly graphite debris [76]. The choice of substrate is crucial for this to be successful as it makes it possible to find the mono layer graphene flakes

using an optical microscope. The colour of the flakes on the substrate indicates the thickness of the graphite flakes [30].

3.1.2 Epitaxial growth on silicon carbide

Epitaxial growth on silicon carbide (SiC) is another method known to produce graphene. With this approach, graphene forms when silicon carbide is annealed in a dense noble gas atmosphere such as argon [77], [78]. Emtsev and co-workers [77] showed that the quality of a graphene film prepared on SiC(0001) can be greatly increased by annealing the SiC sample in an argon atmosphere, close to atmospheric pressure, as opposed to annealing it in high vacuum. When they annealed the SiC in the argon atmosphere, they were able to heat it up to 1650 °C. The graphene forms as a result of silicon evaporation from the substrate.

3.1.3 Epitaxial growth on metal substrates

Large-scale graphene films can be grown by using chemical vapour deposition [79], [80]. Kim *et al* [79] showed that high quality graphene can be grown on a SiO_2/Si substrate using chemical vapour deposition. With this method, a 300 nm layer of nickel is deposited on a Si/SiO_2 layer. The sample is heated in an argon atmosphere up to 1000 °C, after which a reactive gas mixture (CH_4:H_2:Ar = 50:65:200 standard cubic centimetre per minute) is flowed through the system. Using flowing argon, the system is rapidly cooled (-10 °C/min). The nickel is etched away using a $FeCl_3$ solution and the remaining graphene layers that are floating in the solution can be transferred to an arbitrary substrate.

3.1.4 From nanotubes

Another approach that has interesting possible applications is creating graphene from carbon nanotubes, producing graphene nano ribbons [44], [45]. Jiao *et al* [45] produced graphene nano ribbons by depositing multiwalled carbon nanotubes (MWCNT) on a Si substrate and coating it with a poly (methyl methacrylate) (PMMA) layer. The PPMA-MWCNT was removed from the Si substrate and then the exposed area of the CNT was etched away using an argon plasma. Removal of the PPMA then exposed the graphene nano ribbons that were less than 20 nm wide. Kosynkin *et al* [44] had a much different approach as they used sulphuric acid and potassium permanganate to open the nanotubes and create graphene nano ribbons.

3.1.5 From graphite oxide

Graphene can be synthesized by rapidly heating graphite oxide. Aksay and co-workers [17], [18] were the first to show the required steps for optimal

graphite oxide preparation as well as thermal treatment to make the formation of graphene possible. This is the primary method that was used to synthesize graphene during this project and more information regarding the preparation steps and reasons for choosing this method are given in detail later in this chapter.

3.2 The Graphene film sensor

The graphene film sensor refers to the sensor that was used during the majority of the graphene related research. This section will discuss how this graphene was manufactured, transferred to the substrate and electrical connections established to the film.

3.2.1 Manufacturing the graphene

The majority of the graphene related research of this project was done with Professor Nikhil Koratkar's group at Rensselaer Polytechnic Institute in Troy, NY, USA. The method Koratkar's group uses to synthesize graphene is based on the work done by Aksay and co-workers as stated before. With this technique, functionalized graphene sheets are formed through the thermal expansion of graphite oxide [17], [18], [81]. Subsequently, the same method for graphene fabrication was employed during this project.

There have been numerous unsuccessful attempts since 1859 to produce graphene by exfoliation of graphite oxide. Aksay and co-workers [17], [18] showed that with optimal preparation of graphite oxide and heat treatment, bulk quantities of functionalized single graphene sheets can be produced.

The process starts with the acidic treatment of graphite to produce graphite oxide. In order for the process to be successful, it is critical to completely eliminate the intergraphene spacing that is found in bulk graphite during the oxidation phase. When complete oxidation has occurred, the 0.34 nm intergraphene spacing disappears and is replaced by a new spacing of 0.71 nm. After the oxidation process, the graphite oxide is rapidly heated at a rate of >2000 °C/min, up to 1050 °C. This thermal shock causes CO_2 between the graphene layers of the graphite oxide to expand, breaking the van der Waals attraction between the graphite layers resulting in the formation of partially oxygenated graphene sheets. Figure 3.1 shows a schematic representation of the process used to synthesize functionalized graphene sheets.

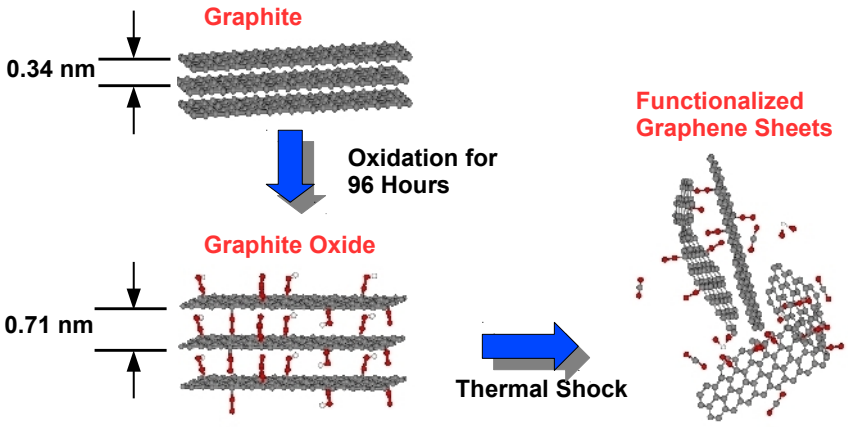

Figure 3.1: Schematic of the oxidation and thermal exfoliation process employed to synthesize bulk quantities of functionalized graphene sheets from graphite [81].

The graphene that was used during this project was prepared by a graduate student in Professor N. Koratkar's group, J. Rafiee. The method used to synthesize the graphene is explained in one of their publications, entitled *Superhydrophobic to Superhydrophilic Wetting Control in Graphene Films* [81]. The following paragraph provides a quote from that article and gives the exact steps to create graphene:

> "Natural graphite flakes with an average diameter of 48 μm were supplied from Huadong Graphite Factory (Pingdu, China). Concentrated sulfuric acid (95-98%), concentrated nitric acid (68%), and hydrochloric acid (36-38%) were purchased from Beijing Chemical Factory (China). Potassium chlorate (99.5%) was obtained from Fuchen Chemical Reagents (Tianjin, China). Graphite oxide was prepared by oxidizing graphite in a solution of sulfuric acid, nitric acid, and potassium chlorate for 96 h based on the work of Aksay and co-workers [17], [18]. Thermal exfoliation of graphite oxide was achieved by placing the graphite oxide powder (200 mg) in a 200-mm-inner-diameter, 1-m-long quartz that was sealed at one end. The other end of the quartz tube was using a rubber stopper. An argon inlet was then inserted through the stopper. The sample was flushed with argon for 10 min, and the quartz was quickly inserted into a tube furnace (Thermolyne 79300, Thermo Scientific Inc., USA) preheated to 1050 °C and held in the furnace for 30 s. Rapid heating (>2000 °C/min) splits the graphite oxide into bulk quantities of few-layered graphene sheets."

Figure 3.2 shows a transmission electron microscopy (TEM) image of a typical graphene flake synthesized using this method and deposited on a

standard TEM grid for imaging. The flake is several micrometers in dimension and has a wrinkled surface texture. Figure 3.3 displays a high-resolution TEM (HRTEM) image of the edge of a typical graphene flake, indicating that each flake is comprised of ∼3 individual graphene sheets. The electron diffraction pattern shown in Figure 3.4 confirms the existence of graphene, as the sp^2 bonding configuration is clearly visible. The atoms are clustered together in groups of two or three, indicating that the graphene consists of a few layers.

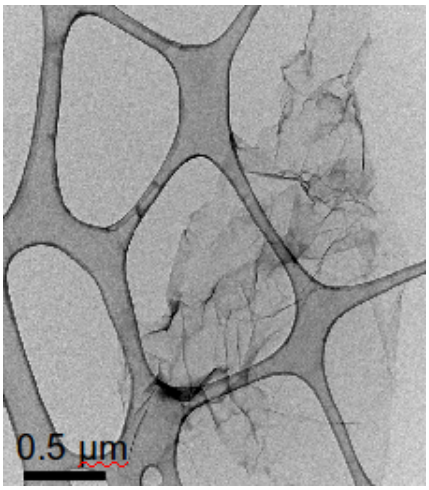

Figure 3.2: TEM image of a graphene flake on a standard TEM grid.

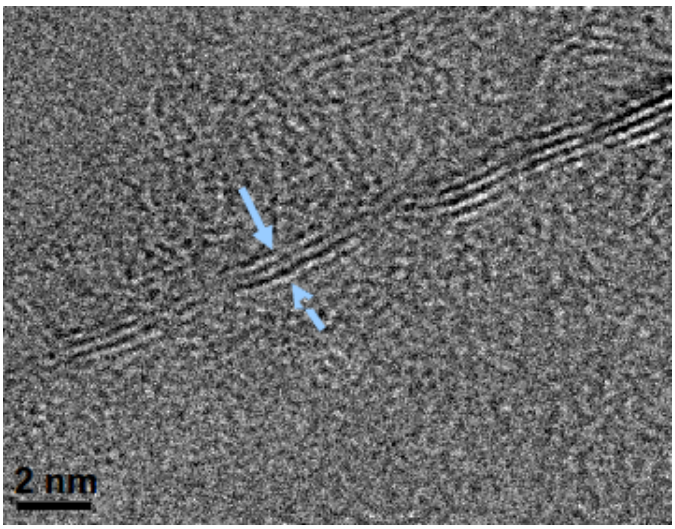

Figure 3.3: HRTEM image of the edges of a typical graphene flake showing ∼2-3 layers.

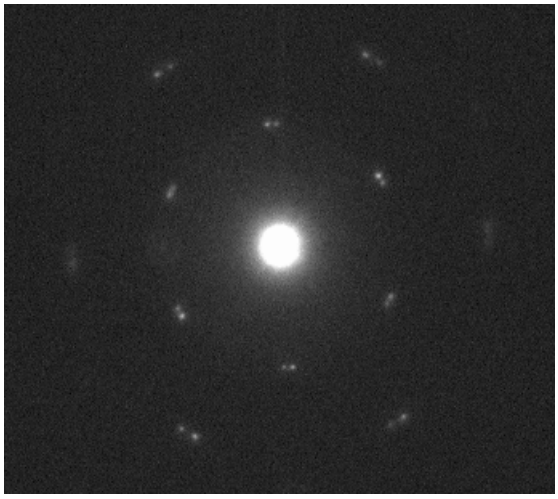

Figure 3.4: The measured electron diffraction pattern which is typical for few-layered graphene.

3.2.2 Deposition of the graphene

To create the sensor, the graphene created in the above section had to be dispersed onto the glass substrate and then an electrical connection to the graphene had to be established. The method used to create the graphene creates what can best be described as graphene powder, which is difficult to work with and nearly impossible to attach contacts to on a macro scale. To solve this problem, high-power ultrasonication was performed on the graphene sheets in deionized water. This transforms the graphene powder to a graphene solution that can be applied to the desired substrate and allowed to dry. To perform the sonification, 25 mg of graphene was mixed with 100 ml deionized water. An ultrasonic probe sonicator (Sonics Vibracell VC 750, Sonics and Materials Inc., USA) was inserted into the mixture for 1 hour at 40% power and a duty cycle of 10 seconds on, 5 seconds off. The mixture was then allowed to cool before depositing it onto the glass substrate.

Two deposition methods were explored. The first technique employed a drop coat method, where the suspension was dropped on the substrate by a dropper and allowed to dry in a fume hood. As the water evaporated, the graphene remained on the glass substrate. This process was repeated two or three times, because a single iteration did not produce an electrically conductive film.

In the second technique, the mixture was sprayed onto the glass substrate using a standard airbrush (Paasche Single-action Siphon Feed external mix airbrush). Very small amounts of the mixture were sprayed onto the substrate to stop the formation of large droplets that degraded the smoothness of the film. The airbrush was held approximately 30 cm from the substrate and

sprayed for about 1 second at an angle of roughly 70°. As small amounts of the mixture was sprayed at a time, the water evaporated within 15 minutes to leave a smooth graphene film. This process had to be repeated a number of times, as a few sprays did not produce an electrically conductive film. The additional sprays caused the graphene flakes to overlap and form the needed conductive path. Table 3.1 shows the relationship between the number of sprays and the measured sheet resistance. Figure 3.5 shows the 5 sensors that were used for this test. Note how the film clearly becomes darker with more sprays. From these results, it was decided to fabricate the sensors using 8 to 10 sprays, as it resulted in a sheet resistance between 50 kΩ to 150 kΩ.

Layers	Resistance
4	∞
6	> 1 MΩ
8	148 kΩ
10	45 kΩ
12	11 kΩ

Table 3.1: Number of sprays versus resistance.

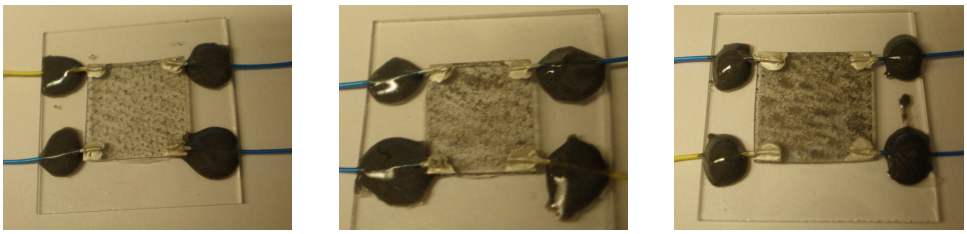

(a) 4 Sprays **(b)** 6 Sprays **(c)** 8 Sprays

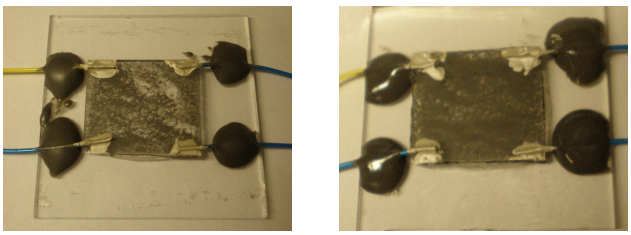

(d) 10 Sprays **(e)** 12 Sprays

Figure 3.5: Samples with different number of sprays.

Figure 3.6 shows the airbrush that was used with the graphene suspension in the reservoir. This technique produced much smoother films that covered the entire area of the substrate as opposed to the drop coat method. For this reason all of the sensors were constructed using the spray coat method.

Figure 3.6: The airbrush that was used to coat the glass substrates with graphene.

3.2.3 Establishing electrical connection to the film

After successfully preparing the graphene film, electrical contacts had to be connected. Four wires were connected to the corners of the film using silver paste. This configuration made it possible to use the van der Pauw method to determine the sheet resistance of the sample (see Section 3.4). During many of the initial tests the contacts broke off when only a small force was applied to the contact. This fragile nature of the sensor made measurements difficult and the contacts had to be connected in a way that ensured that only a minimal force was applied to the contacts at all times. To solve this problem, the substrate with graphene was glued onto an additional glass substrate. The wires were then glued onto this bigger substrate with high strength glue as this removed any force on the contacts when the sensor was handled. Figure 3.7 shows a schematic of this configuration of the sensor. Figure 3.5 shows images of sensors with this configuration.

For tests where the sensor had to be submerged within a liquid, the contacts were covered by a polyurethane coating known as m-coat. This had two advantages. Firstly, it isolated the contacts from the environment so that only the effect of the graphene was measured. Secondly, it further increased the bonding strength of the contact to the graphene's surface.

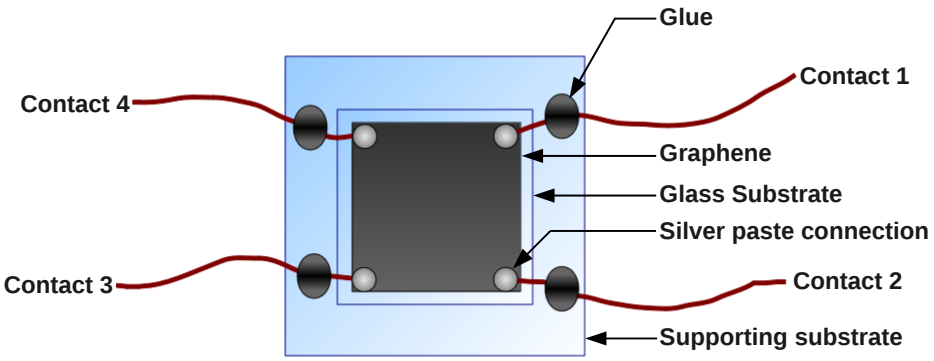

Figure 3.7: Top view of the graphene sensor.

Figures 3.8 to 3.11 shows scanning electron microscopy (SEM) images of the graphene film at various magnification levels after it was deposited on the glass substrate. The overlapping flakes are clearly visible in the images.

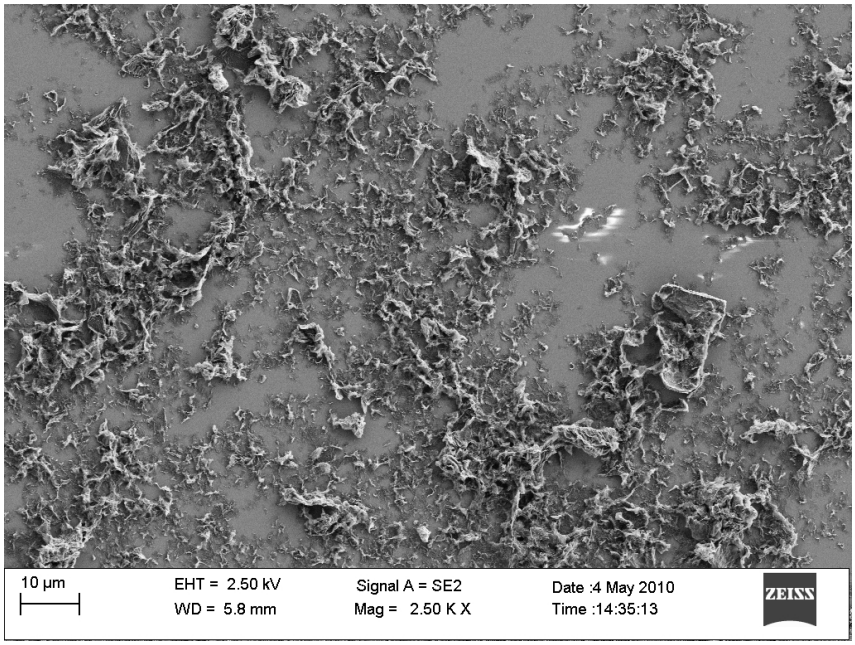

Figure 3.8: SEM image of the sensor's surface at a magnification of 2 500.

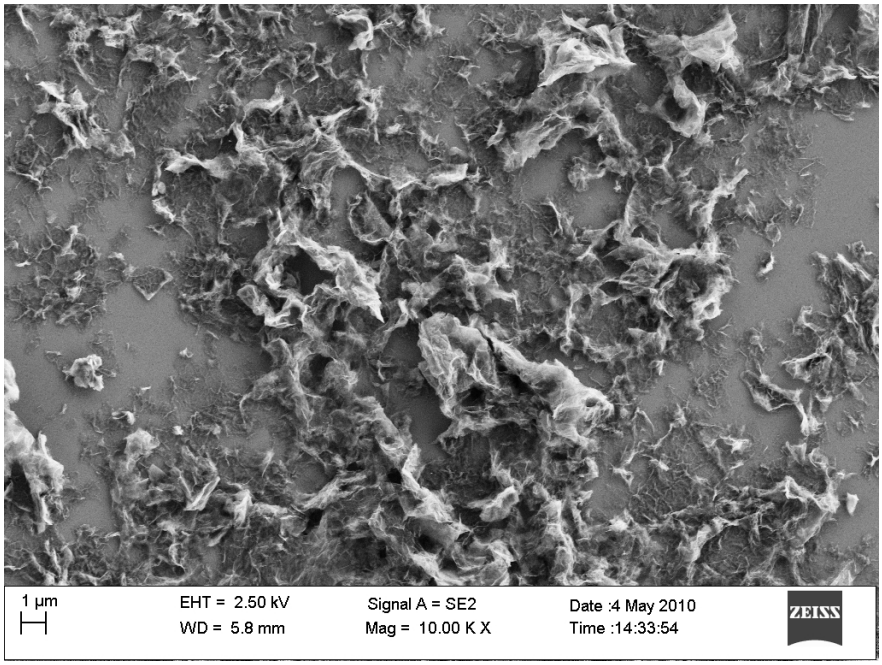

Figure 3.9: SEM image of the sensor's surface at a magnification of 10 000.

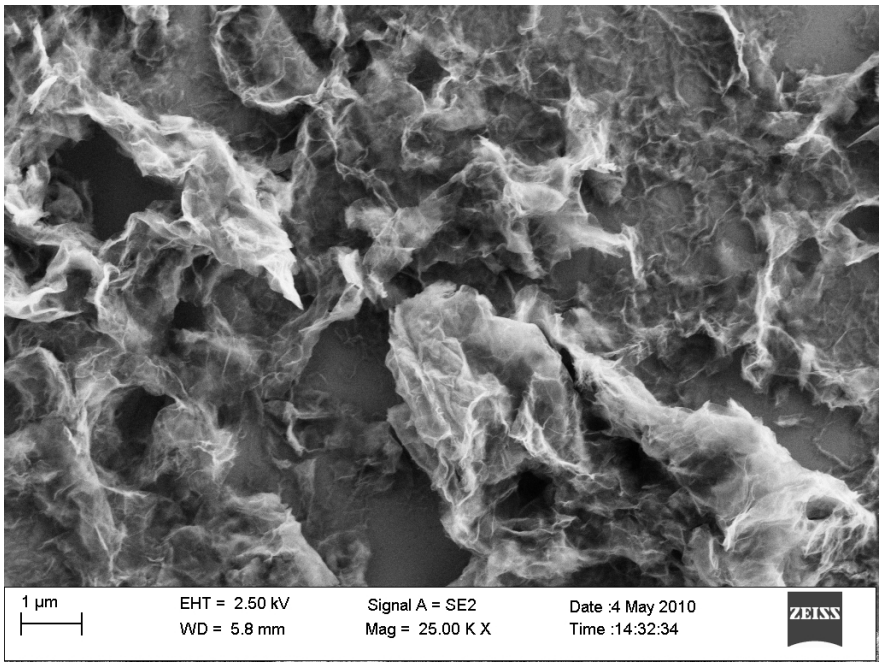

Figure 3.10: SEM image of the sensor's surface at a magnification of 25 000.

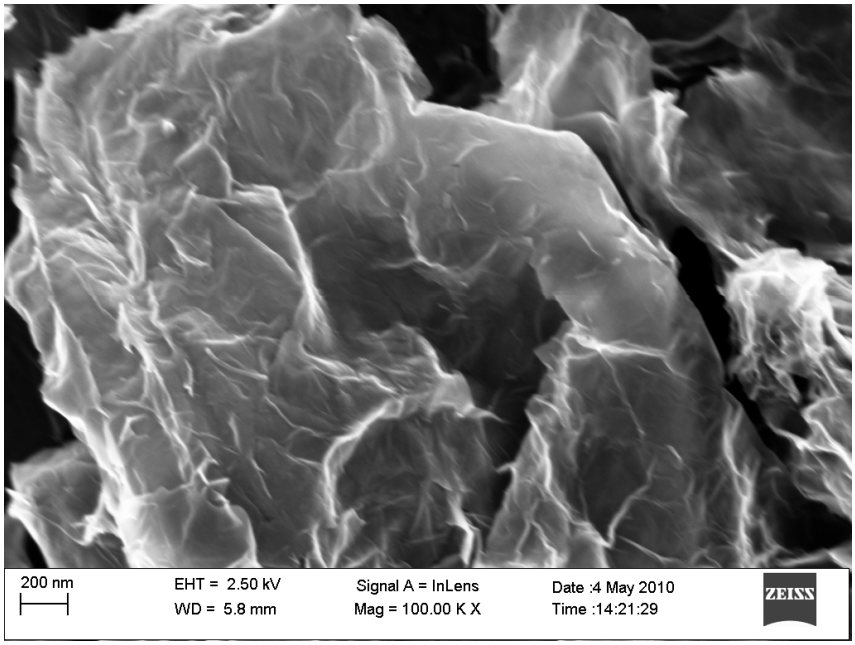

Figure 3.11: SEM image of the sensor's surface at a magnification of 100 000.

It is important to explain the method of electron transfer within the sensor as most of the tests are concerned with resistance changes in the sample. The graphene used is not a single mono-layer graphene sheet as explained in Chapter 2, but rather consists of thousands of graphene platelets that are randomly deposited on the glass substrate during the deposition process. These micro-sized graphene platelets overlap each other and form a resistance path from one end of the sensor to the other. Additionally, each platelet may consist of a few graphene sheets as shown in Figure 3.3. So, in order for an electron to travel from one end of the sample to the other, it must travel from platelet to platelet, but within each platelet it may also encounter some resistance. It is thus important to note that the resistance of the sample is a function of two phenomena, that is, the resistance from platelet to platelet (inter platelet) and the resistance within each platelet (intra platelet). Therefore, a change in resistance of the sensor must be attributed to either one of these effects, or both.

The focus of the research is the use of graphene as a sensor, but as graphene is used for many other applications, most of the results obtained can also be used to characterize graphene under these conditions. For instance, as graphene is likely to be used in various electronic applications, it is important to know how the graphene's resistance changes at different humidity levels.

3.3 Other sensors used

The majority of the experiments performed during this project were done using the graphene film sensor as explained in the previous section. In addition to performing the humidity tests on the graphene film sensor, humidity testing was also done on a SWCNT sensor and on a sensor that consisted of a single graphene sheet (see Chapter 4). This section will discuss the other sensors that were used.

3.3.1 Carbon nanotube sensor

The carbon nanotube (CNT) sensor was made in the exact same fashion as the graphene film sensor, except single-walled carbon nanotubes (SWCNT) were sonicated with the water instead of graphene. The mixture was sprayed on using the same airbrush and contacts were attached using the same process as described before. With the naked eye the sensors look identical. Figures 3.12 and 3.13 show SEM images of the CNT sensor at different magnification levels. The images clearly show the web of inter-tangled nanotubes on the surface of the substrate.

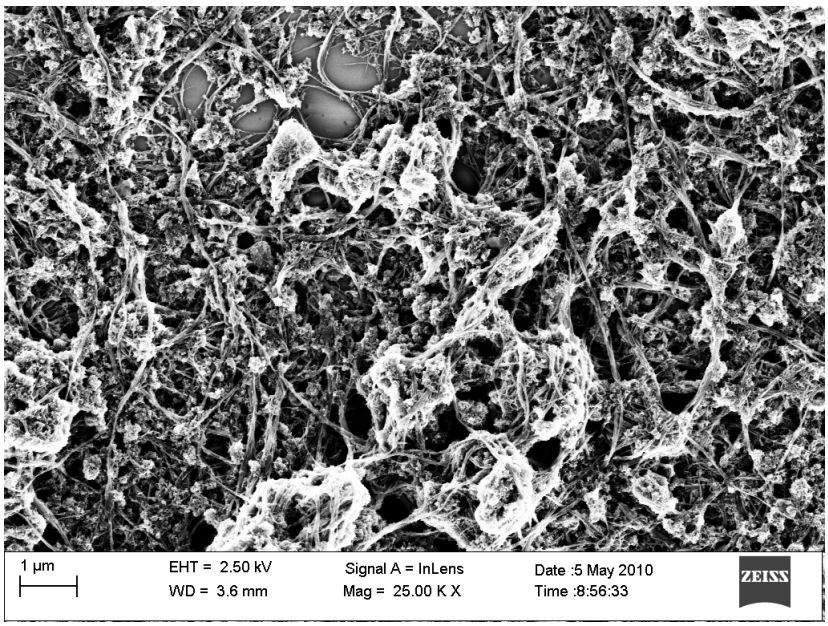

Figure 3.12: SEM image of the CNT sensor's surface at a magnification of 25 000.

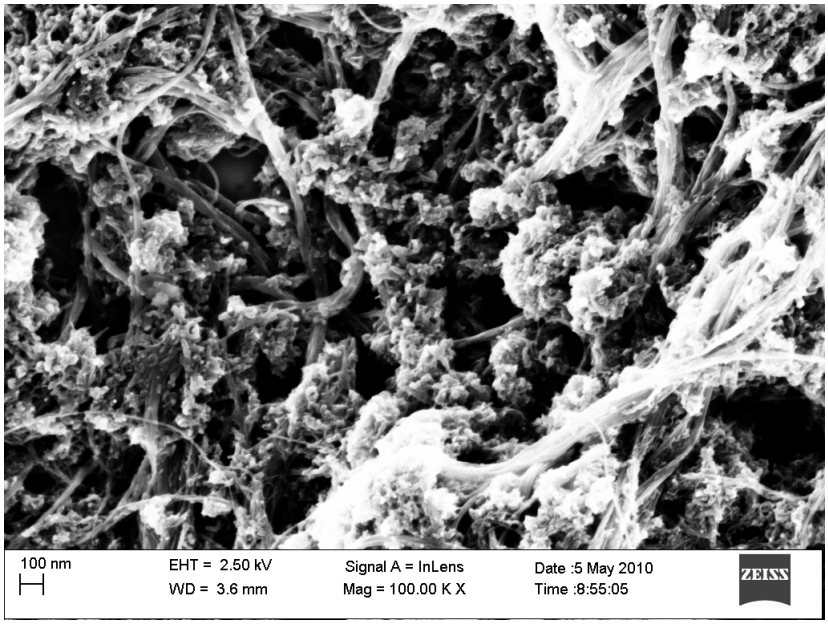

Figure 3.13: SEM image of the CNT sensor's surface at a magnification of 100 000.

3.3.2 Graphene sheet sensor

Another type of graphene sensor was used during the humidity testing: a single graphene sheet sensor. The graphene sheet sensor differs from the graphene film sensor in the fact that it consists only of a single sheet of graphene, but it still contains a few layers of graphene.

The single graphene sheet sample was fabricated by Professor M. Ajayan's group at Rice University, Houston, Texas, USA. The few-layered graphene was grown *in-situ* on a copper substrate using Chemical Vapour Deposition. It was transferred to a silicon substrate with a ∼300 nm thick insulation silicon dioxide layer, after which gold contacts were patterned on the graphene to establish electrical contact [82, 83]. The four contacts make it possible to use the van der Pauw configuration. The sample was then sent to Professor N. Koratkar's group at RPI. The sample was placed on a standard chip carrier where F. Yavari, also from Professor N. Koratkar's group, connected the wires from the sample to the chip carrier using silver epoxy (EJ-2189 two part kit from EPOXY Technology).

Figure 3.14 shows an optical image of the graphene sheet sensor. The graphene can clearly be seen as the blue areas around the contacts against the substrate which is purple. The gold contacts deposited on top of the sheet can also be seen in the image. The small gold pieces between the electrodes on the right is an imperfection of the deposition process. Careful examination

with a SEM confirmed that this did not form a short circuit between the two electrodes and therefore did not influence the sample.

A SEM image of the sample shown in Figure 3.15 indicates a ∼30 μm × 16 μm region of the graphene film that is enclosed within the electrode pattern. This area was characterized using atomic force microscopy (AFM) and the image is shown in Figure 3.16. The wrinkled topography of the graphene sheet is clearly visible and probably caused by the process used to transfer the graphene film from the copper to the silicon dioxide substrate during fabrication of the sample. AFM scans were also performed on the edge of the graphene sheet to determine the thickness of the sheet and is shown in Figure 3.17. The average thickness of the graphene sheet was determined to be ∼2.5 nm which suggests that the film is composed of ∼3–4 individual monolayers of graphene.

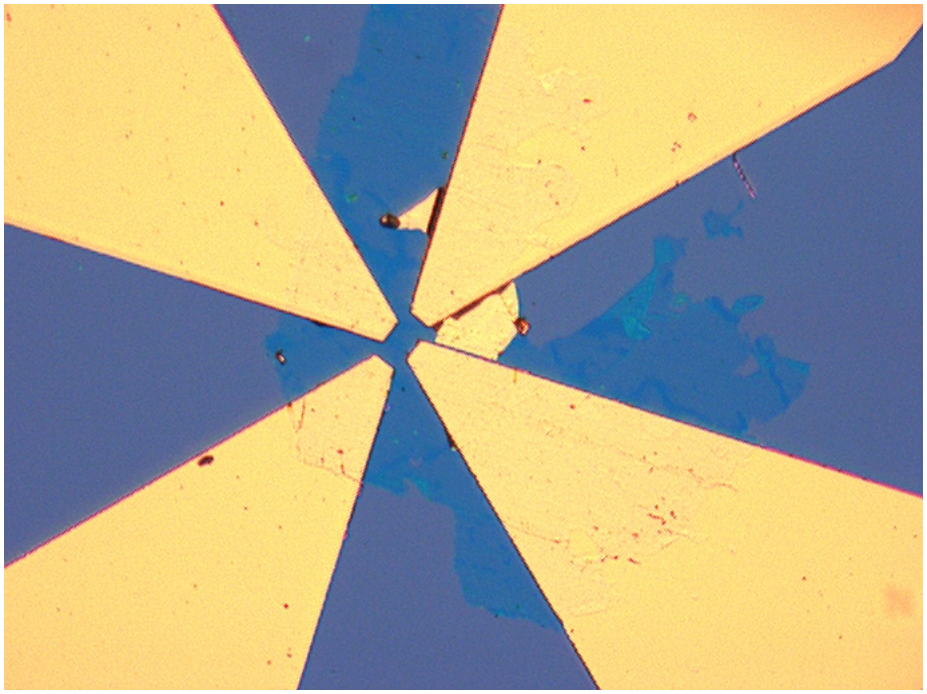

Figure 3.14: Optical image of the graphene sheet sensor.

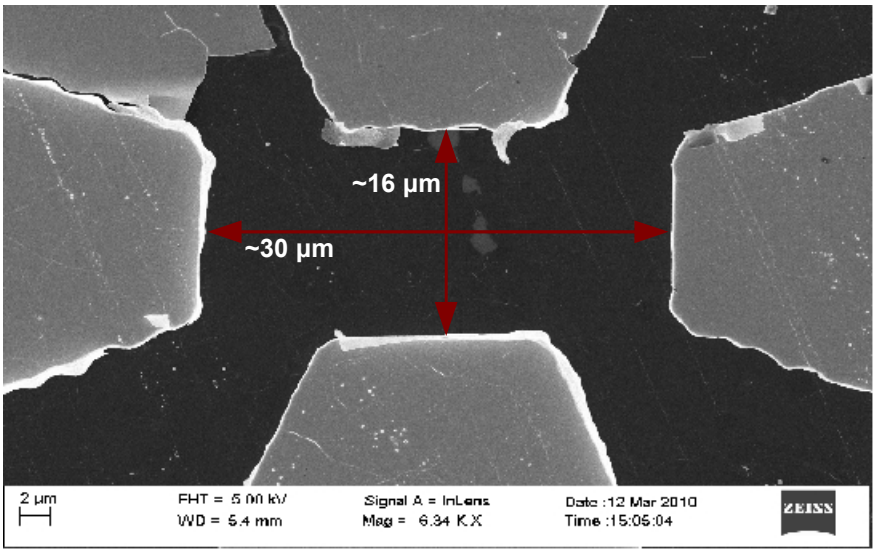

Figure 3.15: SEM image of the region of the graphene sheet that is enclosed within the electrode pattern.

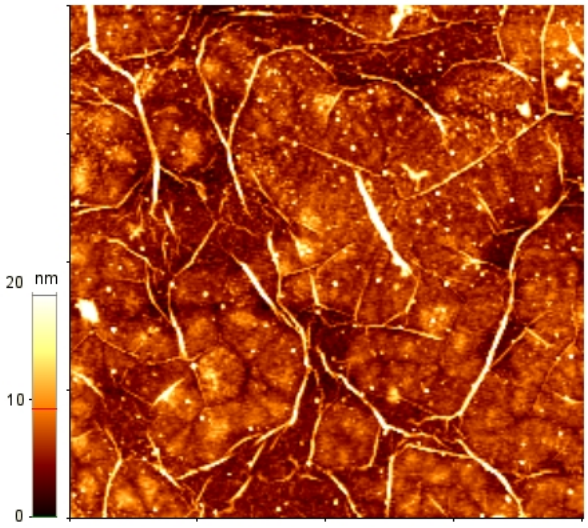

Figure 3.16: AFM image of the topography of the graphene sheet.

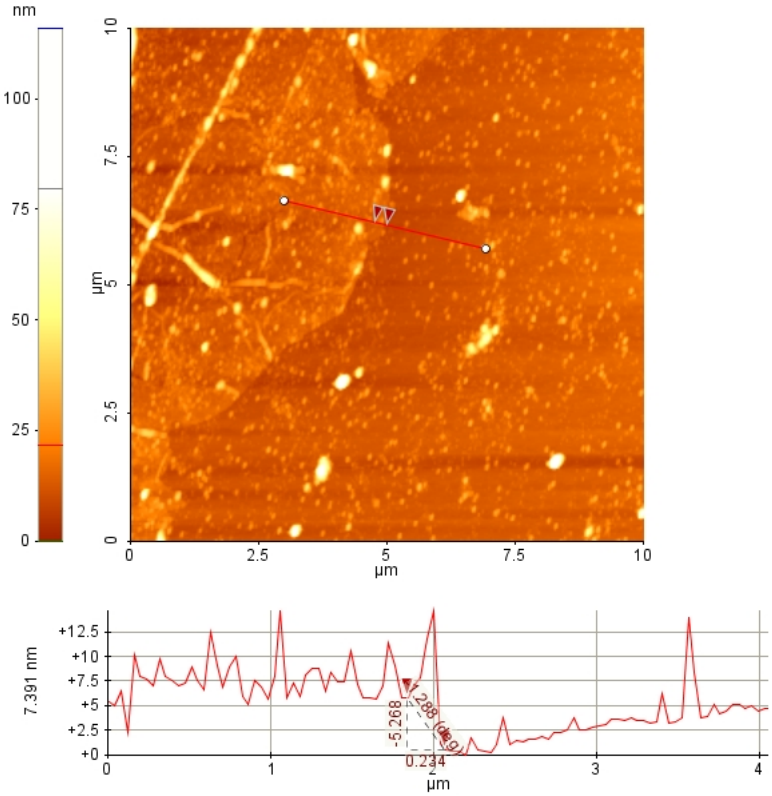

Figure 3.17: AFM image of the edge of the graphene sheet.

3.4 Sheet Resistance: The van der Pauw method

The van der Pauw method is a commonly used technique to measure the sheet resistance of a thin film. Leo J. van der Pauw invented the method in 1958 [84]. The van der Pauw method was used to determine the sheet resistance of all the samples used during this research.

There are two advantages of using the van der Pauw method over a traditional two point measurement. Firstly, the van der Pauw method eliminates contact resistance between the film and the contacts which results in more accurate measurements. This is especially true when the sheet resistance is very low. Secondly, as the four contacts are connected to the corners of the sample, the entire graphene sheet has an effect on the resistance. When only two points are used for the measurements, only the graphene between the contacts influence the resistance. Similarly, when the traditional four point probe method is used, the entire graphene film does not contribute to the measured resistance.

To determine the sheet resistance of the sample, van der Pauw showed that two resistance measurements need to be made, one resistance along a vertical

edge and another along a horizontal edge [84].

This can be achieved as follows: The contacts are connected to the corners of the sample and are numbered in an anti-clockwise direction starting at the top left corner. A current is applied between contacts one and two (I_{12}), which produces a voltage between contacts three and four (V_{34}). Using Ohm's law:

$$R_{12,34} = V_{34}/I_{12}. \tag{3.1}$$

This represents the vertical resistance of the sample and similarly a horizontal resistance, $R_{23,41}$, can be found. Using these two resistances, the actual sheet resistance can be found by using what is known as the van der Pauw formula [84]:

$$e^{-\pi R_{12,34}/R_S} + e^{-\pi R_{23,41}/R_S} = 1. \tag{3.2}$$

To make more accurate measurements, two vertical and two horizontal measurements can be made and averaging the results as shown in the following equations:

$$R_{Vertical} = (R_{12,34} + R_{34,12})/2, \tag{3.3}$$

$$R_{Horizontal} = (R_{23,41} + R_{41,23})/2. \tag{3.4}$$

Using the van der Pauw formula again (Equation 3.2) with the averaged resistance values, the equation looks as follows:

$$e^{-\pi R_{Vertical}/R_S} + e^{-\pi R_{Horizontal}/R_S} = 1. \tag{3.5}$$

Unfortunately there is no closed loop solution for this equation unless $R_{Vertical}$ and $R_{Horizontal}$ are equal, which is rarely the case. Iterative methods are usually used to determine R_S. C code was written to solve the problem and it is shown in Appendix A. Figure 3.18 shows a schematic of how the two resistance values are determined.

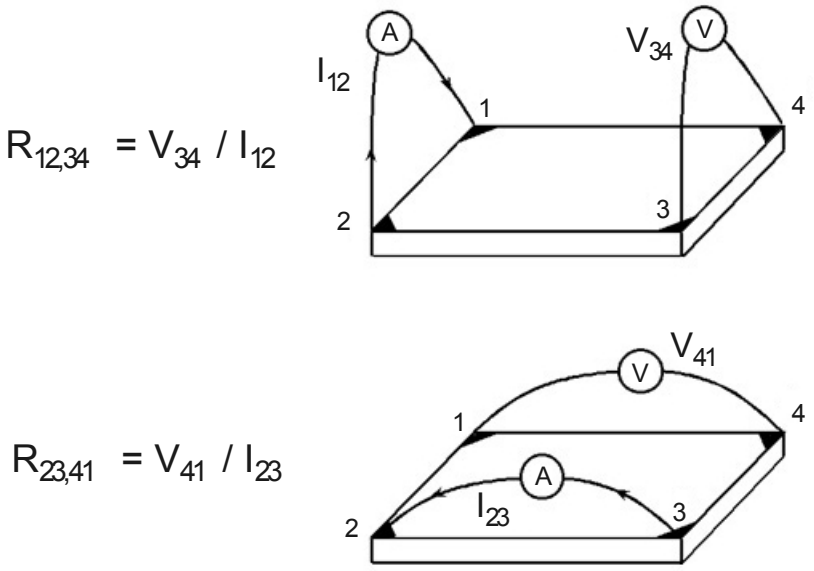

Figure 3.18: Schematic of the van der Pauw configuration.

For all of the resistance values reported in this research, each of the four resistivity measurements were taken at five different voltages, and then the average value of these five measurements were used. If any of the measured samples did not show ohmic behaviour, the test was discarded and repeated with a new sample. Therefore, all of the resistance values reported did show ohmic behaviour.

There are a few considerations that should be taken into account when using the van der Pauw Method. These considerations include: The sample must be symmetrical to minimize errors and there should not be any isolated holes in the sample. The contacts should be placed as close to the boundary as possible. The contacts should be as small as possible, as an error in the order of D/L is introduced into the system, where D is the average diameter of the contacts and L is the distance that the contacts are apart.

This chapter contains the main sensors that experiments were performed on. The following chapters contain the results of the experiments performed that set out to investigate the feasibility of using the sensors discussed here.

Chapter 4

Humidity and Temperature Sensing

This chapter discusses the results of experiments that were conducted to determine the effect of humidity and temperature on various carbon nanostructured sensors. The effect of humidity on the resistance of the graphene film, graphene sheet and CNT film sensor were investigated. The results of a temperature test that was performed on the graphene film sensor and the subsequent bandgap calculation is given. This bandgap experiment led to further testing where the bandgap of the graphene sheet sensor was calculated at various humidity levels.

4.1 Humidity

Moisture measurements are important as it is used in several areas such as weather prediction, heating, ventilating, and air conditioning (HVAC) systems, electronics, vehicles, airplanes and various other industrial processes [85].

It is an important parameter in HVAC systems as humans are very sensitive to changes in humidity. The body is cooled by sweating and as the humidity increases, the sweat evaporates much slower and it feels much warmer. At low levels of humidity, it feels colder as the sweat evaporates easily, cooling the body down much quicker. As humans perceive temperature as the rate of heat transfer from the body and not the actual temperature, days of high humidity feel much warmer and vice versa.

Another important reason for measuring humidity is the effect that it has on electronics. Most electronic devices work only in a certain range of relative humidity values and operating the device outside of these values may cause permanent damage. When used at high humidity values, condensation can form which could result in water droplets that may cause a short circuit. When the device is powered on before the droplets evaporates, high currents may

form that permanently damage the device. Low humidity levels favours the build up of static electricity that can form spontaneous electrical discharges of high potentials that can permanently damage the device, even when it is not powered on.

Humidity refers to the amount of water vapour in the atmosphere (or any other carrier gas) and there are different ways in which humidity can be expressed, such as specific humidity or absolute humidity. When working with HVAC applications and process control, the method most commonly used to express moisture levels is relative humidity [86]. Relative humidity is defined as the ratio between the actual vapour density and the saturation vapour density and is usually expressed as a percentage [87]. The saturation vapour density is the point where the water vapour in the air condenses and it forms either dew, clouds or fog [88]. During the bandgap calculation, the absolute humidity level was used, which refers to the weight of water vapour in every kilogram of air.

4.1.1 Experimental

The humidity chamber that was used has two temperature controllers (Chromalox 1600), one to control the dry bulb temperature and another to control the wet bulb temperature. The relative humidity level can then be calculated from the two temperatures using a psychrometric chart. Figure 4.1 shows a picture of the humidity chamber.

Figure 4.1: The humidity chamber used in all the humidity related experiments.

The experiments were conducted using the following methodology: The humidity level in the environmental chamber was set to the desired level with the sensor inside. After the chamber reached the set humidity level, 15 minutes were waited to allow the sensor to reach its steady state value. The resistance was then measured using the van der Pauw method as explained in Section 3.4.

Graphene film sensor

The first humidity test was performed on the graphene film sensor (Section 3.2). The test was done at two temperatures, 100 °F (37.8 °C) and 110 °F (43.3 °C). Each test was also done twice to determine the repeatability of the

sensor. Figure 4.2 shows the result of the experiments. From the graph it is clear that the resistance of the sample increases with an increase in humidity. The test was repeated several times with different samples and in all cases the resistance increased with an increase in the relative humidity level. The trend lines added indicate that this increase is relatively linear. From the graph it is evident that the sensor shows signs of hysteresis. The cause of the hysteresis is discussed later in this chapter when the mechanism behind the increase in resistance is explained.

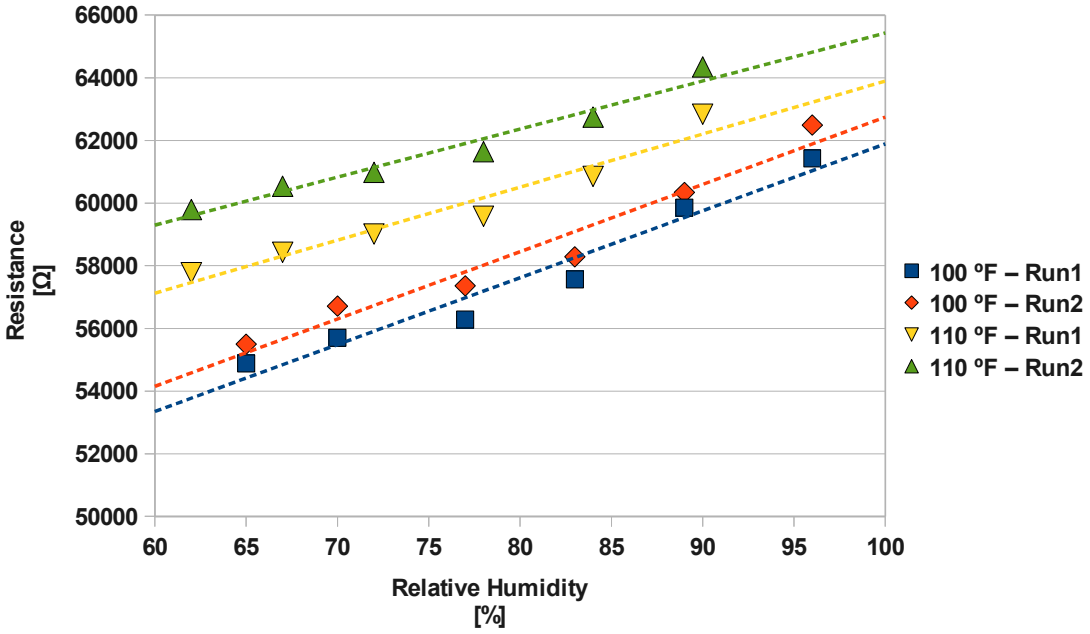

Figure 4.2: Graphene film sample's resistance value at various relative humidity levels.

SWCNT film sensor

To test whether this increase in resistance with an increase in humidity is observed in other carbon materials, the test was repeated using a single-walled carbon nanotube (CNT) sensor. The fabrication process of this sensor is explained in Section 3.3.1. The exact same test was performed on the CNT film sensor as on the graphene film sensor, but each test was done once. Figure 4.3 shows the result of the experiment, and the CNT film sample clearly did not respond to the change in humidity as the graphene film sensor did. At 110 °F there was a slight increase in the resistance of the sample, while at 100 °F, the trend was decreasing. The results of this test prove that the humidity sensing capability of graphene is unique to graphene and not all carbon based materials.

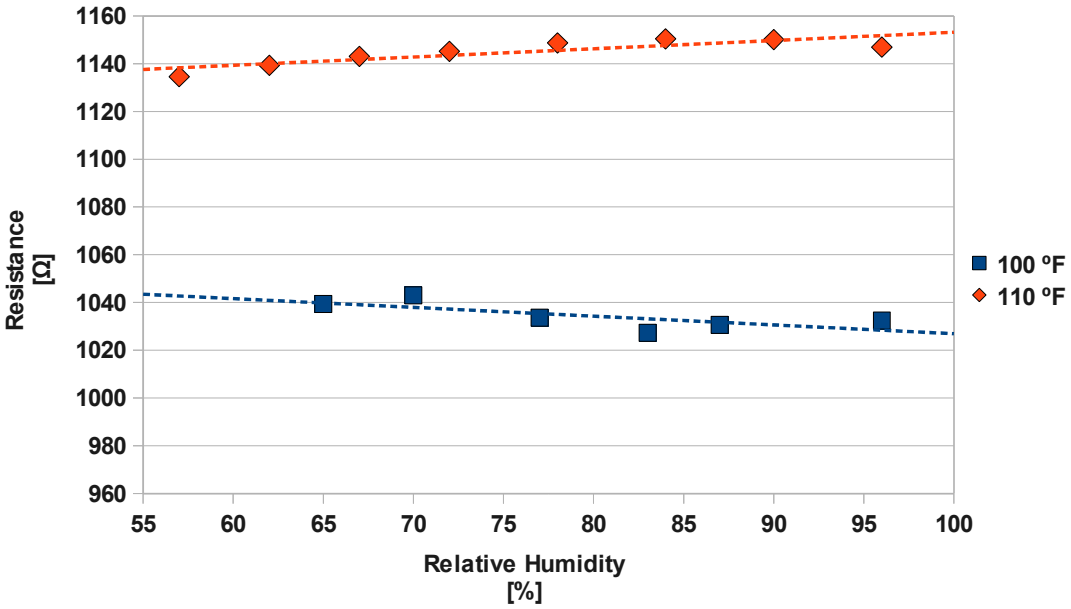

Figure 4.3: The SWCNT film sample's resistance value at various relative humidity levels.

As explained in Chapter 3, the resistance of the sample is a function of two phenomena, that is, the resistance from platelet to platelet (inter platelet) and the resistance within each platelet (intra platelet). To determine whether the total increase in resistance is caused by the inter- or intra platelet resistance increase, a third test was done. For this test, the graphene sheet sensor was used. As explained in Section 3.3.2, the graphene sheet sensor consists of a few layers of graphene, which means that there is no inter platelet resistance, only intra platelet resistance. The response of the graphene sheet sample should thus give insight into the cause of the resistance change.

Graphene sheet sensor

The test was repeated on the graphene sheet sample at 100 °F. Figure 4.4 shows the results of the experiments. Similar to the graphene film sensor, the graphene sheet sensor's resistance increases with a increase in humidity. The results of this experiment prove that the resistance change of graphene due to humidity is predominantly caused by a change in resistance on an intra platelet level.

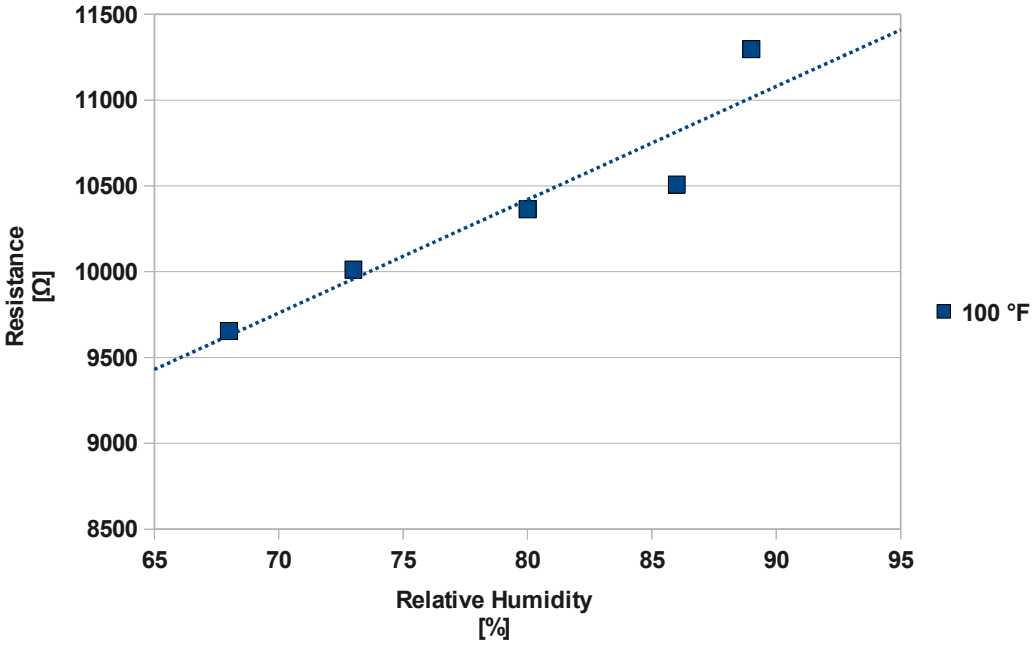

Figure 4.4: The graphene sheet sample's resistance value at various relative humidity levels.

The cause for this increase in resistance was investigated. Buchsteiner and co-workers showed that the intra platelet spacing of graphene oxide layers increases with an increase in humidity [89]. They used X-ray scattering to measure the layer distance and found that it varies reversibly from 0.6 to 1.2 nm depending on the relative humidity. Park and co-workers used this principle to fabricate a device that uses this phenomenon and changes shape according to the current humidity level [90]. They created bi-layer paper, with one layer consisting of multiwalled carbon nanotubes and the other layer consisting of graphene oxide. When the paper was exposed to low levels of humidity (∼12%), the paper curled with the MWCNT facing outwards, around 60% relative humidity the paper was flat and at higher values the paper curled with the MWCNT facing inward. They also performed tests where they heated graphene oxide paper and MWCNT paper to 100 °C and recorded weight loss as a result of water evaporation. The graphene paper had a 17% loss in weight while the weight of the MWCNT paper remained unchanged. This is a clear indication that the graphene absorbs water vapour and the CNTs do not.

The graphene used during these tests has a similar structure as the graphene oxide layers used by Buchsteiner and co-workers, as it consists of a few layers. The graphene therefore swells and shrinks in relation to the relative humidity level. It is believed that this swelling and shrinking is the cause of the resistance change observed at various humidity levels. As a result,

the change in resistance is directly influenced by the amount of water vapour absorbed by the graphene.

4.2 Wetting experiments

Wetting experiments were subsequently done on the graphene and carbon nanotube sensor to further prove the operating principles of the sensor. Static contact angle measurements between a drop of deionized water and both sensors' surfaces were made using RameHart M500 digital goniometer equipped with a dispensing needle (VICI Precision Sampling Co., CA, USA). A 1 μL water droplet was formed on the tip of the needle using the automatic dispenser of the goniometer. The sample's surface was then brought closer to the needle's tip until it touched. Once it touched the drop spontaneously detached itself from the needle's tip and moved to the sample's surface. The axisymmetric-drop-shape analysis profile (ADSA-P) method was then used for estimating the contact angle of the drop on the sample's surface. For each sensor the measurement was repeated four times to find an average value of the contact angle. The results are shown in Figures 4.5 and 4.6.

The results supported the humidity sensing results. Graphene showed hydrophilic behaviour with an average contact angle of 58.6°, while the CNT showed hydrophobic behaviour with an average contact angle of 138.1°. This means the graphene is more likely to absorb the water vapour than the CNTs. These results together with the results of Buchsteiner and co-workers [89] show the mechanism responsible for the increased resistance must be due to absorption of water vapour by the graphene.

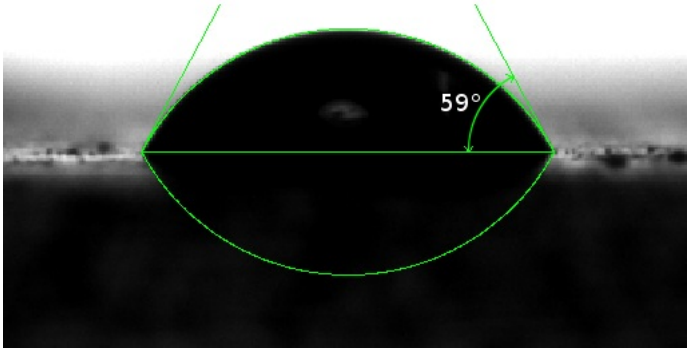

Figure 4.5: 1 μL drop on the graphene sensor's surface. Note the hydrophilic behaviour.

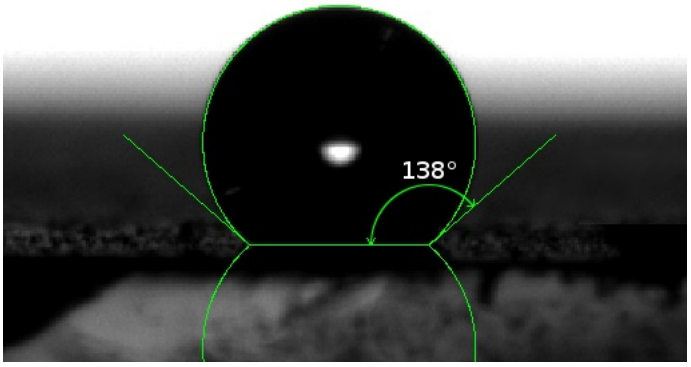

Figure 4.6: 1 μL drop on the SWCNT sensor's surface. Note the hydrophobic behaviour.

As stated earlier, the sensor did display some hysteresis effects. The initial resistance of the first test done at 100 °F was 54.9 kΩ, but when the test was repeated, the initial resistance increased to 55.5 kΩ. This is caused by water vapour that is absorbed by the graphene is not released immediately when exposed to lower levels of humidity. The response time of the sensor is consequently not very high, and when the measurements are taken in quick succession it appears as if the sensor exhibits hysteresis. This can be solved by gently heating the sensor before a measurement is taken to speed up the desorption of water in the graphene.

4.3 Temperature

Temperature tests were also performed on the sample to determine how the graphene film sensor's resistance changed as a function of temperature. There are currently various methods available to measure temperature and it is doubtful that graphene will have an advantage for temperature sensing applications. Therefore, the temperature tests were primarily undertaken to determine the effect that temperature would have on the sensor's resistance when used in other applications such as humidity and gas sensing.

The first test was done in vacuum with the pressure $< 10^{-5}$ mbar. Figure 4.7 shows the change in resistance versus temperature. The linear trend line clearly shows the resistances decreases linearly with an increase in temperature. From the trend line it was calculated that the sensor has a negative temperature coefficient equal to -0.0041 K^{-1}, which is 8 times more than carbon.

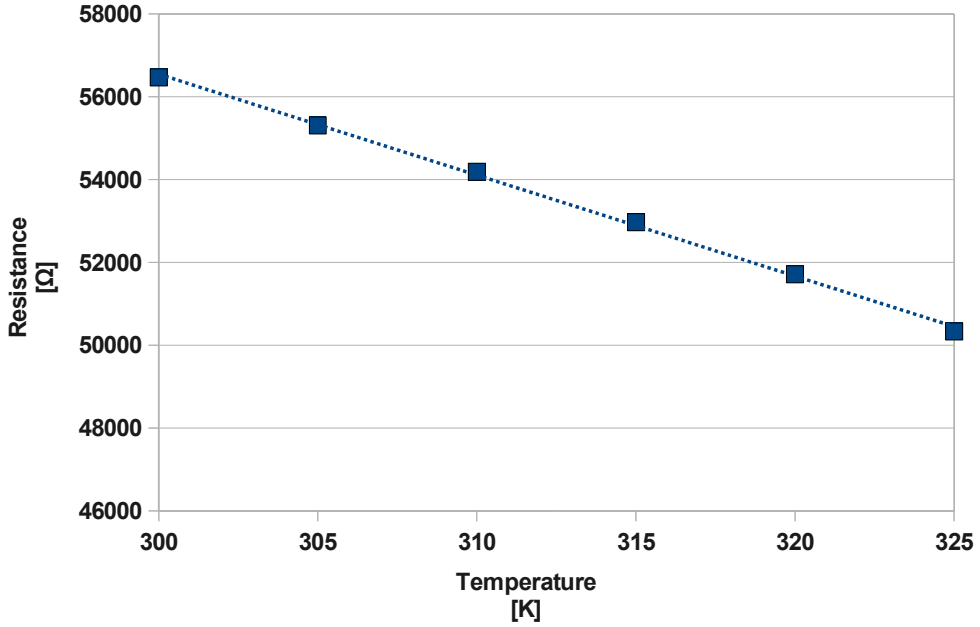

Figure 4.7: The temperature response of the sensor under vacuum (pressure $< 10^{-5}$ mbar). The resistance of the sample decreased in a linear fashion as the temperature increased.

The decrease in resistance with an increase in temperature means that the graphene contains a certain bandgap. The next section will elaborate on this and explain how the bandgap was calculated.

4.4 Bandgap

Electrons in atoms have different energy states or bands that they can exist in. When looking at the electrical properties of materials, the two most important energy states that exist in materials are the conduction band and valence band. The valance band contains an atom's highest energy electrons in their ground state and in this band each electron is bound to a specific atom. The conduction band is the next higher energy band above the valence band. Importantly, in this band, electrons are not bound to a specific atom and can move freely in the material. These electrons are the charge carriers that are responsible for electrical conduction in solids. The difference between these two bands is called the energy gap or bandgap [67].

In metals these bands overlap, causing metals to be excellent conductors of electricity. In semiconductors and insulators there is a gap between these bands and the electrons require a certain amount of energy to move from the valence band to the conduction band. In semiconductors the bandgap is much smaller than in insulators and usually in the order of 1 eV. A relatively small

applied potential can excite electrons into the conduction band resulting in a moderate current [67].

When dealing with metals, an increase in temperature increases phonon vibrations, which in turn, scatters free electrons, and decrease their mobility. Therefore, the conductivity of a metal decreases with increasing temperature. On the other hand, when dealing with semiconductors, an increase in temperature increases the energy of the electrons and more electrons move from the valence band to the conduction band. This effect is much more significant than the decrease in their mobility due to phonon vibrations and as a result, the conductivity of a semiconductor increases with increasing temperature.

The graphene therefore displays semiconductive behaviour as the resistance decreases with an increase in temperature. As this is a thermally activated process, the conductivity can be related to temperature by an Arrhenius relationship, using the following equation [91], [92]:

$$\sigma = \sigma_0 exp(-\frac{Eg}{2kT}), \tag{4.1}$$

where σ is the conductivity, Eg the energy bandgap of the material, k is the Boltzmanns constant and the T is the temperature.

An Arrhenius plot can be constructed to determine the bandgap of the graphene film. It is constructed by plotting the logarithm of film conductivity ($ln(\sigma)$) versus the inverse of temperature. If the points form a linear distribution, a linear trend line is then constructed from the points which is used to calculate the bandgap. The y-axis intercept of the trend line equals $ln(\sigma_0)$ and the gradient equals $-\frac{Eg}{2kT}$.

To find the value of σ, the equation used to calculate the resistivity of a material must be used and rearranged. The resistance of a material can be calculated with the equation:

$$R = \rho\frac{L}{A}, \tag{4.2}$$

where ρ is the resistivity of the material, L is the length and A is the area. This can be expanded and rearranged to show that

$$R = \rho\frac{L}{Wt} = \frac{\rho}{t}\frac{L}{W} = R_S\frac{L}{W}, \tag{4.3}$$

where R_S is the sheet resistance, W is the width and t is the thickness. As the sensor is a square, $L = W$. The equation can be written as follow:

$$R = R_S = \frac{\rho}{t}. \tag{4.4}$$

Furthermore, $\sigma = \frac{1}{\rho}$ and by using the above mentioned equations, it is clear that,

$$\sigma = \frac{1}{R.t}. \tag{4.5}$$

The average thickness was measured to be approximately 15 μm. With the data from the temperature measurements and these equations, the Arrhenius plot could be constructed and is shown in Figure 4.8.

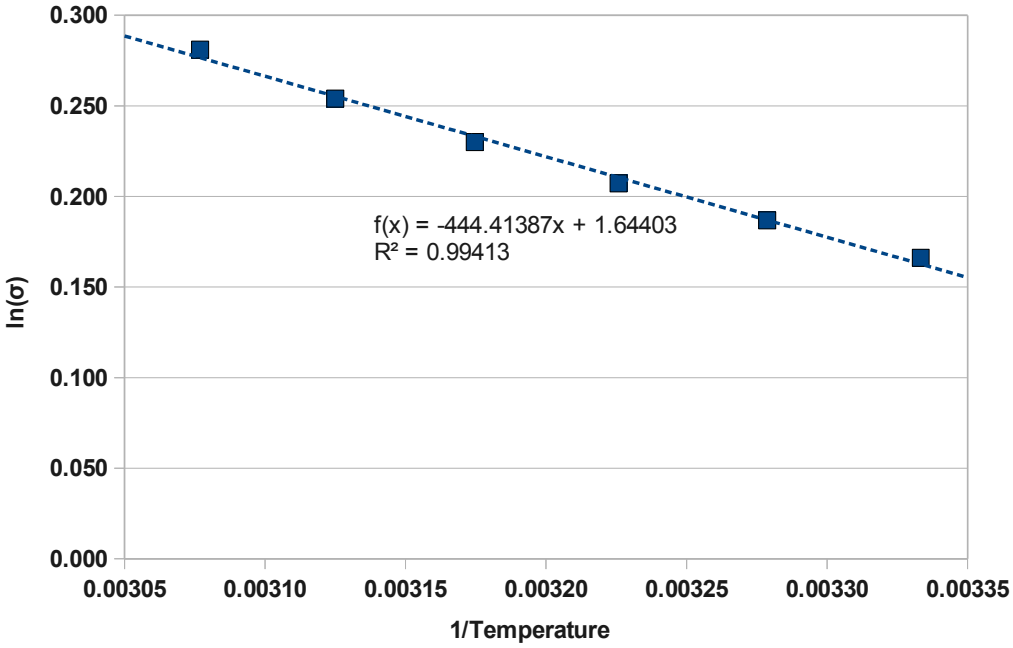

Figure 4.8: Arrhenius conductivity relationship of the graphene film sensor.

Using the above mentioned method, the bandgap in the graphene film sensor was calculated to be 0.08 eV over the tested temperature range. As this test was done under vacuum, the humidity level was zero. The subsequent step was to calculate the bandgap at various humidity levels, while keeping the temperature constant. Unfortunately, due to timing constraints, the work had to be completed by F. Yavari who is also a student in Prof N. Koratkar's group. The tests were performed using the graphene sheet sensor as explained in Section 3.3.2. The results of the tests provided some very interesting results. Figure 4.9 shows the results of the measurements with a logarithmic trend line added.

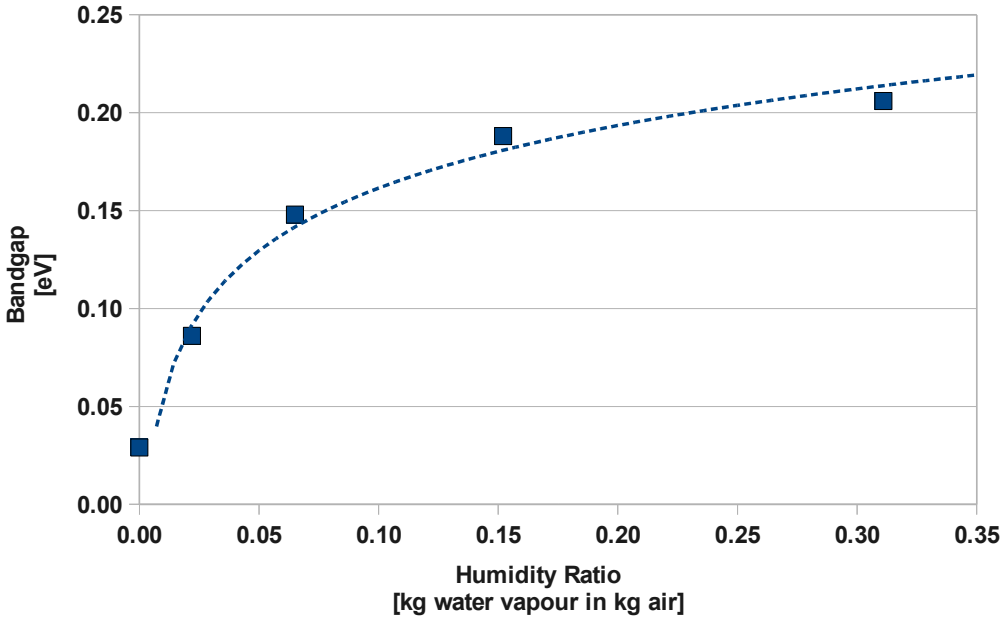

Figure 4.9: The bandgap (Eg) is plotted as a function of the absolute humidity. The bandgap increases sharply with humidity and then saturates at a level of ∼0.21 eV for a humidity level of ∼0.31 kg/kg.

The graph clearly shows that it is possible to vary the bandgap of graphene by exposing it to different humidity levels. By varying the humidity between 0 and 0.3 kg/kg (i.e. 0.3 kg of water in 1 kg of air), the bandgap varied between 0.03 eV to 0.21 eV and the effect was reversible. The small non-zero bandgap at zero humidity is probably an artifact of impurity scattering. It is this change in bandgap that caused the resistance of the graphene film to change at the different humidity levels.

Perfect graphene is a semi-metal and has no bandgap. This lack of bandgap is a major hindrance for graphene's application in semiconductor devices. There has been other methods proposed to introduce this bandgap such as through defect generation [93], doping [94] (e.g. with potassium), applied bias [95] and interaction with gases [96] (e.g. nitrogen dioxide).

The results presented here showed that it is possible to tune the bandgap in graphene based on water adsorption to the graphene surface. This technique is much simpler than other proposed methods as it does not involve any modifications to the graphene sheet or complex configuration of the layers.

Berashevich and co-workers studied the effect of water molecules absorbed on nanoscale graphene sheets. They found that the water molecules act as defects that break the sublattice and molecular symmetries of graphene and this results in the opening of a bandgap [97].

A paper containing the results has been accepted in the nanoscience journal, *Small*. The paper is entitled *Tunable Bandgap in Graphene by the*

Controlled Adsorption of Water Molecules by F. Yavari, P. C. Kritzinger, C. Gaire, L. Song, H. Gulapalli, T. Borca-Tasciuc, P. M. Ajayan and N. Koratkar [16].

4.5 Conclusion

The results of the humidity experiments showed that graphene has the potential to be used as a humidity sensor. The response was repeatable, but did suffer some hysteresis effects. Further investigation found that the mechanism behind the change is based on absorption of water molecules by the graphene film. Currently available commercial humidity sensors such as the Honeywell HIH-4000 Series Humidity Sensor also relies on absorption based sensing. Water vapour is absorbed by a sensing capacitor's active dielectric layer, causing the capacitance to change according to the amount of water vapour that is absorbed. The output of all absorption based humidity sensors are affected by both temperature and relative humidity [98]. As the primary investigation into graphene as active material for humidity sensing, these findings are the first steps to develop a fully working graphene based humidity sensor.

The temperature and subsequent bandgap calculations led to the discovery that the bandgap in graphene can be tuned simply by exposing the graphene to a certain humidity level. This result is even more significant than the humidity sensor application result as this ability to vary the bandgap may enable the use of graphene in nanoelectronics.

Chapter 5

Gas Sensing and Pressure Sensing

This chapter first discusses the results of experiments that measured the effect of gas pressure on the resistance of the sensor. Secondly, the results of experiments that investigated whether the graphene's resistance changed with exposure to various concentrations of pure carbon dioxide (CO_2) and also mixtures of CO_2 and air, are given. Finally, experiments were performed to investigate whether the detection sensitivity can be improved by using the graphene in conjunction with a surface acoustic wave device.

The focus of the gas sensing experiments was on the detection of CO_2. CO_2 is the largest volume of man made greenhouse gas in the atmosphere and is involved in various industrial processes [99]. There are therefore various application areas where CO_2 gas sensors can be used, especially environmental monitoring situations.

A gas chamber that was custom built for gas testing was used for all of the gas experiments. The chamber was fitted with a vacuum and turbo pump (Pfeiffer Vacuum) that can reduce the pressure in the chamber down to 10^{-6} Torr (1.3×10^{-6} mbar). It was also fitted with five pressure sensors connected to a vacuum measurement and control unit (Pfeiffer Vacuum MaxiGauge TPG 256 A). Four of the pressure sensors were ceramic capacitance gauges (Pfeiffer Vacuum CMR 261 to CMR 264) and together they had a detection range of 1 bar to 10^{-4} bar. The fifth sensor was an ion gauge sensor that was used to measure lower pressures. The chamber featured four gas connections and every connection was equipped with a needle valve. This made it possible to introduce four different gases, each with a precise flow rate, into the chamber. Using the vacuum pump and pressure sensors together with the needle valves, the amount of each gas in the chamber could be controlled very accurately. The chamber also had four electrical connectors which made using the van der Pauw method possible. Figure 5.1 shows a picture of the chamber.

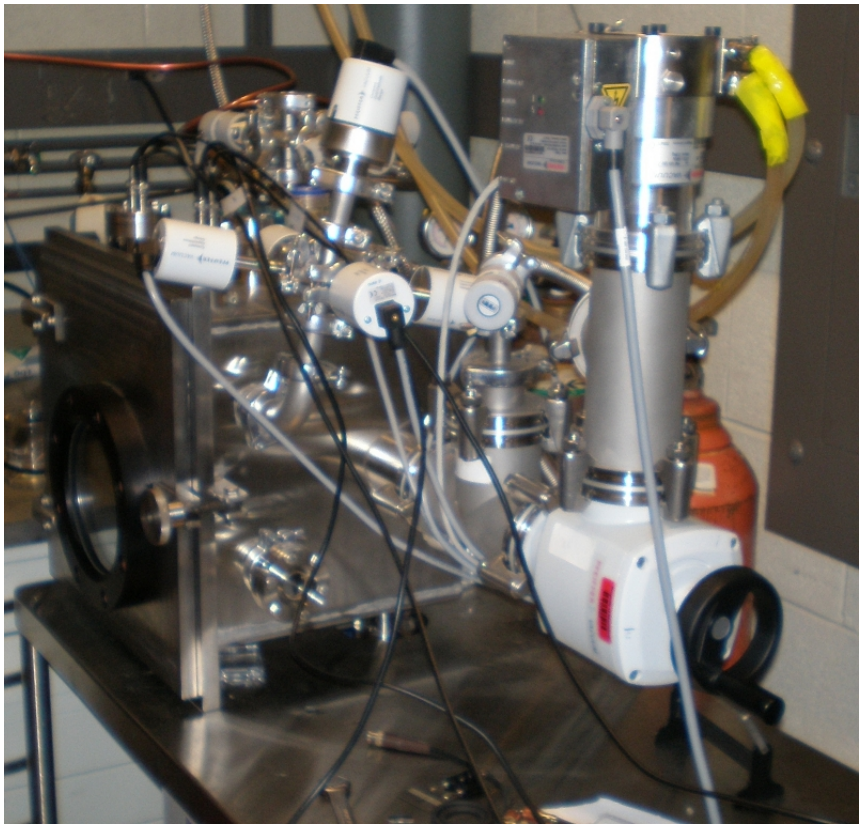

Figure 5.1: The chamber used during gas tests.

5.1 Resistivity measurements

Resistivity measurements were performed on the sample in a similar fashion to the humidity testing. The testing methodology was fairly straightforward: The sensor was exposed to a certain gas at a certain pressure and the resistance was measured using the van der Pauw method.

5.1.1 Results

The results of three resistivity measurements performed are discussed in this section.

Resistance change caused by pressure

The first experiment performed was used to determine whether the graphene's resistance changes with a change in air pressure. The test was performed, because when gas tests are performed and a change in resistance is observed, it is important to know that this change is caused by the gas and not by

the change in pressure. The tests were also done to investigate whether the graphene can be used as a pressure sensor.

The pressure in the chamber was decreased in logarithmic intervals. When the required pressure level was reached, the pump was switched off and resistivity measurements were taken. After the last pressure level was reached and the resistance measured, the pressure was increased back to atmospheric pressure by stopping the pump and opening a needle valve that caused air to flow back into the chamber. This process was repeated three times.

After the third time the pressure was decreased to the lowest measured value (0.02 Torr), the pressure was increased with argon instead of air as opposed to the other tests. As the pressure increased due to the argon flowing into the chamber, the resistance of the sample was measured at the same pressures as the air measurements. This determined whether it was a change in pressure or some other mechanism that caused the change in resistance. Argon was used because it is a noble gas and known to react with very few substances. Figure 5.2 shows the results of the measurements.

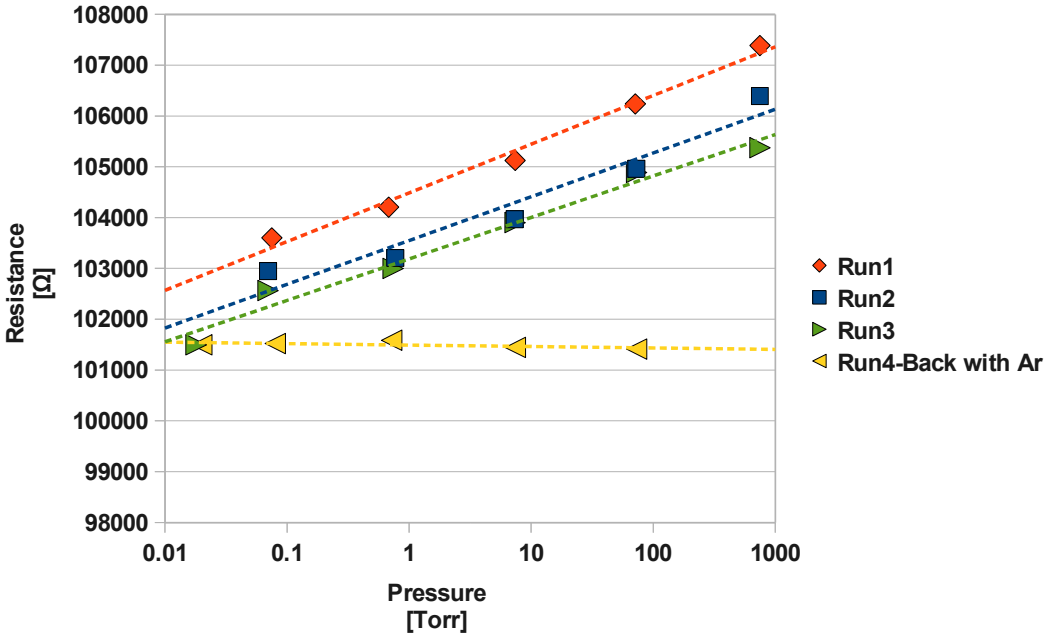

Figure 5.2: The resistance of the graphene film sample at various pressures.

During the first three runs of the test, the resistance decreased logarithmically. However, when the pressure was increased using argon, the resistance of the sample stayed fairly constant. This proved that the change in resistance was not caused by a change in pressure. A humidity and temperature sensor was then placed in the chamber to determine how these variables changed when the pressure was decreased. When the pressure was decreased from

atmospheric pressure to 1 Torr, the temperature only decreased by 1 °C, but the humidity halved from 46% relative humidity down to 23% relative humidity. The change in resistance was therefore attributed to the change in humidity as seen in Chapter 4. The resistance of the graphene sheet is therefore largely unaffected by a change in pressure.

Resistance change caused by CO_2 and Ar

In the second experiment, the change in resistance caused by exposure of the graphene to CO_2 and argon was determined. For the CO_2 measurements, the pressure in the chamber was decreased to just under 0.1 Torr. The chamber was then flushed a couple of times with CO_2 to ensure no other gas was in the chamber. The pressure was set to 0.08 Torr and the measurements were started. The CO_2 pressure was increased logarithmically and at each interval the resistance value of the sample was taken. The exact same process was followed to measure the effect of argon on the sample's resistance. Figure 5.3 shows the results of the measurements.

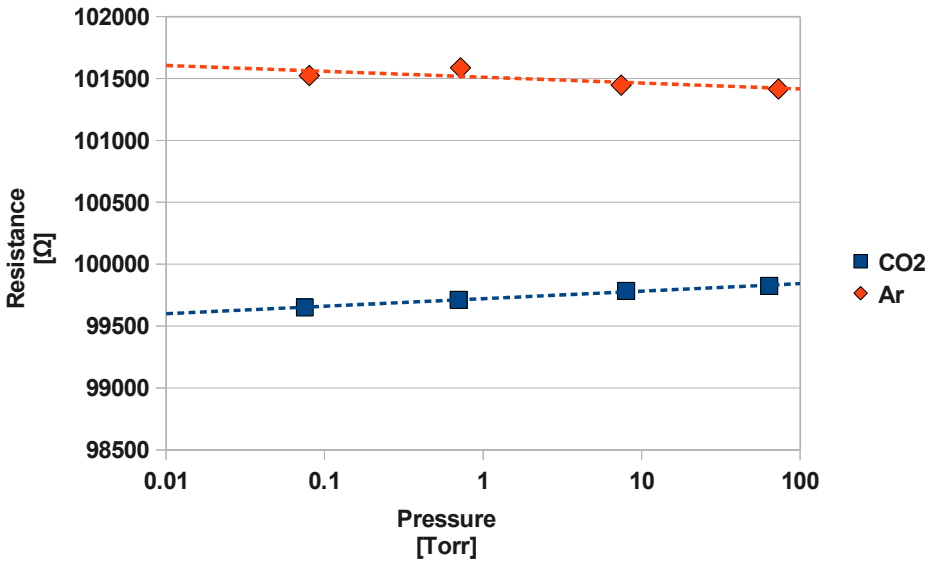

Figure 5.3: The resistance of the graphene film sample with exposure to CO_2 and Ar at various pressures.

Both these gases produced a small change in resistance, and the logarithmic regression line shows that the resistance changes logarithmically. The exposure to CO_2 caused the resistance to increase 0.176% over a pressure range from 0.08 to 64 Torr and the argon caused the resistance to decrease by 0.107% over the same pressure range.

Resistance change caused by CO_2 in Air

The last of the three experiments performed, investigated the change in resistance of the sample when CO_2 was mixed with air in various ratios. The resistance was measured over a range of 1% to 15% CO_2 at a base pressure just under atmospheric pressure (569.2 Torr or 0.76 bar). Figure 5.4 shows the results of the measurements.

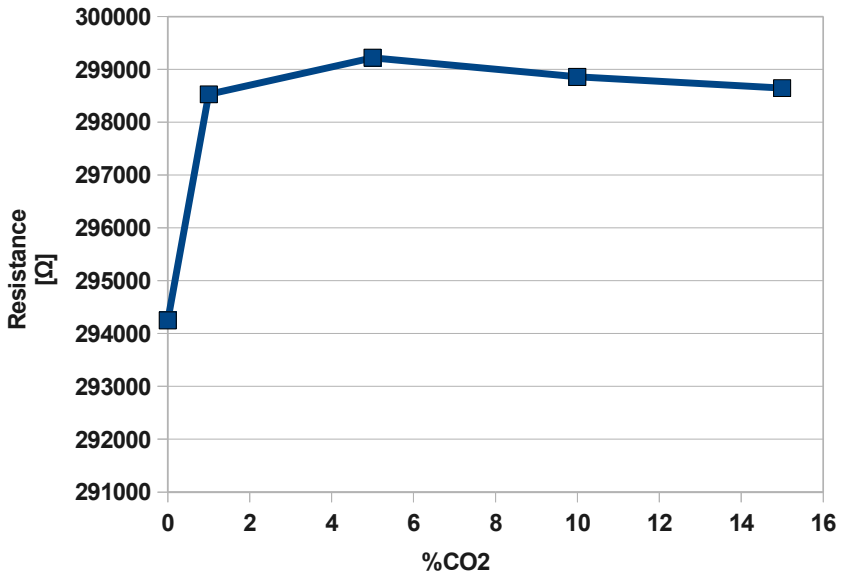

Figure 5.4: The resistance of the graphene film sample with exposure to various concentration of CO_2 in air.

There was a 1.45% increase in resistance when the sample was exposed to 1% CO_2, but further exposure did not increase the resistance significantly. It is believed that at these levels of CO_2, the graphene has absorbed the maximum amount of CO_2 that it is capable of and therefore the resistance does not increase further when exposed to higher levels CO_2.

Although changes in resistance of the sample were observed, these changes were not large enough to justify the use of graphene as a sensor that operates on resistivity changes alone. It did however show the graphene does have the ability to absorb CO_2, even if it is very small quantities. The following section will discuss a device that is capable of using the small quantities of absorbed CO_2 and amplifying it to a more usable level.

5.2 Surface acoustic wave measurements

Acoustic wave devices have been used commercially for over 70 years. Its main use is in the mobile telecommunication industry where ~3 billion

devices are used annually. These are mostly surface acoustic wave (SAW) devices and predominantly used as band pass filters. SAW devices are being used more frequently in sensing applications with a whole range of sensing possibilities including but not limited to pressure, chemical, vapour, humidity, temperature, and mass sensors [100].

A surface acoustic wave (SAW) is an ultrasonic acoustic wave that propagates on the surface of a solid. SAW devices are created by placing an interdigitated transducer (IDT) on the surface of a piezoelectric material [101]. Piezoelectric materials are crystals that are able to convert mechanical stress to a potential difference across the crystal and vice versa. It is observable in many crystals, but only a few such as quartz (SiO_2) show this effect strong enough to be of practical significance [102]. SAW devices exploit the piezoelectric phenomenon to form devices with novel electronic properties. An IDT is therefore responsible for the conversion of an electrical signal to a SAW and back again to an electrical signal [103]. An IDT is typically a comb shape structure and the precise shape and size of the IDT determines the frequency and other characteristics of the SAW that it generates. When a signal is applied to the IDT, it generates a SAW on the surface of the piezoelectric material. Sensor applications generally contain a transmitting IDT and a receiving IDT on the piezoelectric material. The sensing is then performed between the two IDTs on the substrate and this interaction produces a change in the signal received by the IDT. This change can subsequently be used for sensing purposes. Figure 5.5 shows a schematic of a typical SAW device. SAW devices that are used in the telecommunication industry use other types of IDTs, such as reflectors, to implement filters or resonators [104].

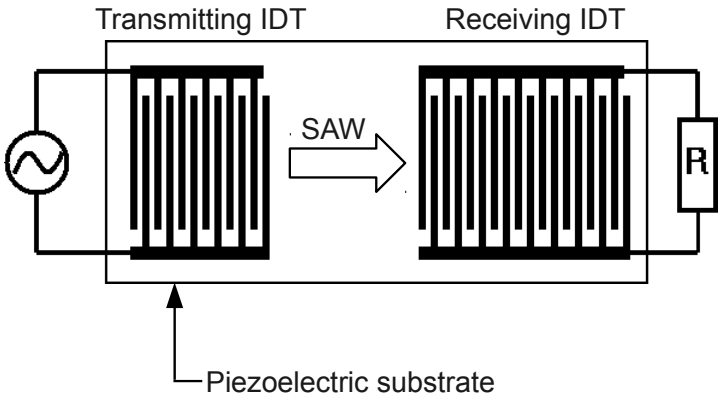

Figure 5.5: Schematic of a typical SAW device.

As SAW devices are constructed by depositing IDTs on a piezoelectric substrate, the hard work in creating a SAW device is to determine the exact shape of the IDT. Once the shape has been determined, the IDTs are created on the substrate using standard lithography techniques and a deposition

process. The exact shape and size of the IDT determines the centre frequency, bandwidth and various other parameters of the device.

Jakubik *et al* has demonstrated that it is possible to detect hydrogen using a SAW sensor [105]. During their study, they experimented with a layered structure of palladium/metal-free phthalocyanine deposited on the SAW sensor's surface. They were able to detect 0.5% to 3% hydrogen in air at 30 °C using their SAW device. The detection mechanism is based on frequency changes in the acoustic surface wave dual delay line system.

5.2.1 The Surface Acoustic Wave Sensor

As the acoustic wave propagates through or on the surface of the material, any changes to the characteristics of the propagation path affect the velocity and/or amplitude of the wave. Changes in velocity can be monitored by measuring the frequency or phase characteristics of the sensor and can then be correlated to the corresponding physical quantity being measured.

SAW sensors are very promising candidates to be used for sensitive gas sensing due to the fact that almost the entire energy of the travelling acoustic wave is on the surface of the substrate [105]. Any change to the characteristics of the propagation path affects the velocity and/or amplitude of the wave. This means that any environmental change can easily influence the travelling wave, making it possible to detect very small environmental changes. By depositing graphene, which has already proved itself as a highly sensitive material, on the surface of the SAW device, the creation of an extremely sensitive detection device should be possible. Moreover, SAW sensors are competitively priced, rugged and reliable [100].

Sensor construction and operation

The SAW sensor used during this research, consisted of two IDTs on opposites side of a lithium niobate ($LiNbO_3$) crystal. The SAWs were generated by aluminium thin film IDTs of 1.5 mm width and 100 finger pairs with 18 μm period. This resulted in the SAW sensor to have a centre frequency of 96 MHz. RF connections were subsequently connected to the IDTs. Graphene was spray coated onto the centre of the $LiNbO_3$ substrate using the exact same process that was used to fabricate the graphene film sensor as explained in Section 3.2. The IDTs were covered during the spray-coat process and only an area that was 3 mm long and the entire width of the substrate was exposed to the spray-coat process. Figure 5.6 shows the SAW device that was used during testing. Note the graphene in the centre of the device and the two IDTs on either side of the substrate connected to the RF connections. The sample was mounted on a piece of aluminium to make handling it easier.

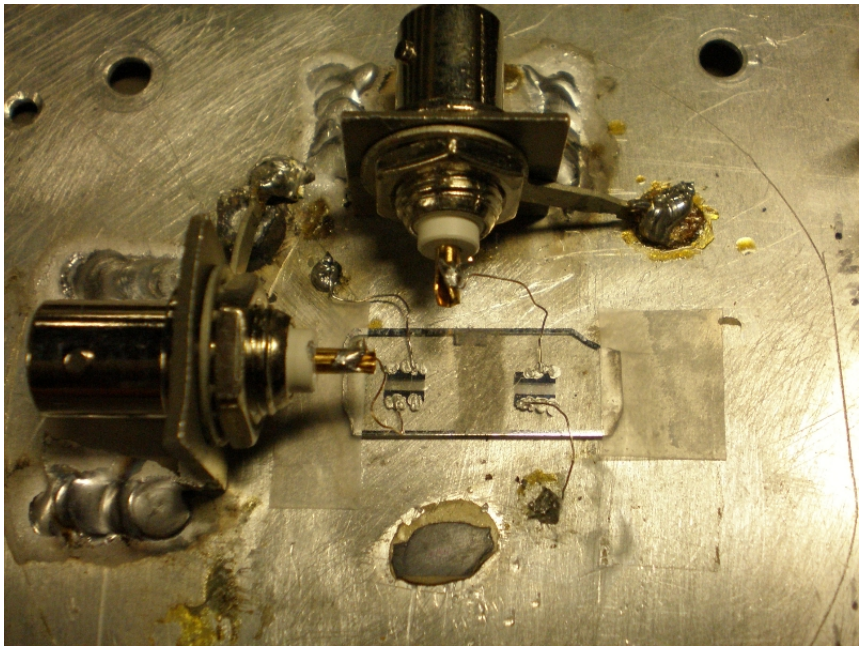

Figure 5.6: The surface acoustic wave sensor used during gas testing. The dark area in the middle of the substrate is the graphene.

The SAW device operates as follows: A 96 MHz sine wave was applied to the transmitting IDT and compared to the signal received at the receiving IDT. By comparing the two signals, attenuation and phase changes can be determined. The SAW attenuation measurements were performed using RF pulse modulator (Matec 7700) and SAW phase response was monitored by measuring the S-parameters using network analyser (Agilent 4396B).

Phase change measurements were the primary detection mechanism during the experiments. Attenuation measurements were only performed to study the effect of the graphene on the amplitude of the received signal. If the attenuation was too large, it could result in a small signal-to-noise ratio when the phase change was measured.

After each experiment the graphene was gently removed from the SAW substrate using acetone. The spray-coat process was then repeated. The results from each individual experiment can therefore not be compared directly as the precise amount of graphene on the substrate was not exactly the same for every experiment.

5.2.2 Results

The results of three surface acoustic wave (SAW) measurements performed are discussed in this section. The SAW gas sensing experiments proved to be the most interesting part of the research and it provided very interesting results.

Phase change caused by CO_2

In the first test the phase change response of the SAW sensor without any graphene was compared to a SAW sensor with graphene when exposed to various pressures of CO_2. Figure 5.7 shows the results of the measurements. Each point on the graph corresponds to 400 measurements over a 2 minute period. An average value for these measurements were calculated and plotted on the graph. This measurement technique eliminates a lot of the noise that would otherwise be present in the measurement if only a few measurements were taken.

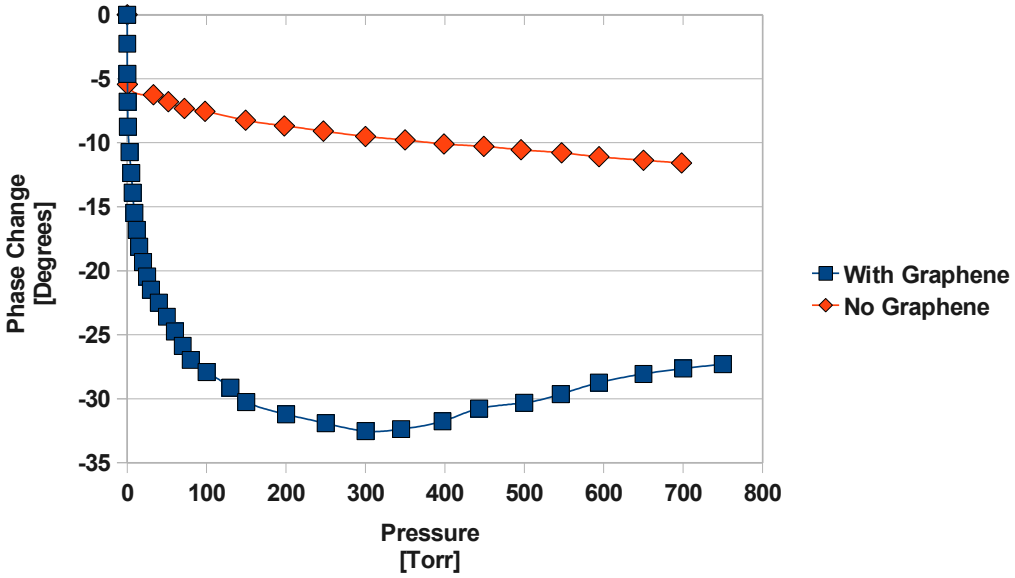

Figure 5.7: The phase change of the SAW sensor coated with graphene compared to a SAW sensor without any graphene when exposed to different pressures of CO_2.

The SAW sensor coated with graphene underwent a maximum phase change of 32.5° compared to a 9.5° phase change of the SAW sensor without graphene at 300 Torr. The graphene SAW sensor was especially sensitive in the lower pressure ranges, as seen in the graph. The reason the blank SAW sensor underwent a phase change with the increased pressure is due to mass loading that is caused by an increase in pressure.

The graphene can have two effects on the SAW that propagates along the surface of the substrate. The first effect is if the graphene's weight changes, it will change the phase of the received signal. The second effect is if the graphene's resistance changes, it will also impact the phase of the received signal. Resistance and mass changes of the graphene film can occur due to absorption of a specific gas as shown in Section 5.1. The SAW device can

therefore be seen as a type of amplifier for this change to the graphene film. The graphene film can be tailored to respond to a specific gas and in the process become an ultra sensitive detector.

Time response of exposure to CO_2

The second experiment was used to record the phase change versus time of the graphene SAW sensor when it was exposed to CO_2. The sensor was exposed to a CO_2 atmosphere of 182 Torr or 0.43 mg/cm^3 for 50 minutes. Figure 5.8 shows the results of the measurements. The sensor underwent a phase change of just over 4° during that period. When a blank SAW sensor was used, a phase change of only 0.7° was observed (not shown in the graph). This translates into a 5.7 times enlargement of the phase change.

The CO_2 was then purged from the chamber and the sensor recovered to its initial value in just over 30 minutes.

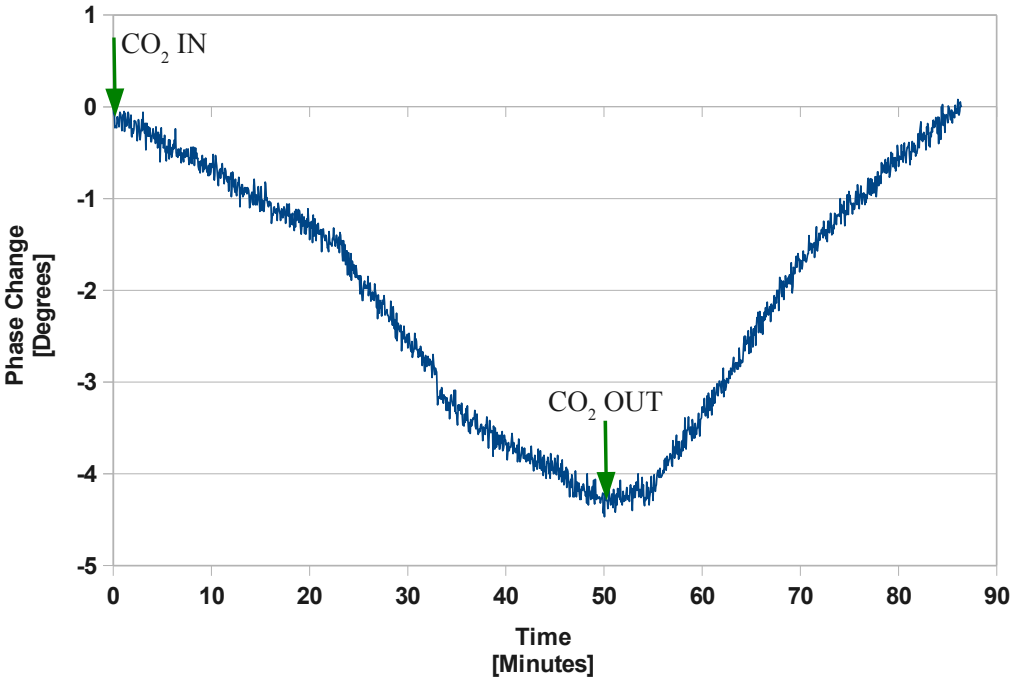

Figure 5.8: The phase response of the graphene SAW sensor over time when exposed to a CO_2 atmosphere of 182 Torr.

The delays in the graphene SAW sensor's performance is due to the fact that it is based on absorption effects on the graphene's surface. The absorption and desorption is not an instant process. In contrast, when the blank sensor was used, the phase change was much quicker as the change is purely a function

of pressure. Consequently, there is a trade-off between the increased sensitivity and response time.

It might be noted there is a difference in the phase change of this experiment compared to the first one. This is due to the fact that different amounts of graphene were sprayed onto the SAW sensor for each test. The results should therefore not be compared directly to each other.

CO_2 in air

The results of the previous two tests have shown that the graphene SAW sensor has potential to detect different concentrations of CO_2. The following test was used to determine whether a similar trend can be seen when a certain percentage of CO_2 in air was exposed to the graphene SAW sensor. Figure 5.9 shows the results of the experiment. The graphene SAW sensor underwent a phase change of just over 1° when the CO_2 concentration was increased to 20%. Although the phase change was not precisely linear, it did follow an increasing trend with an increase of the CO_2 concentration. Each point on the graph once again corresponds to 400 measurements over a two minute period, as this minimizes the effect on noise on the measurements.

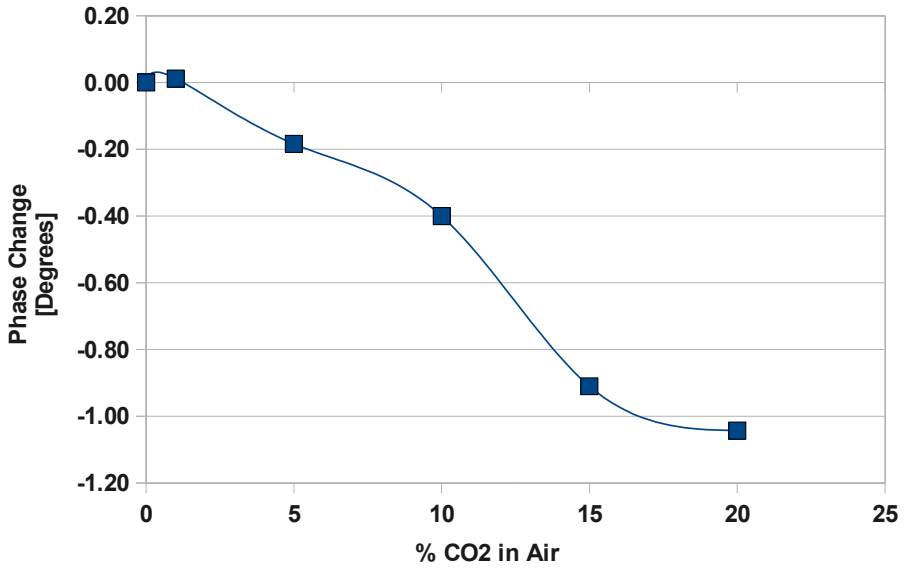

Figure 5.9: The phase change of the SAW sensor coated with graphene with exposure to various concentration of CO_2 in air.

The SAW sensor is much more sensitive to changes in CO_2 concentration when it is only exposed to CO_2. The sensitivity decreases when the CO_2 is mixed with air. It is believed that the air interacts with the graphene and this causes the absorption of CO_2 to be less effective.

5.3 Conclusion

The results of the resistive experiments showed that graphene is an unlikely candidate to be used in resistive based gas sensing. For that reason it was used in conjunction with a SAW device.

The results of the SAW experiments were conclusive in showing that a SAW sensor can be used to measure absorption changes in graphene. This novel method is so far unreported on the detection of CO_2 using graphene together with a SAW device. Although only CO_2 experiments were performed, the sensor can also be used to detect various other gases. The graphene can be tailored with some chemical doping techniques to absorb a certain gas which will lead to a wide range of possible gas sensing applications.

There is also room for improvement of the SAW sensor. As the primary investigation into whether graphene can be used with a SAW device to form a highly sensitive gas sensor, the main goal was to determine whether it is feasible. Consequently, it is believed that the operating characteristics of the sensors should be able to be increased significantly. It is difficult to determine what the optimum amount of graphene on the surface of the SAW sensor should be. The type of graphene and deposition method can also influence the performance of the sensor. Subsequent experiments can determine this and it could result in an even more sensitive sensor with an increased response time.

Chapter 6

Liquid Based Applications

In this section three experiments that were performed in a liquid environment are discussed. The first experiment looked into using graphene as a pH sensor. The second experiment investigated whether graphene can be used to increase the efficiency of a water electrolysis process. Lastly, an experiment was conducted to determine if the sensor has any potential to be used as a flow sensor.

6.1 pH Sensing

pH meters are used for simple applications such as home-based testing of pool water as well as in complex industrial processes. pH measurements are important in medicine, biology, chemistry, food science, environmental science, oceanography and many other applications.

pH refers to the hydronium ion concentration ($[H_3O^+]$) in an aqueous solution. As the hydronium ion concentration can vary from 10 M down to 10^{-15} M, it can result in a very wide range of numbers to work with. The pH scale makes handling of this enormous range and negative exponents easier by taking the negative logarithm of this number, similarly how the decibel scale is used [19]. The pH of a solution can therefore be calculated as follows [19]:

$$pH = -log([H_3O^+]). \tag{6.1}$$

When substances dissolve in water they produce ions. Certain substances produce hydronium (H_3O^+) ions and others hydroxyl (OH^-) ions. Acidic water contains extra hydronium ions (H_3O^+) and basic water contains extra hydroxyl (OH^-) ions. Similarly to how the pH is calculated, the pOH can be calculated as follows [19]:

$$pOH = -log([OH^-]). \tag{6.2}$$

As pH + pOH = 14 (at 25 °C), when one of these concentrations are known the other can be easily calculated [19].

pH can be seen as a measuring unit used to determine the acidity or basicity of a solution. The values usually fall in a range from 0 to 14, but higher and lower values are possible. The lower side of the scale (pH < 7) represents acids and the higher values represents the bases or alkalines (pH > 7). The lower the value, the stronger the acid and the higher the value, the stronger the base. A value of 7 represents a neutral pH, which is the pH of pure water [106].

A rough indication of the pH value can be obtained by using pH paper, which contains organic molecules whose colour depends on the pH level. A few drops of the solution to be measured can be dropped onto the paper, and the colour of the paper can be compared to a colour chart to estimate the pH level. A more precise value can be obtained by using a pH meter. A pH meter contains two electrodes. The one electrode provides a stable fixed voltage while the other electrode contains a known [H_3O^+] solution separated from the unknown [H_3O^+] solution with an extremely thin, conduction, glass membrane. The difference in concentration of the two solutions generates a voltage that is proportional to the pH level [19].

6.1.1 Motivation

In a recent study conducted by J. Rafiee from Rensselaer Polytechnic Institute, a graduate student in Professor Nikhil Koratkar's group, it was showed that graphene holds a lot of potential for hydrogen storage [107]. The results of the study showed that graphene has a hydrogen storage capacity of 14 percent by weight, surpassing the US department of Energy's 2015 target by 6%. Given that pH is a function of H_3O^+ ion concentration in the solution and the fact that the exact same graphene was used during this study, it may well be possible that the H_3O^+ ions also get absorbed similar to H_2 gas. Should this absorption occur, the resistance or some other electrical property of the sample could change, making it possible to use the graphene as a pH sensor.

6.1.2 Experimental

The pH testing was done by preparing solutions of different pH values, exposing the graphene sample to these solutions and then measuring the resistance of the graphene film.

Basic pH solutions were prepared by dissolving KOH in water. To make basic solutions of different pH values, a solution with a pH of 13 had to be prepared first. This solution was then diluted to prepare more solutions with lower pH values. A 200 ml solution with a pH of 13 was prepared using the following method:

As pH + pOH = 14 (at 25 °C), a solution with an OH^- concentration of 0.1 mole per litre will yield a solution with a pH of 13. KOH dissolves completely in water, therefore dissolving 0.02 moles of KOH in 0.2 L of distilled water

will produce the required concentration of 0.1 mole per litre. The molar mass of KOH is 56 g, so using the equation: $n = m/M$, where n is the number of Moles, M is the molar mass of the substance and m is the mass of the substance [19], it can be calculated that 1.12 g of KOH equals 0.02 moles of KOH. Thus, the solution with a pH of 13 was obtained by dissolving 1.12 g of KOH in 200 ml of water.

A solution with a pH of 12 was obtained by taking 20 ml of the pH 13 solution and adding 180 ml of distilled water to it. This dilution process was repeated and solutions with a pH range from 9 to 13 with increments of 1 pH were prepared.

LabVIEW (Laboratory Virtual Instrumentation Engineering Workbench) was used to do the testing. LabVIEW is a visual programming language and the data acquisition capabilities of the software were used for the testing. A program was specifically developed for van der Pauw type measurements, which has the ability to apply a voltage and then measure two different voltages. The one voltage represented the required voltage in the van der Pauw equation, while the other voltage was used to measure the voltage over a small current sensing series resistor, which was used to calculate the current. The measured voltage and current can then be used to calculate one of the four required resistance values when using the van der Pauw method as explained in Section 3.4. The remaining three resistance values can be determined by switching the contacts and repeating the process.

The process was in fact more complicated than simply measuring two voltages. A wide range of voltages were applied to ensure that the sample showed ohmic behaviour and that the values were reliable. The code was therefore written to perform the following actions: A series of voltages from 1 V to 5 V in a step size of 1 V was applied to the sample. At each voltage step, the measurement was done ten times within one second. From these ten measurements, an average value and standard deviation could be calculated. If the standard deviation was large, the test was discarded and repeated from the beginning. After each voltage step, a few seconds were waited before the next ten measurements were taken to ignore any transient response of the system. All of the voltages were recorded to a file from where it was processed to determine one of the four required resistance values when using the van der Pauw method. The contacts were switched and the process was repeated until all of the required resistance values were known and the sheet resistance of the sample could be determined using the van der Pauw method.

To keep the results consistent and to minimize any external influences, the following work methodology was implemented: For all of the tests the temperature was fairly constant, as the tests were done in an air conditioned room with constant temperature setting. The sensor was also securely attached to the beaker containing the solution. Due to the logarithmic nature of the pH scale, the tests were performed in order of increasing pH to minimize contamination issues. After every experiment was completed, all

of the equipment was rinsed three times with distilled water.

Various tests were performed to determine whether graphene could be used for pH testing. The following results were obtained from the experiments:

Resistive measurements

The first experiment performed was used in an attempt to find a relationship between the resistance of the graphene film and the pH value. Figure 6.1 shows the results of the experiments. Initially it seemed as though the graphene responded to the change of pH, as it increased from 9 to 10, but then decreases significantly from 10 to 13. This test was done three times in order to test for repeatability. In the Figure 6.1 it is indicated as Run1, Run2 and Run3. The test was also done by only exposing four electrodes to the solution while keeping the distance between them fixed. The four electrodes had a similar response to the change in pH as the graphene sample. This shows that the graphene sample provides no advantage for pH sensing. As the pH increased, the concentration of ions also increased and it is believed that this higher concentration lowered the resistance of the solution, which was basically what the graphene sample measured.

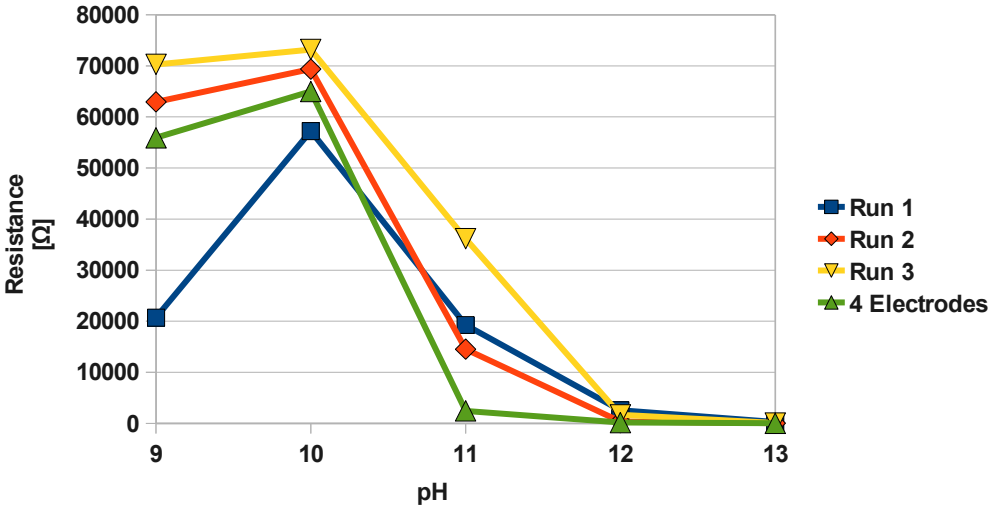

Figure 6.1: The resistance of the sample at various pH levels. The test was repeated three times with graphene and once with a sample without any graphene.

Voltage measurements

Even though these tests were discouraging at first, an interesting observation was made when the sample was placed in the solution. A spontaneous voltage appeared between the contacts of the sample. Initially it was not clear how

this voltage originated, so various test were conducted to determine the cause of this voltage. The test were also performed to determine whether this voltage can be used to measure a certain property of the solution. The first experiment conducted was to investigate whether there was a correlation between the pH level of the solution and the generated voltage. The sample was placed in the solution starting with a pH of 7 up to a pH of 14. The experiment was then repeated to determine the repeatability of the voltages. Figure 6.2 shows the results of the experiment. It plots the voltage generated versus time for each solution. The voltage was recorded using LABVIEW. For pH values lower than 13, the voltage was very close to 0. At a pH of 14, there was a voltage over 100 mV, but with poor repeatability.

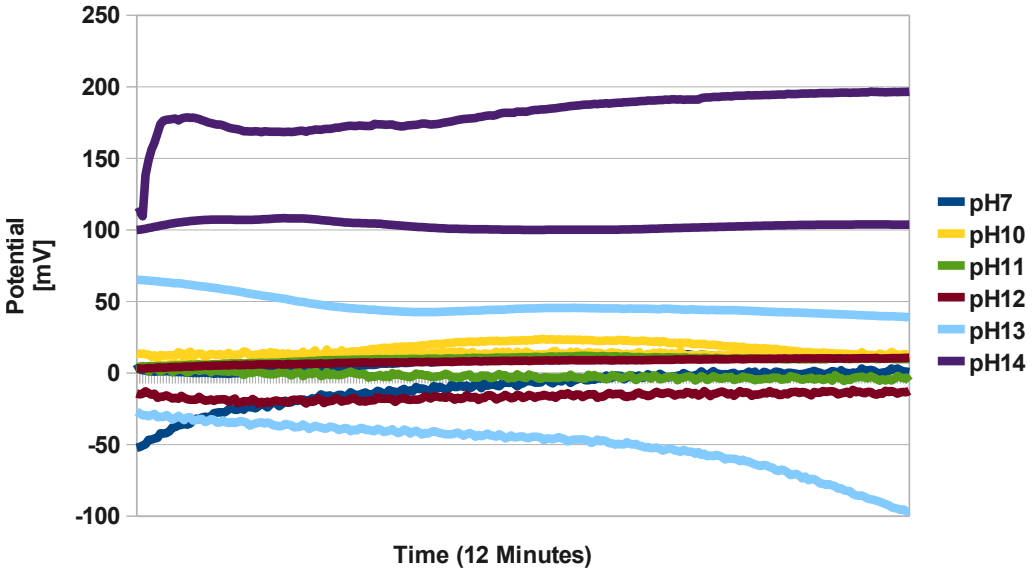

Figure 6.2: The voltage of the sample versus time at various pH levels. Each test was done twice.

Additional measurements

Additional experiments were performed to determine if it was truly the graphene that was generating the voltage or an electro chemical reaction at the contacts. A sample was created with two contacts connected to the glass substrate with no graphene on the surface. Figure 6.3 shows the value of the voltage between these two contacts. At a pH level of 13, the voltage measured was around 100 mV which confirmed that the graphene was not the reason for this voltage.

When two different metals are placed in an acidic or basic solution, a voltage is generated. This is due to difference in the electron affinity of the two metals [19]. When two of the same metals are placed in such a solution,

no voltage should be generated as they have identical electron affinities. The voltage generated in this case can be attributed to slight differences in the electrodes and when it was placed in a solution with a large concentration of ions, this voltage appeared. The m-coat that was used to isolate the contacts from the solution seems not to have isolated it properly. The value of the generated voltage can therefore not be used for the pH sensor as it is attributed to the contacts and not to the graphene.

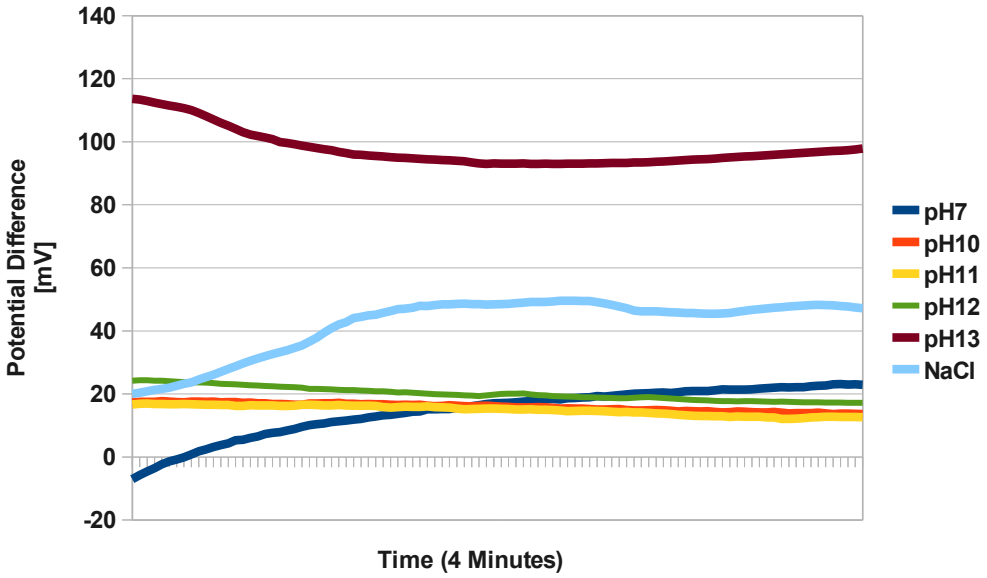

Figure 6.3: The voltage of a sample with no graphene versus time.

A last experiment was performed to establish whether this graphene has any potential as a pH sensor. During this test, the contacts were not exposed to the solution. Figure 6.4 shows the set up of this experiment. The sample was constructed in a similar fashion as explained in Chapter 3, but a glass substrate was used where the length was three times the width. Also, only two contacts could be connected as the experiments aims not to expose the contacts to the solution. The resistance was measured by applying a voltage and measuring a current at various voltage levels to ensure ohmic behaviour. A model of the sample can be approximated as two resistors that are in parallel. The one resistor is the part of the sample that is exposed to the solution and the other resistor is the part not exposed to the solution. A change in the resistor that is exposed to the solution (in either direction) should then produce a change in the total resistance of the sample.

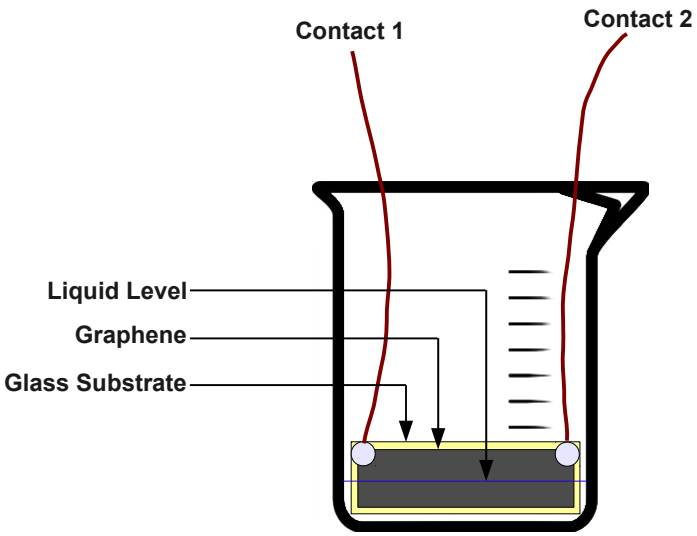

Figure 6.4: Test setup of the final pH test. In this experiment the contacts were not exposed to the solution.

Two tests were performed on the sample. The first test consisted of resistive measurements. Figure 6.5 shows the relationship between the resistance of the sample in air, various pH levels and in a NaCl solution. The pH level of a NaCl solution should be neutral (7) as it contains no H_3O^+ ions. Consequently, the NaCl solution can be used to determine whether the sensor measured the pH level or conductivity of the solution. For the sensor to operate successfully as a pH sensor, it should give a similar output for pure water (pH 7) and the NaCl solution. From Figure 6.5, it is clear that the graphene responded to a change in conductivity and not the pH level.

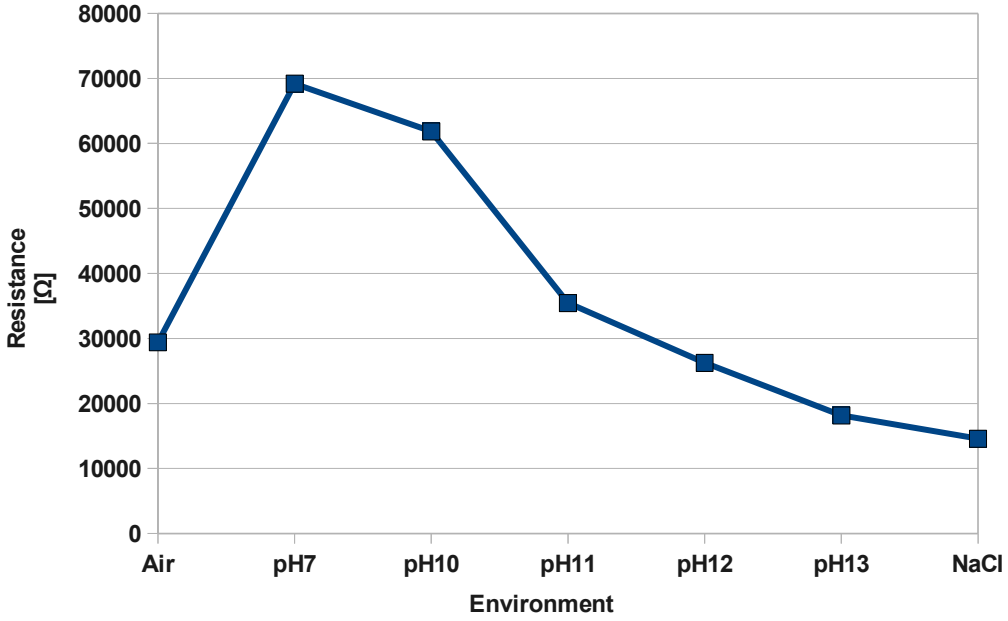

Figure 6.5: The resistance of the sample used in Figure 6.4 in different solutions.

The second test performed was used to determine the frequency response of the sample at various pH levels as well in a NaCl solution. Figure 6.6 shows the results. In all the test cases the impedance of the sample decreased dramatically around 100 kHz. This decrease does not seem to convey extra information about the sample and the frequency response does not provide additional information to Figure 6.5

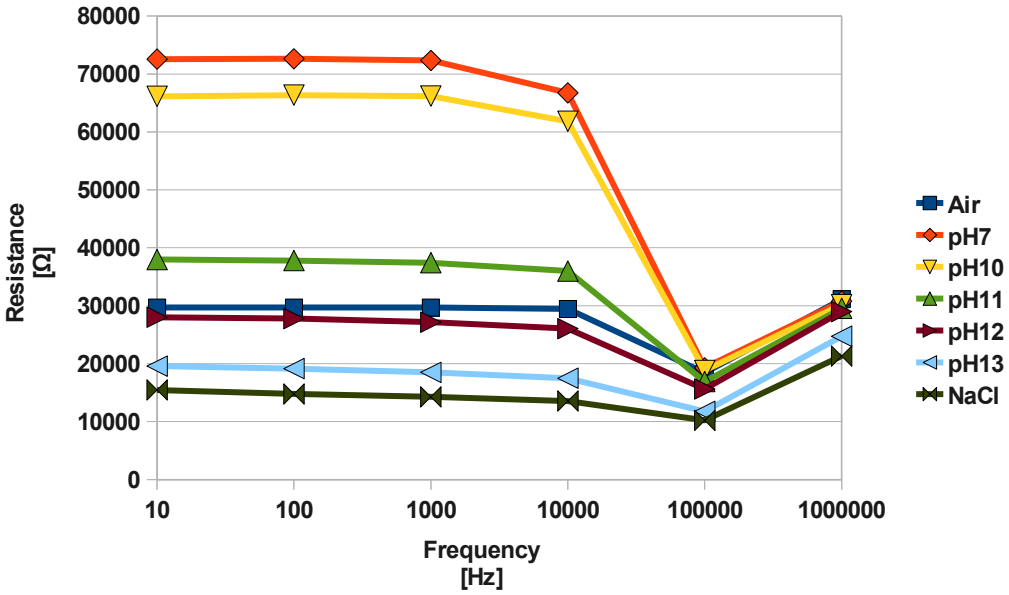

Figure 6.6: The frequency response of the graphene film sample in various solutions.

6.1.3 Conclusion

Although the sensor produced changes, no correlation between the pH value and the change could be found. These changes seem to be caused by a change in conductance of the solutions and not by a change in concentration of H_3O^+ ions. Prolonged exposure of the graphene sensor to the liquid also caused the graphene to dissolve, especially at higher concentrations of KOH. If H_3O^+ ions do indeed react with the graphene, it does not produce a significant change in the resistance of the sample. The resistance of the sample is dominated by the conductance of the solution. There are obviously much simpler methods to measure the conductance of a liquid than using graphene. In summary, the graphene used in this study seems unable to be used as the detection mechanism for H_3O^+ ion concentration and therefore, pH levels.

6.2 Water electrolysis

Electrolysis of water is the decomposition of water (H_2O) into oxygen (O_2) and hydrogen gas (H_2) due to an electric current being passed through the water [19]. During this process, water is oxidised at the anode:

$$2H_2O \rightarrow O_2 + 4H^+ + 4e^-,$$

and reduced at the cathode:

$$4H_2O + 4e^- \rightarrow 2H_2 + 4OH^-.$$

Both these gases have numerous applications over a wide range of industries. Hydrogen is used to produce ammonia and other industrial chemicals, but more importantly, is the vital role that hydrogen is to play in the so called hydrogen economy. In the hydrogen economy, hydrogen is used to replace fossil fuels, especially in cars. In a car, the water electrolysis process can be reversed to produce electricity from hydrogen and oxygen. This could eliminate mankind's dependence on fossil fuels as well as reduce greenhouse gases that cause climate change.

Unfortunately, hydrogen does not occur naturally in large quantities anywhere on earth and another energy source has to be used to create the hydrogen. Hydrogen can therefore be thought of as an energy carrier similar to electricity. Currently, the most economical and commonly used method to produce hydrogen is through steam reforming from hydrocarbons, mostly methane. With this process, high temperature steam is used to produce hydrogen from methane. The process has the following reaction: [108]

$$CH_4 + H_2O(+heat) \rightarrow CO + 3H_2,$$

and it clearly still produces a pollutant in the form of CO. Although this method produces hydrogen, it does not solve the original problems as it still produces pollutants and it still uses fossil fuels. The alternative is to use water electrolysis to produce the hydrogen and use a renewable energy source such as solar power or wind power to deliver the energy to the water electrolysis process. This technique produces no pollutants and requires no fossil fuel.

Producing hydrogen with water electrolysis is unfortunately not a very efficient process. The minimum thermodynamic voltage required to start this process is 1.23 V. In reality this voltage is usually 0.4 to 0.6 V more and is called the overpotential. This overpotential is caused by diffusion, losses by reaction and resistances in the system [109] and is the main cause of the inefficiency of the system. Any approach that can minimize this overpotential has the ability to increase the overall efficiency of the system and it would be of great significance to the entire hydrogen economy.

6.2.1 Motivation

Kim *et al* showed in their paper, *Water Electrolysis Activated by Ru Nanorod Array Electrodes*, that the efficiency of water electrolysis can be increased by using ruthenium nanorod arrays as the cathode [109]. Using this configuration, they decreased the over potential by 25% and the energy consumption by 20%. They attribute this improvement to an increase in the active area of the electrode, which causes the current density of the electrolyzer to decrease.

During this research, graphite rods were spray coated with graphene to determine whether the graphene might play a similar role as described above. The unique structure and high surface to volume ratio of graphene might

increase the active area of the electrolyzer that would result in a more efficient water electrolysis process.

6.2.2 Experimental

Setting up the experiment consisted of the following steps. Two graphite rods were spray coated using the exact same graphene and airbrush as described in Chapter 3. The graphite rods were attached to a spacer to ensure that the rods remained in the exact same position during all of the tests. An electrical connection was attached to the top of the graphite rods. An adjustable voltage source together with an ammeter was then connected to the contacts. Figure 6.7 shows a schematic of the setup used during testing. Pure water has a high resistance because it contains very little ions. A salt that produces ions when dissolved can be added to lower the resistance of the water. Hydrogen will still form at the cathode, as long as it is easier to reduce the water than the positive ions of the salt. Similarly, oxygen will form at the anode if a lower potential is required to oxidise the water than the negative ions of the salt [19]. During this experiment, a KOH 30 wt% aqueous solution (30 g KOH in 70 ml distilled water) was used throughout all of the tests, with hydrogen still forming at the cathode and oxygen at the anode.

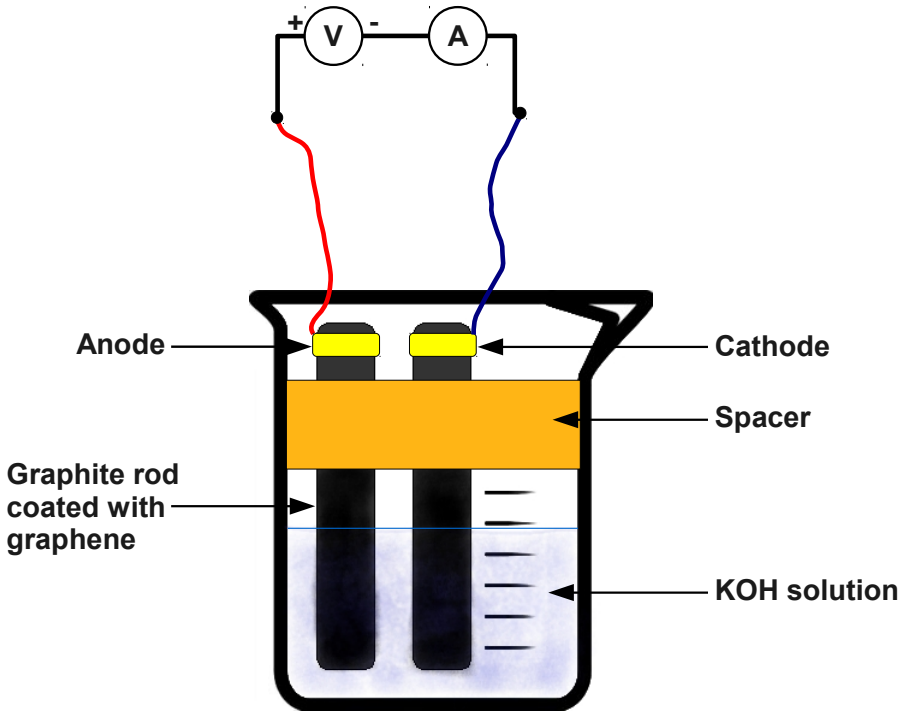

Figure 6.7: Water electrolysis test setup.

The experiment methodology is fairly straight forward. A range of voltages were first applied to the graphite rods without any graphene and the corresponding current was recorded. This process was then repeated with the graphite rods covered with graphene. More graphene was then applied to the rods and the measurements were repeated. Figure 6.8 shows the voltage current relationship of all of the tests performed. The blue line shows the response of the two plain graphite rods. In the experiment with the red line, the rods were coated with a small amount of graphene. Lastly, in the experiment with the yellow line, the rods were coated with a larger amount of graphene.

If the graphene is able to decrease the overpotential it will result in an increased efficiency. This will be observed as an increase in current at a specific voltage. A slight improvement was observed when the rods with a small amount of graphene were used, but it was not large enough to be of practical significance. The KOH solution that was used as electrolyte was very strong and as seen during the pH experiments, some of the graphene were dissolved by the strong basic solution as was evident by the graphene flakes floating in the water. However, this was not observed during the first experiment with graphene, when a small amount of graphene was used.

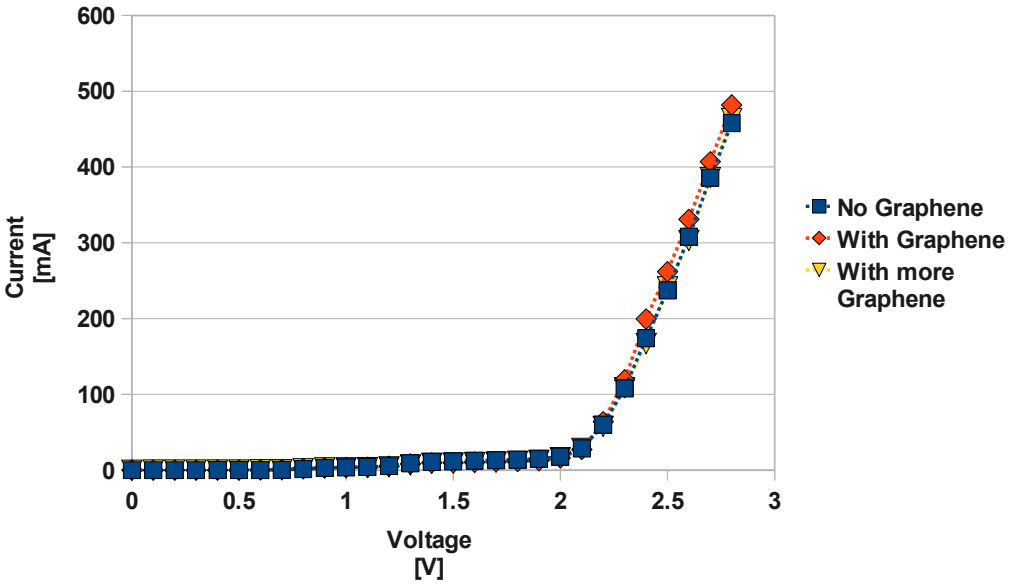

Figure 6.8: The current versus voltage relationship of the water electrolysis experiment.

6.2.3 Conclusion

Although the slight increase in current is not significant, it does not rule out the possibility of using graphene to increase the efficiency of water electrolysis.

Future experiments should experiment with different types of graphene and also better methods of depositing the graphene on the graphite rods. As stated before, the unique structure of graphene makes it an ideal candidate to improve the efficiency of a water electrolysis process. Such an improvement has the potential to significantly impact the hydrogen economy.

6.3 Flow speed sensing

The last liquid based test that was performed on the graphene sensor is flow speed sensing. Ghosh and co-workers designed a carbon nanotube flow sensor that is capable of detecting flow speeds as low as 10^{-7} m/s [14]. The sensor they fabricated produced a voltage that fit a logarithmic velocity dependence over nearly six decades of velocity.

Prof N. Koratkar's group at Rensselaer Polytechnic Institute (RPI) received a grant from the Advanced Energy Consortium (AEC) to the value of $1 000 000 to be used from 2010 to 2013 to investigate whether graphene or carbon nanotubes can be used to extract energy from a flowing liquid and use it for power generation. Leading this research is P. Dhiman and he has designed and built a complete test area that is capable of varying the flow speed. The idea is that large graphene areas can be placed in river beds to generate electricity.

The first step to generate power form the flowing liquid is to generate a voltage. Even if it does not produce any power, the possibility exists that the induced voltage can be used to measure the velocity of the flowing liquid.

6.3.1 Experimental

This experiment attempted to determine whether a voltage is generated across the surface of the graphene film when water flows over it. Experiments were conducted to determine whether there is a correlation between the flow speed and the generated voltage. If a correlation is found, the possibility exists that the graphene sensor can be used for flow speed sensing. Figure 6.9 shows a schematic of the setup that was used during the flow experiments.

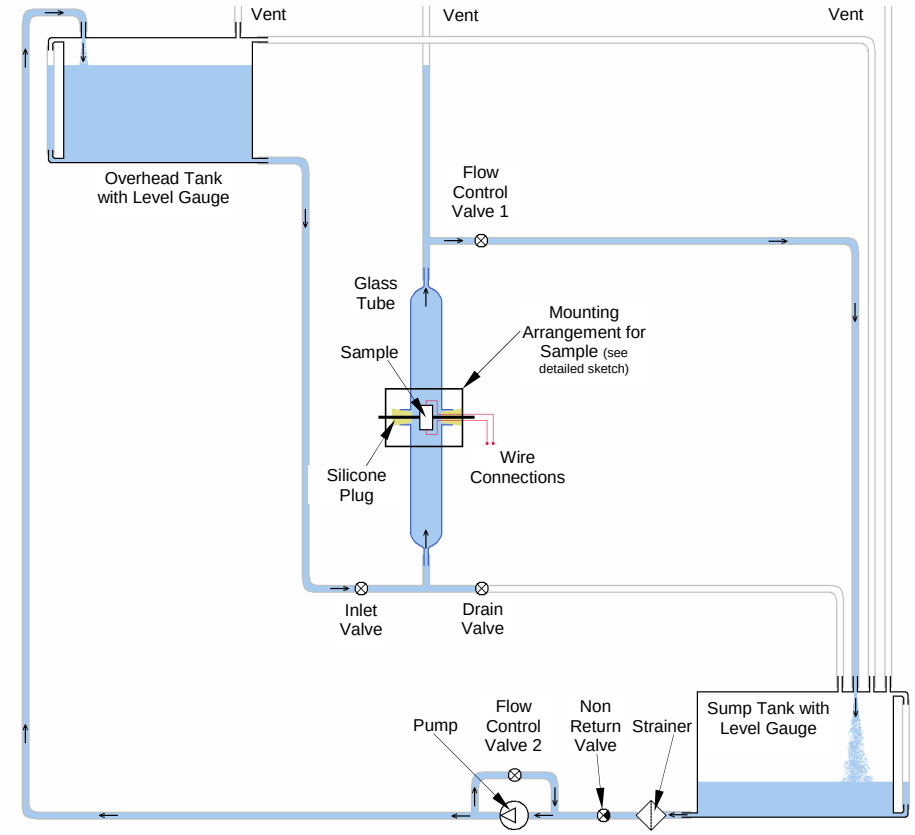

Figure 6.9: Schematic of the setup that was used during the flow experiments.

The setup basically contained two tanks. The water flowed from the top tank through a tube into the bottom tank. Note that the liquid entered the glass tube that contained the sample against gravity to prevent the formation of air pockets. When the water level in the top tank was low, a pump was switched on that pumped the water from the bottom tank back to the top tank. The setup also contained various drain valves and overflow protection devices. Figure 6.10 shows a picture of the glass tube where the sample was housed.

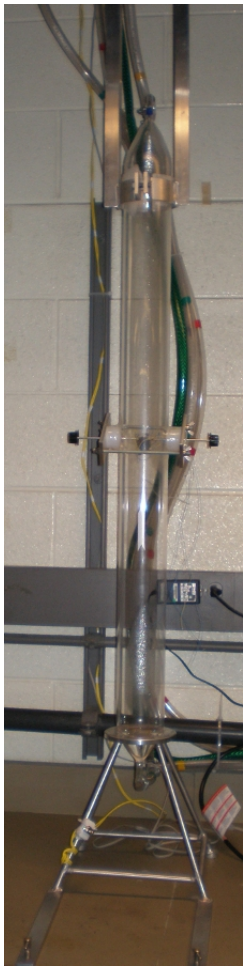

Figure 6.10: The glass tube where the sensor was housed during testing.

The sensor that was used for the measurements, was once again constructed by spray coating a glass substrate with graphene. The sensor was in the shape of a rectangle with its dimensions measuring 10 × 5 mm. Two contacts were connected to the edge of the sample over the length of the sample.

The sample was exposed to a variety of flow rates, to observe whether a relationship can be found between the flow rate and the voltage generated. The orientation of the sample against the flow rate was also changed to determine whether this has an effect on the voltage. Figure 6.11 shows the result of the experiment. The voltage was recorded over a 25 minute period. The arrows on the graph indicate where changes to the flow rate or orientation occurred.

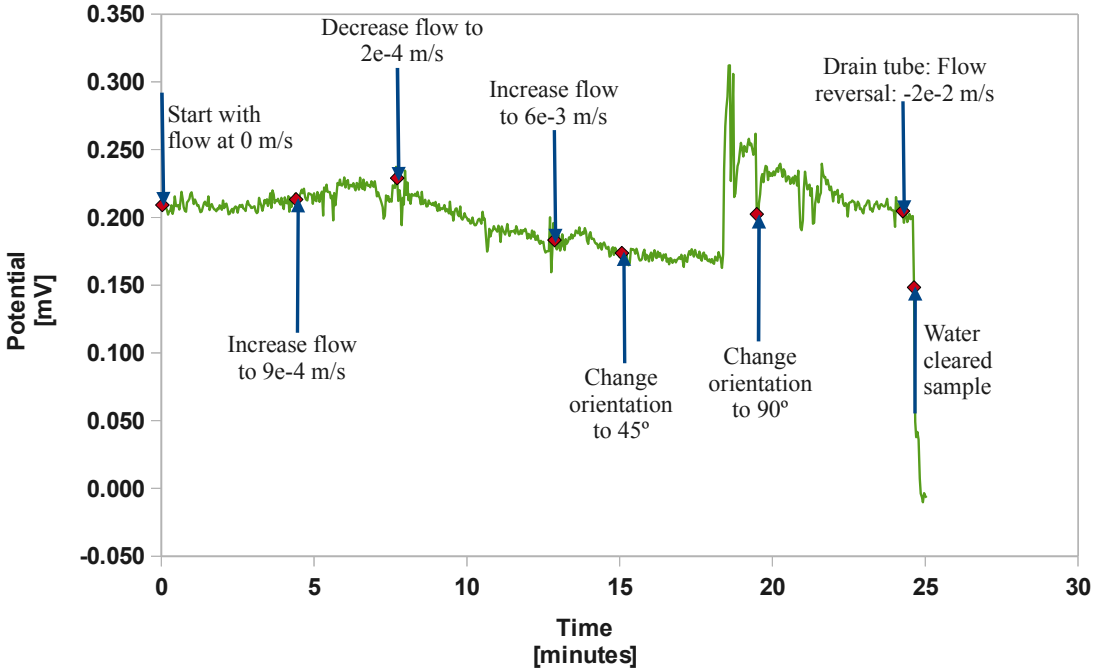

Figure 6.11: The sample's voltage in various flow conditions.

Form the figure it can be seen that the flow rate did not have a significant effect on the voltage. The orientation changes also produced little to no effect on the voltage. The only clearly visible change to the voltage occurred when the flow direction switched around during the tube draining process and especially after the water level cleared the sample.

Although the results were not very positive, this test was the first test performed to investigate the use of graphene as a flow sensor. The graphene used in this project does not seem suitable for flow speed sensing and a different type of graphene should be used to investigate the possibility of using a graphene based flow sensor.

6.4 Conclusion

All three liquid based experiments did not produce any significant results as opposed to the other application areas in this research. The graphene used in this project is therefore not a feasible candidate to be used in these types of applications. The graphene sample was not very robust in liquid and prolonged exposure of a few hours caused some of the graphene to dissolve. Other methods to synthesize graphene and creating the sensor may well show potential to be used in one of these applications.

Chapter 7

Carbon Nanotube Gas Sensor

As stated in the introduction (Chapter 1), the carbon nanotube (CNT) gas sensor that was constructed was based on the work done by Modi *et al* entitled *Miniaturized gas ionization sensors using carbon nanotubes*. Gas sensors are important as they are used in various applications, from large industrial processes to home smoke detectors.

This chapter first discusses the structure and operating principles of the sensor, followed by the method that was used to construct the sensor. The various methods available to synthesize CNTs are investigated and the method used to fabricate CNTs for this sensor is explained. A model that was used to calculate the electric field around the tips of the nanotubes, as well the equipment that was created to perform the experiments, are given.

7.1 Operating principles of the CNT gas sensor

The CNT sensor consists of two parallel spaced electrodes, one of the electrodes was covered with vertically aligned multiwalled carbon nanotubes (MWCNT) and the other was a plain aluminium electrode. The electrodes were separated by a thin insulating material, leaving the two electrodes roughly 150 μm apart.

The sensor's operating principle lies in the fact that each gas has a unique breakdown voltage. An electric potential is applied across the electrodes and by monitoring the voltage at which breakdown occurs, the unknown gas can be identified. The sharp tips of the nanotubes create very large electric fields, thereby lowering this breakdown voltage. This makes the device more portable than traditional ionization sensors, as risky high voltages are not involved.

7.1.1 Sensor construction

The construction of the sensor consisted of the following steps:

- Grow vertically aligned CNTs on a conducting substrate.

- Establish an electrical connection to the CNTs where the positive terminal of the voltage source would be connected.
- Place a smooth electrode in parallel to the CNT film, 150 μm away, without making electrical contact.
- Establish an electrical connection to this smooth electrode for the ground connection of the voltage source.

Figure 7.1 shows a three dimensional schematic of the sensor and Figure 7.2 shows a two dimensional diagram of the sensor.

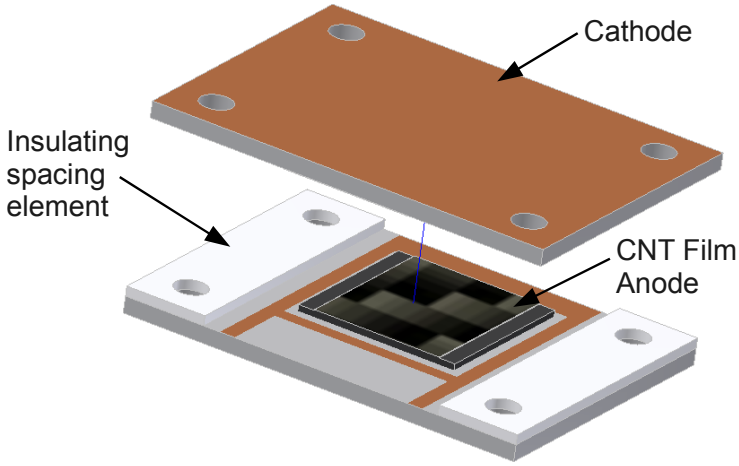

Figure 7.1: Exploded view of the CNT gas sensor.

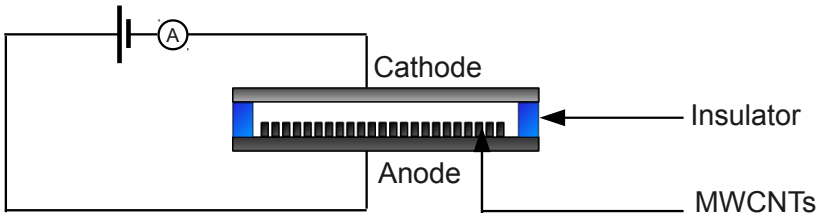

Figure 7.2: Diagram of the CNT gas sensor.

7.2 Fabrication of the sensor

The most challenging aspect of fabricating the sensor proved to be the growth of vertically aligned CNTs. This section will discuss the various methods available to synthesize CNTs, as well as the method that was used, and finally the results obtained from it.

7.2.1 CNT synthesis

A study was undertaken to determine which method can be used to produce the required vertically aligned CNTs. There are three techniques that are most often used to produce carbon nanotubes, namely carbon arc discharge, laser ablation and chemical vapour deposition. This section will briefly discuss these three methods and then comment on the practicality of each of these methods for the sensor.

Arc-Discharge

The arc-discharge method was the first method used to produce CNTs. An arc is produced across two graphite rods in an inert gas atmosphere using a sufficiently large DC voltage. When the two rods are pure graphite, MWCNTs are produced, but Iijima *et al* found that a metal catalyst needs to be added to the anode to produce single-walled carbon nanotubes (SWCNTs) [49]. The inert gas is usually a mixture of argon and helium and interestingly, the Ar:He gas ratio controls the diameter of the nanotubes [110]. Various metal catalysts such as Ni, Co, Fe, Pt and Pd have been used to produce SWCNTs. Other important parameters in the process are the pressure of the inert gas and the arcing current. With this method it is possible to produce high quality CNTs, although purification steps are required [3].

Laser ablation

Laser Ablation is another technique used to produce CNTs. With this technique, a laser is used to ablate and vaporize a graphite composite target. The target consists of graphite doped with metallic catalysts and is placed in a tube furnace that contains a high temperature argon atmosphere. Metal nanoparticles form when the target is vaporized and these particles catalyse the growth of CNTs. The CNTs are then collected via condensation on a cooled copper collector at the end of the tube. By-products such as graphitic and amorphous carbon also form in the process [110]. Purification techniques can then be applied to separate the CNTs from the by-products. The parameters that influence the shape of the CNTs are furnace temperature, type of metallic catalyst and the flow rate of the inert gas [3].

Chemical Vapour Deposition

A chemical vapour deposition (CVD) system consists of a furnace with a quartz tube inside. A substrate together with a metal catalyst is then placed in the quartz tube. The tube is heated while an inert gas, typically argon, flows through the tube. When the desired temperature is reached, the gas flow is switched to a hydrocarbon, such as methane, ethane or acetylene. After the growth process, the gas is switched back to the inert gas until a temperature

of 300 °C is reached. Exposing the nanotubes to higher temperatures can damage the CNTs [1].

For growth on substrates, the catalyst has to be applied directly onto the substrate. Preparing the catalyst is one of the most crucial steps in the growth process. Catalysts can either be directly applied to the substrate, or it can be applied in solution form. Solution based catalyst preparation is a time consuming and tedious process. It involves various chemicals and it is difficult to confine the solution to a specific pattern. Physical deposition techniques is a more attractive approach as the catalyst can be applied to the substrate in the form of thin films, using a deposition technique such as thermal evaporation, pulsed laser deposition or sputtering [1].

Although each method has its own advantages and disadvantages, only the CVD method was a viable option for this project as the other methods produces a tangle web on intertwined nanotubes and a vertically aligned array of CNTs that is directly grown on a substrate was required.

7.2.2 CNT growth attempts

A literature study was undertaken to find a method that produces vertically aligned CNTs with the CVD method. Various methods were found, most of them using a similar approach, where a metal catalyst is deposited on a substrate. However, nanotubes do not grow from smooth films and a pretreatment step is needed to form nanosized catalyst particles that act as growth sites for the nanotubes [111]. For this reason, most methods involved this pretreatment step, where a certain gas such as ammonia is used to etch the smooth film into nano sized particles. The method used by Delzeit and co-workers entitled *Multiwalled Carbon Nanotubes by Chemical Vapor Deposition Using Multilayered Metal Catalysts* [111], eliminates the need for this pretreatment step by introducing a metal underlayer between the substrate and the catalyst. It is believed that this underlayer increased the surface roughness and formed catalyst nanoparticle growth sites. This is a big advantage as it is generally much easier and quicker to deposit the underlayer than performing a pretreatment step. The underlayer also made the optimization of the catalyst layer thickness easier, because excess catalyst can contaminate the top of the CNT film. This can result in multiple CNT films growing on top of each other. Based on an extensive literature survey, the method used by Delzeit *et al* to grow vertically aligned CNTs was believed to be the simplest and quickest. Moreover, everything that was needed to attempt the growth process was readily available in the laboratory.

Delzeit and co-workers published two papers on the growth of CNTs using multilayered metal catalyst. Their first paper entitled *Multilayered metal catalyst for controlling the density of single-walled carbon nanotube growth* [112] experimented with the use of aluminium, iridium, niobium and titanium as metal underlayer and iron as catalyst in the growth of SWCNTs. They

found that aluminium produced the best growth results and therefore focused on the optimization of aluminium thickness. The iron layer was kept fixed at 1 nm and they found that an increase in aluminium thickness increased the density of SWCNT up to a thickness of 10 nm. Thicker aluminium layers did not seem to influence the growth density. The sample was then placed in a quartz tube inside a furnace. Argon (99.999% pure) was flowed through the tube at a rate of 1000 sccm (standard cubic centimetres per minute), while it was heated to 900 °C. After reaching the required temperature, argon was flowed through the tube for an additional 10 minutes. This was to ensure that the temperature equilibrated before the gas flow was changed to 1000 sccm of methane for 10 minutes. Afterwards, the gas was switched back to argon and the furnace switched off. The gas flow was stopped when the furnace temperature reached 300 °C, because as stated earlier, exposure to higher temperatures can damage the nanotubes.

The second paper entitled *Multiwalled Carbon Nanotube by Chemical Vapor Deposition Using Multilayered Metal Catalysts* [111] focused on the production of MWCNTs using aluminium as underlayer and iron or nickel as catalyst. They found that an aluminium layer of 10 – 20 nm used together with a Fe layer of 10 – 20 nm produced a continuous film of CNTs. They additionally found that an aluminium layer of 5 – 20 nm used together with a nickel layer of 5 – 10 nm also produced a continuous film of CNTs. The CVD process they used was exactly the same as described above, except the temperature in the furnace was set at 750 °C. They found that this produced a mixture of SWCNTs and MWCNTs. When they replaced the methane with ethylene they had a greater success growing MWCNTs.

Through the use of the methods described above the growth of a continuous film of CNTs were undertaken, using the following steps:

- Deposit a 10 – 20 nm layer of aluminium on a silicon substrate.
- Deposit a 10 – 20 nm layer of iron on top of the aluminium.
- Perform the following steps in the CVD reactor:
  - Place the sample in a quartz tube furnace and heat it to 750 °C while argon flows through the system at 1000 sccm.
  - After the temperature reaches 750 °C, maintain the 1000 sccm flow rate of argon for 10 minutes.
  - Switch the gas flow to methane at 1000 sccm for 10 minutes.
  - Switch the gas flow back to 1000 sccm of argon and wait until the temperature in the furnace drops to under 300 °C before the gas flow is turned off and the sample is exposed to the atmosphere.

Delzeit *et al* found that ethylene favours the formation of MWCNTs over a mixture of SWCNTs and MWCNTs. The CNTs that were required for this

sensor can be either single-walled or multiwalled, as it was the sharp tips found in both types of CNTs that were required. Methane could therefore be used as feedstock for the growth process.

The catalyst and the metal underlayer were deposited on specific areas on a silicon substrate, making it possible to measure the exact growth achieved. To do this, lithography techniques were employed. It was found that the following method produced the best results:

- Prepare a 10 × 10 mm silicon substrate.
- Drop a single drop of S1818 photoresist on the substrate and spin at 4000 rpm for 30 seconds.
- Place on a heat plate heated to 90 °C for 80 seconds.
- Expose a specific area of the sample to UV light using a mask.
- Place in MF24A developer for 40 seconds to reveal the pattern.
- Rinse with deionized water to remove remaining developer.

This process caused some areas of the sample to be covered in photoresist. Deposition techniques could subsequently be performed on the sample. The thin films were deposited on the sample using a thermal evaporator. In a thermal evaporator, a material is heated under vacuum until it starts to evaporate. The evaporated material then condenses against a substrate that is placed above the heating area. Thermal evaporation is performed under high vacuum to ensure a straight line path for most of the evaporated particles. This type of evaporation is called resistive thermal evaporation and is one of the most common evaporation techniques. A crystal sensor is also placed in the chamber to measure the thickness and deposition rate of the deposited material. The quality of the film is dependant of the vacuum level as well as the purity of the source material used. The deposition was performed at a pressure between 1 and 2×10^{-5} mbar.

After the 10 – 20 nm layer aluminium was deposited, the sample was placed in an ultra sonic acetone bath. The acetone etched away the areas on the substrate where photoresist remained, while the aluminium remained in the uncovered areas of the sample.

Figure 7.3 (a) shows an AFM scan that was performed on the sample after the deposition of aluminium. The scan was performed on one of the small features of the pattern. The cross section image (Figure 7.3 (b)) was used to calculate the thickness of the aluminium layer and it was in the middle of the required range at 15 nm. The AFM scans were used to calibrate the sensor in the thermal evaporator that measured the thickness of the deposited material. It was therefore unnecessary to perform an AFM scan after each deposition.

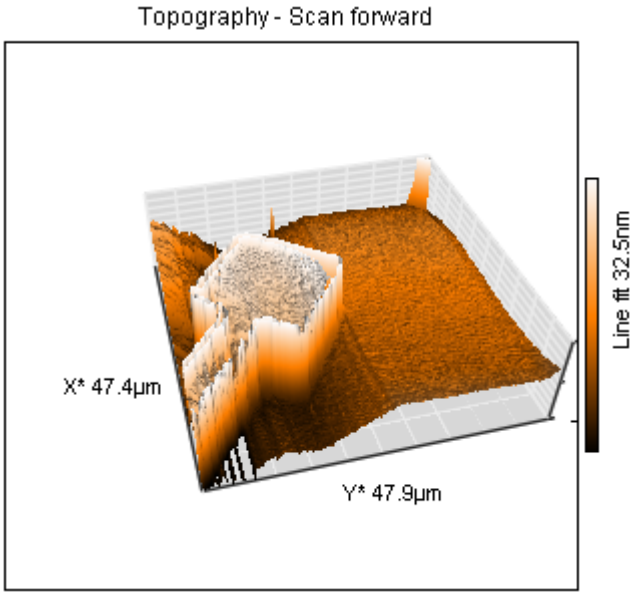

(a) 3D AFM scan.

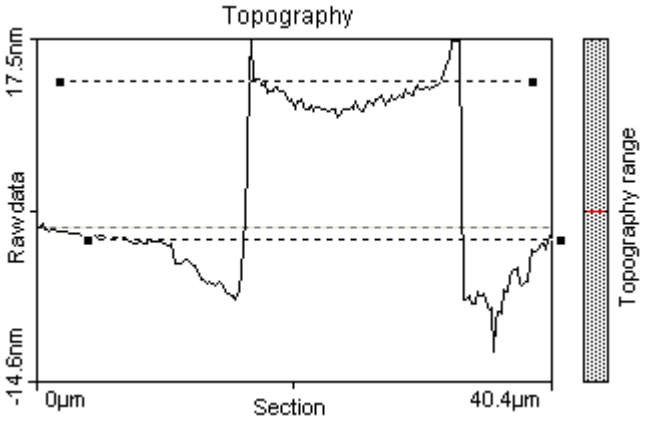

(b) Al step height equals 15 nm.

Figure 7.3: AFM scan after aluminium deposition.

Another AFM scan was performed to calibrate a different sensor, which was used to measure the deposition of iron (not shown). Each material deposited must be calibrated individually. The 10 – 20 nm layer of iron was subsequently deposited uniformly all over the sample. This made it possible to observe the effect of the aluminium underlayer on the growth process. The sample was studied under an optical microscope and the deposition appeared successful. The sample was then taken to the CVD reactor, where the steps described above were followed to begin the growth process. Figure 7.4 shows the optical image of the sample after each step of the process.

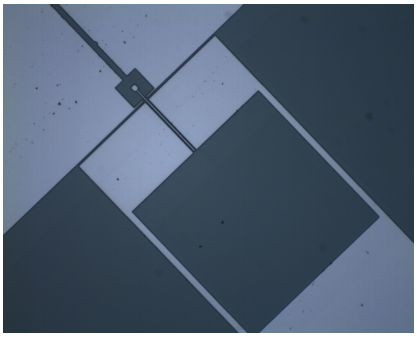

(a) Photoresist.

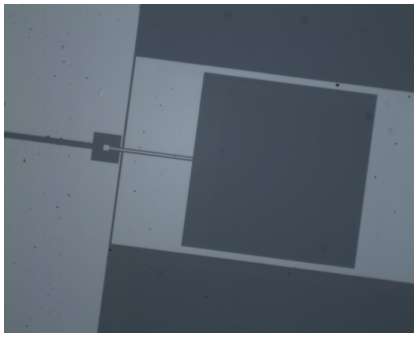

(b) 15 nm Al layer on pattern.

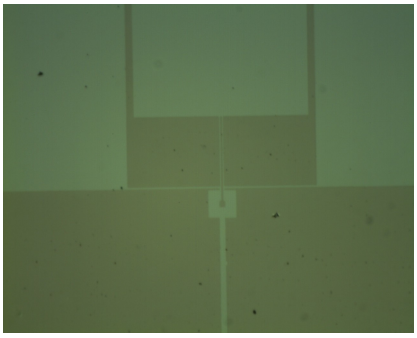

(c) 20 nm Fe layer everywhere.

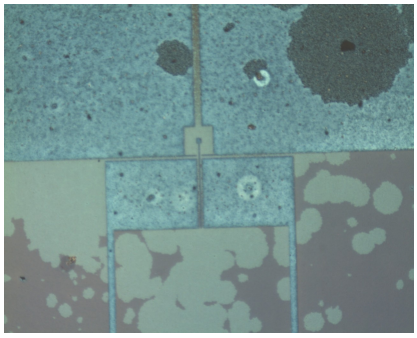

(d) After CVD.

Figure 7.4: Optical image of the sample after each step in the catalyst preparation and CNT growth process.

7.2.3 CNT growth results

The seemingly simple method for the production of CNTs by Delzeit and co-workers turned out to be difficult to repeat. The optical image after the CVD process indicated that there was some growth on isolated areas of the sample. The AFM scan revealed that the height of these growth sites to be less than 100 nm. Raman spectroscopy was performed at the National Centre for Nano-Structures Materials at the CSIR in Pretoria. Raman spectroscopy is one of the most widely used CNT characterization techniques [113]. The Raman spectroscopy showed no indication of any CNT growth.

It was crucial to deposit the metals in some type of pattern to be able to measure the amount of CNT growth achieved. In addition to the configuration described above, where aluminium was deposited in a pattern and iron deposited uniformly all over the sample, two other configurations were tested. In one of the configurations, the aluminium was deposited uniformly across the entire surface of the sample, and iron was deposited in a pattern on the aluminium. In the other configuration, the aluminium and iron were deposited on the same pattern. The growth attempts were repeated numerous

times without any success. The above configurations were then repeated using nickel instead of iron. All these attempts resulted in growth less than 300 nm. This method was expected to produce CNT well in excess of 10 μm and was therefore unsuccessful.

In the method used by Delzeit and co-workers [111], an ion beam sputterer was used to deposit the thin metal film onto the substrate. As an ion beam sputterer was not available at Stellenbosch University, it was decided to use a thermal evaporation system as a replacement. Lance Delzeit was contacted and asked for assistance and whether a thermal evaporator can be used to perform the deposition. He responded with the following:

> "The thermal evaporator should probably work provided that you are able to control the deposition. First, make sure it is a thin film of the appropriate thickness, and second that it is a thin film and not a bunch of large blobs of metal being deposited. A little SEM work should verify this. Assuming that the deposition is good, is the evaporator dedicated to Al and Fe, or is it a work horse with all sorts of metals being deposited in it. As with most catalysts, cross contamination can be a serious issue. Finally, what about the vacuum system that pumps the chamber. Is it an oil free system? If there is some backstreaming of oil or silicon fluid from the pump, that could be causing contamination also.
>
> Catalyst work can be as much an art as it is a science, particularly when you don't have a dedicated machine. Maybe try cleaning the chamber and then depositing a layer of Al or Fe on the inner surfaces to prevent cross contamination. Also, are you maybe getting some contamination from the boat you are using to do the evaporation?
>
> That is all I am able to think of at this moment."
>
> — L. Delzeit

The AFM scans that were performed confirmed that the difficulty in growing CNTs did not lie in the correct thickness or quality of the thin films. The exact temperature was not critical as they have grown CNTs at 750 °C and 900 °C. As can be deducted from the feedback received, the main concern therefore was the purity of the metals used and cross contamination occurring when depositing the thin films.

The depositions in the growth attempts described were performed using iron powder and aluminium pieces that were available in the laboratory. The purity of these metals were unknown but was assured by the head of the laboratory that they were extremely pure. After the initial failures of the experiment, the purity of these metals came under scrutiny. Moreover, the thermal evaporator was indeed a work horse used for various projects and

depositions, which could result in cross contamination issues as highlighted by L. Delzeit.

The experiments were repeated using newly ordered metals with a purity of at least 99.9%, as used by Delzeit *et al.* Furthermore, before every deposition performed, the thermal evaporator was thoroughly cleaned and a layer of the deposition material was deposited all over the inner surface of the thermal evaporator in an attempt to prevent cross contamination. Despite of all these procedures, the growth attempts remained unsuccessful. The reason the growth attempts remain unsuccessful has to be attributed to catalyst cross contamination issues, as every other step was followed exactly as reported by Delzeit *et al.*

Although the growth of CNTs was unsuccessful, a blank sensor was constructed. Aluminium was deposited on the substrate instead of CNTs and then glued to a PCB. An electrical connection between the sample and the PCB was established using a wire bonder. Spacing elements were placed on the sides of the PCB and another PCB was placed on the spacing elements to form the other electrode. The whole assembly was held together by small screws. This made it possible to change the spacing elements and thereby varying the spacing between the electrodes. Figure 7.1 shows an Autodesk Inventor drawing of the sensor, where the CNT sample was replaced with the aluminium sample. Breakdown voltage tests were performed on the blank sample to use it as a baseline when performing the CNT sensor experiments. These results are not given, as the CNT sensor was never successfully completed.

It was at this point that the focus of the research shifted towards graphene based sensors. It was decided to focus on creating a model of the CNT gas sensor, something that Modi *et al* did not report on in their article, thereby moving away from trying to replicate their work.

7.3 Modelling the sensor

The main purpose for creating a model is that the operating environment and the use of the sensor can be simulated. This minimizes the amount of trial and error steps in the development of the sensor. It can also be used to determine the important parameters of the sensor such as the shape, size and distribution of the nanotubes. This can be used to design the sensor optimally. Furthermore, the model provides insight into the fundamental operating principles of the device.

The model was created using COMSOL Multiphysics, which is a finite element analysis software package that can be used for various physics and engineering applications. The advanced capabilities of the software results in a relatively steep learning curve to use the program. A COMSOL course was therefore attended, which was presented by Yeswanth Rao, Applications Engineer at COMSOL in Troy, NY, USA. The information gained in the course

proved to be valuable when the model was designed. Moreover, the knowledge gained can also be used in a wide range of modelling applications.

Modi *et al* reported that the breakdown voltage of two parallel spaced electrodes in air can be reduced by nearly 65% through the use of MWCNTs. They did however not give an exact quantitative analysis of the electric field enhancement.

The model of the sensor was created by approximating the nanotubes as round cylinders with dome shaped caps. Due to the symmetry involved in the sensor, the model could be simplified as a two dimensional structure. This drastically reduced the complexity of the calculations as well as the construction of the model. The cylinders were enclosed in a rectangle that represented the gas around the CNTs. The properties of the rectangle, such as the relative permittivity, could be set to correspond to a specific gas. The one side of the rectangle on the opposite side of the CNTs represented the other electrode of the sensor.

The electric field around the nanotubes was then calculated by setting the boundary conditions as follows: 1 V was applied to the nanotubes and the other electrode was grounded. The electric field was then calculated and the results are shown in Figure 7.5. Note the large electric fields around the tip of the nanotubes. Figure 7.6 is a cross section of the electric field through one of the nanotubes that was located in the centre of the device. It shows the size of the electric field as a function of distance from the nanotube tip. It clearly shows the incredibly strong electric field in close proximity to the nanotube tip.

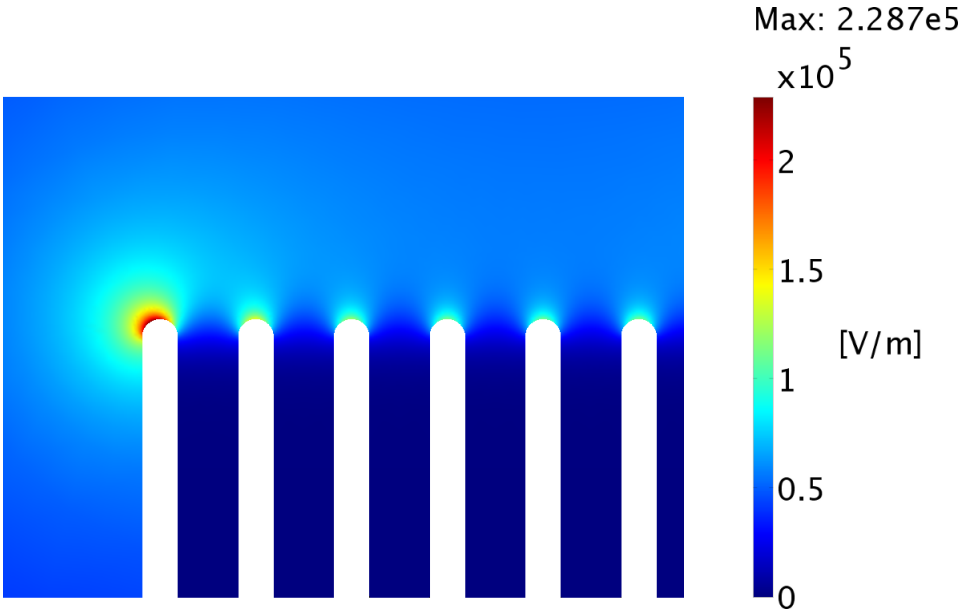

Figure 7.5: Electric field around the tip of 30 nm diameter CNTs.

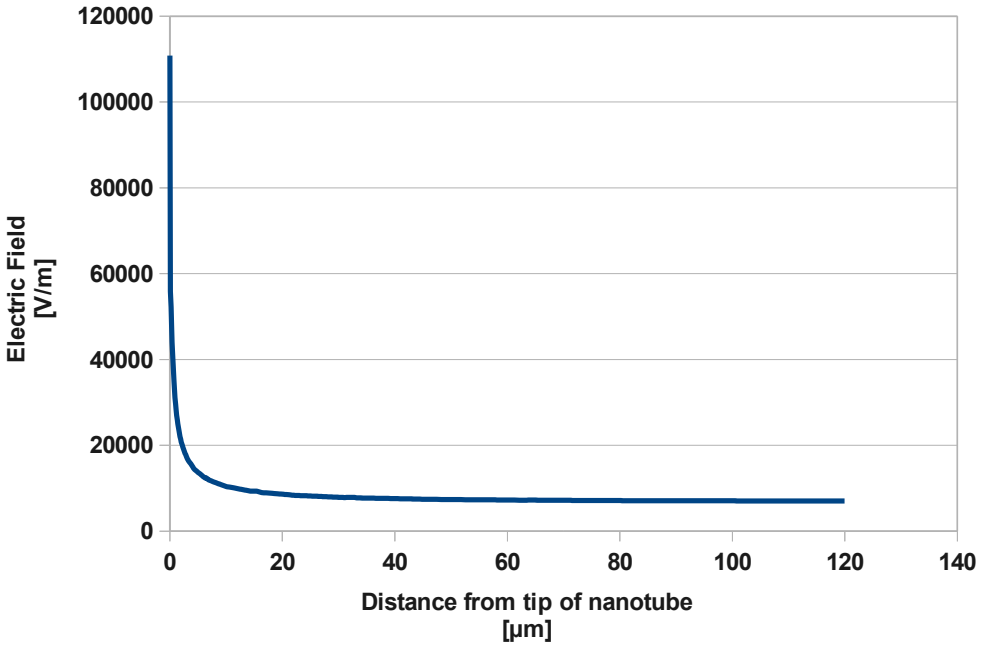

Figure 7.6: A cross section of the electric field around the tip of a CNT shown in Figure 7.5.

The reduction in breakdown voltage is influenced by the actual field enhancement achieved and is therefore important to determine. The field enhancement factor is the ratio between the local field, E_{loc}, and the applied field, E_{app}, and is given by the following equation:

$$\beta = E_{loc}/E_{app}. \tag{7.1}$$

One of the main reasons for creating the model is to determine E_{loc} and from Figure 7.6 it is approximately 110 kV/m.

The applied field can be calculated with the following equation [114]:

$$E_{app} = V/d, \tag{7.2}$$

where V is the applied voltage and d is the minimum distance between the electrodes.

In this case the applied field was 1 V and the distance between the electrodes was 150 μm. Using Equation 7.2, E_{app} equals 6.67 kV/m. This corresponds closely with the value shown in Figure 7.6 when the distance from the nanotube was increased.

With these two values known the field enhancement can be calculated. Using Equation 7.1, β equals 16.5. In actual applications the real value of β can be higher due to rough edges that are difficult to model [114].

Another model was created where the diameter of the nanotube equalled 1 μm. This resulted in a field enhancement β equal to 3. This shows that

thinner nanotubes results in higher field enhancements. This model was created for illustrative purposes as nanotubes this size do not exist.

Sadeghian *et al* fabricated a similar device that uses gold nanowires instead of CNTs. Additionally, the nanowires were covered in nanowhiskers that further enhanced the electric field and enabled the field ionization of gas species at exceptionally low voltages [115], [116]. This confirms the results obtained from the model that showed that thinner nanowires results in higher field enhancement.

Although the model is relatively simple, the results obtained from it can be used to design the sensor optimally and explain the operating principles of the sensor.

7.4 Testing chamber

A testing environment was created in order to perform experiments on the gas sensor. The testing environment had to be able to expose the sensor to a specific concentration of a certain gas or mixture of gases. A testing chamber was designed and manufactured with these specifications in mind. The chamber that was built sealed tightly and featured an input valve, output valve, two electric feed-trough connections and a pressure gauge. The gas that the sensor needed to be exposed to was connected to the input valve, and the output was connected to a vacuum pump. The chamber was then flushed a few times with the gas to ensure that no other gas such as air remained in the chamber.

The chamber also featured a pressure gauge and from the pressure is it possible to calculate the concentration using the ideal gas law [19]:

$$P = nRT/V, \tag{7.3}$$

where P is the absolute pressure, n the amount of substance, R the gas constant, T the absolute temperature and V the volume.

With T and R being constant, it is clear from Equation 7.3 that the pressure, P, is directly proportional to n/V, which is the amount of gas divided by the volume of the chamber. Therefore, the pressure in the chamber is directly proportional to the concentration of the gas. Although this equation is based on an ideal gas, working within a certain range of temperature, pressure and types of gases, this equation will give very accurate results.

The chamber was fabricated from aluminium at the *Sentrale Elektroniese Dienste* department at Stellenbosch University. Figure 7.7 shows a graphical image of the testing chamber. Appendix B shows detailed CAD drawings of the testing chamber.

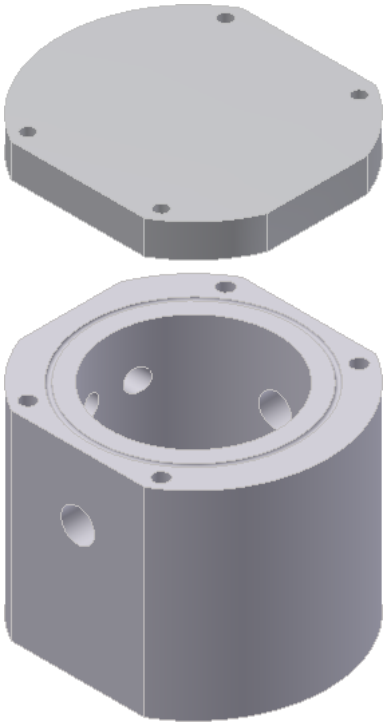

Figure 7.7: The testing chamber that was used for the CNT gas sensor tests.

7.5 Sample holder

A sample holder was created in order to make the handling of samples easier and avoid contamination when using the thermal evaporator. The sample holder can hold five 10 × 10 mm and two 20 × 10 mm Si samples. It was made of stainless steel as this makes heating the samples possible, without contaminating the system. Some applications require the sample to be heated when the deposition is performed.

The sample holder can be used by any person using the thermal evaporator, replacing the current method of using 'Prestik' or double sided tape.

Figure 7.8 shows a graphical view of the sample holder. Appendix B shows a detailed CAD drawing of the sample holder.

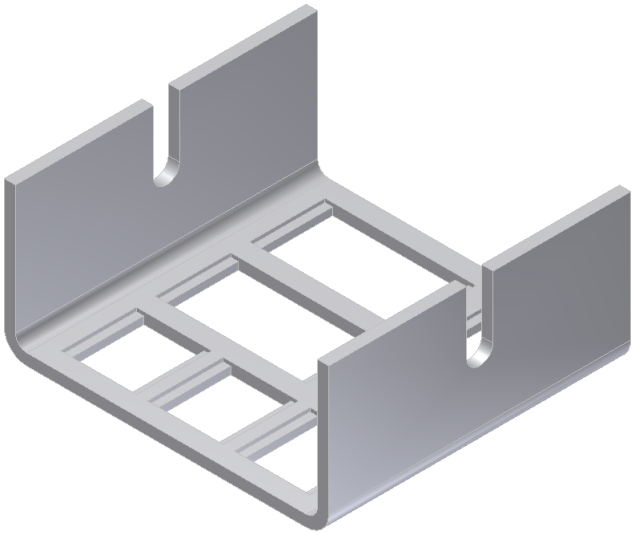

Figure 7.8: The sample holder that was used to hold the silicon samples in place during thermal evaporation.

7.6 Conclusion

Although the sensor did not operate successfully, many of the original objectives at the onset of this research have been completed. The work of Modi *et al* was followed to gain experience in nano-growth techniques, learn how to operate equipment such as an AFM, learn how to use a simulation software package and study a nanomaterial such as CNTs. Most of these objectives were therefore accomplished and if the sensor operated successfully, the work performed would have been more rewarding, but not necessarily more insightful.

Chapter 8

Conclusions

The use of graphene as active material in sensing devices has been further confirmed during this research. It was well suited to applications that involved gas absorption, but it unfortunately did not show any potential to be used in liquid based applications, especially were strong acids and bases were involved.

The results of the humidity experiments showed that the graphene absorbs water vapour which in turn changes the resistance of the graphene. The test was repeated with a carbon nanotube sample and was unaffected by changes in humidity. Before the graphene can be used in an actual humidity sensing application, the slow response time of the sensor which leads to hysteresis needs to be addressed. Possible ways of desorbing the water vapour out of the graphene faster should be explored, thereby improving the response time and eliminating the hysteresis.

Additional testing led to the discovery that the bandgap in graphene can be altered by the controlled absorption of water molecules to the graphene surface. This is a significant result, because a lack of bandgap in pristine graphene is hampering its use in semiconductor devices. This is a simple method compared to previously proposed methods of bandgap modification. The experiment performed showed that the effect is reversible and future experiments should explore the possibility of using this method to fix the the bandgap at a specific value. As stated previously, the results have been published in the nanotechnology journal, *Small* [16].

The other absorption based application that had very positive results was the detection of CO_2 using graphene in conjunction with a surface acoustic wave (SAW) device. The initial resistive experiments performed showed that the graphene absorbs a small amount of CO_2 when exposed to the gas. This absorption of CO_2 slightly altered the resistance of the sample, but a method was needed to amplify this change. A surface acoustic wave (SAW) device was used and it was able to successfully detect small changes to the graphene's properties that were caused by the absorption of CO_2. Additional tests are planned to investigate the performance of the sensor when graphene is directly

grown on the surface of the SAW device using chemical vapour deposition.

This is the first time that surface acoustic waves have been used to detect the absorption of CO_2 in graphene and this method has the potential to be expanded to detect a wide range of gases. Future studies can investigate methods of modifying the graphene to only respond to specific gases. An array of these devices can be incorporated into a single sensor to create an ultra sensitive gas sensor that can detect and identify various gases. The study could also determine the optimal amount of graphene to use as well as the type of graphene and deposition method. During this research a network analyser was used to measure the phase changes, but in an actual application this can be accomplished using quite simple electronics.

The first liquid based experiments of this study attempted to use graphene as a pH sensor. In the initial pH experiments, the graphene sample's resistance changed at different pH levels, but additional testing showed that the sample responded to the conductivity of the liquid instead of the pH level. The graphene was therefore an unlikely candidate to be used as a pH sensor. If graphene is used to measure the pH of a solution, the sensor would have to be very robust to survive the harsh environments faced when measuring strong acids and bases.

Graphene could not significantly improve the efficiency of a water electrolysis process. However, given the impact that such an improvement can have on the hydrogen economy, additional experiments should be continued. The high surface to volume ratio of graphene makes it an ideal candidate to be used to improve the efficiency of a water electrolysis process. The high surface area of graphene will increase the active area of the electrode, which could cause the current density of the electrolyser to decrease. The first step to achieve this is to design the electrodes with the graphene strongly attached and to optimally use the surface area of the graphene. Future experiments should be conducted where the graphene is grown directly on the electrodes.

The flow experiments were the first performed in a three year research project conducted at Rensselaer Polytechnic Institute (RPI), which investigates the use of graphene or carbon nanotubes (CNTs) for power generation from a flowing liquid. Before power can be generated, a voltage needs to be generated, and the first experiment investigated whether a voltage was observed when a liquid flows over graphene. In this experiment, a small voltage was observed, and a second experiment was used to determine whether there was a correlation between this voltage and the flow speed. No correlation was found to exist between the voltage and the flow speed. Similar to the other two liquid based experiments, the results obtained here do not rule out the use of graphene in a flow sensor, or more importantly, power generation. Other types of graphene can be used and the device would have to be carefully designed. A model of the device created in a program such as COMSOL could provide insight into designing the device.

A CNT based gas sensor, based on the work of Modi *et al*, was developed

and identifies a gas by fingerprinting its ionization characteristic. The main challenge in creating this sensor was the fabrication of vertically aligned CNTs that were required in the sensor. Although various growth attempts were undertaken, CNTs of the required height could not be fabricated. It was therefore decided to focus on the creation of a model of the sensor, because more knowledge can be gained from the model than from experimental results using the sensor. The model was designed in COMSOL and it was used to calculate the electric field around the tips of the nanotubes. This model can be used to explain the operating principles of the device and to optimize the distribution of CNTs.

In applications where the main objective is not the growth of the nanostructure, but rather the use of the nanostructure, it may be more productive to purchase the nanostructure after failed growth attempts. Another advantage of buying the nanostructures is the wide field of nanotechnology can be explored without investing too heavily in expensive equipment that is needed to successfully create and view these nanostructures.

As discussed in Chapter 3, there are various methods available to manufacture graphene. Although each of these methods produces graphene with the same basic structure, the resulting graphene can have slightly different properties due to defects produced by each of the methods. In each application it should be consider which graphene synthesis method would produce the best results. The graphene used in this project conclusively proved to be well suited for absorption based applications, but a different manufacturing method should be used in liquid applications.

Although nanostructures such as CNTs and graphene have shown ample potential to be used in sensors, certain challenges remain that must be overcome before it can be realized into an actual device. The current inability to mass produce nanostructured materials in an economical fashion is currently limiting its adoption in a wide range of applications and devices. Continual improvements in nanostructured manufacturing techniques and society's continual demand for an increase in performance of products and devices, would inevitably lead to the main stream adoption of nanostructured materials in various products and devices.

Appendices

Appendix A

Code

```
/* Source: vanderpauw.c
* Revision: 1.0
* Date: 2010/03/01
* Author: PC Kritzinger
*--------------------------------------
* Calculate the sheet resistance using the van der Pauw Method
*--------------------------------------
*/
#include <stdlib.h>
#include <stdio.h>
#include <math.h>
int main() {
const double PI = 3.14159265358979323846264 3;
const double E = 2.718281828;
double x=0;
double Rs = 0, R1, R2;
double sum=0;
char quit=0;

while(1)
{
printf("Enter R1(0 to quit): ");
scanf("%lf",&R1);
if (R1 == 0)
break;

printf("Enter R2: ");
scanf("%lf",&R2);
```

```
x=R1;
sum=0;
while(sum<1)
{
    x=x+0.1;//the step size is 0.1
    sum = pow(E, (-PI*R1/x))+pow(E,(-PI*R2/x));

}
printf("Answer = %f. Sum = %f\n",x, sum);
}
return 0;
}
```

Appendix B

Drawings

This appendix contains the detailed CAD drawings of the gas testing chamber that was used during the CNT gas sensor experiments.

It also contains the drawing of the sample holder that was used to hold the silicon samples in place during thermal evaporations.

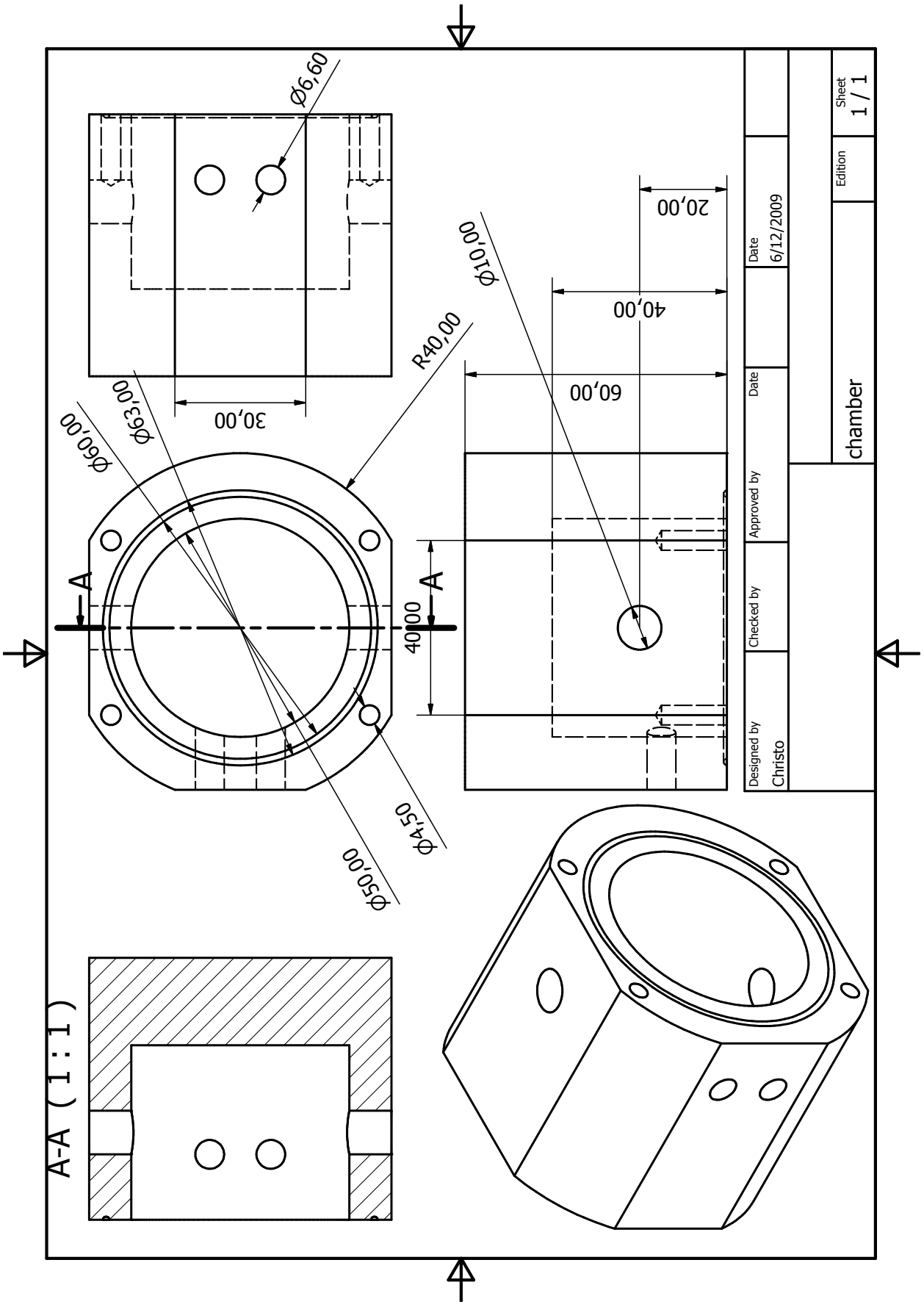
Ø6,60
30,00
R40,00
Φ63,00
Φ60,00
Φ50,00
Φ45,00
A
A
40,00
ϕ10,00
20,00
40,00
60,00
A-A (1 : 1)
Designed by
Christo
Checked by
Approved by
Date
6/12/2009
Date
Edition
Sheet
1 / 1
chamber

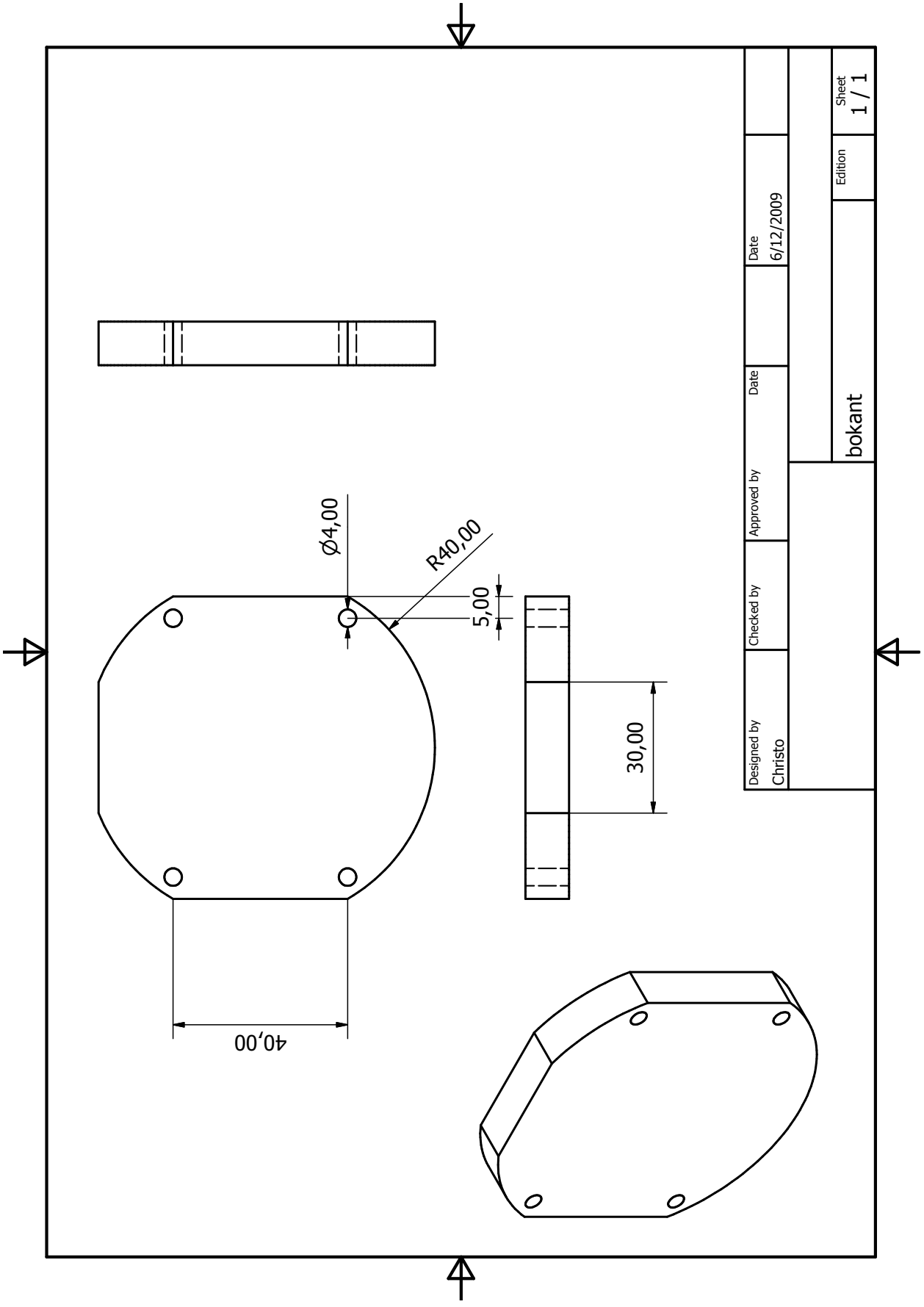
Ø4,00
R40,00
5,00
30,00
40,00
Designed by
Christo
Checked by
Approved by
Date
Date
6/12/2009
Edition
Sheet
1 / 1
bokant

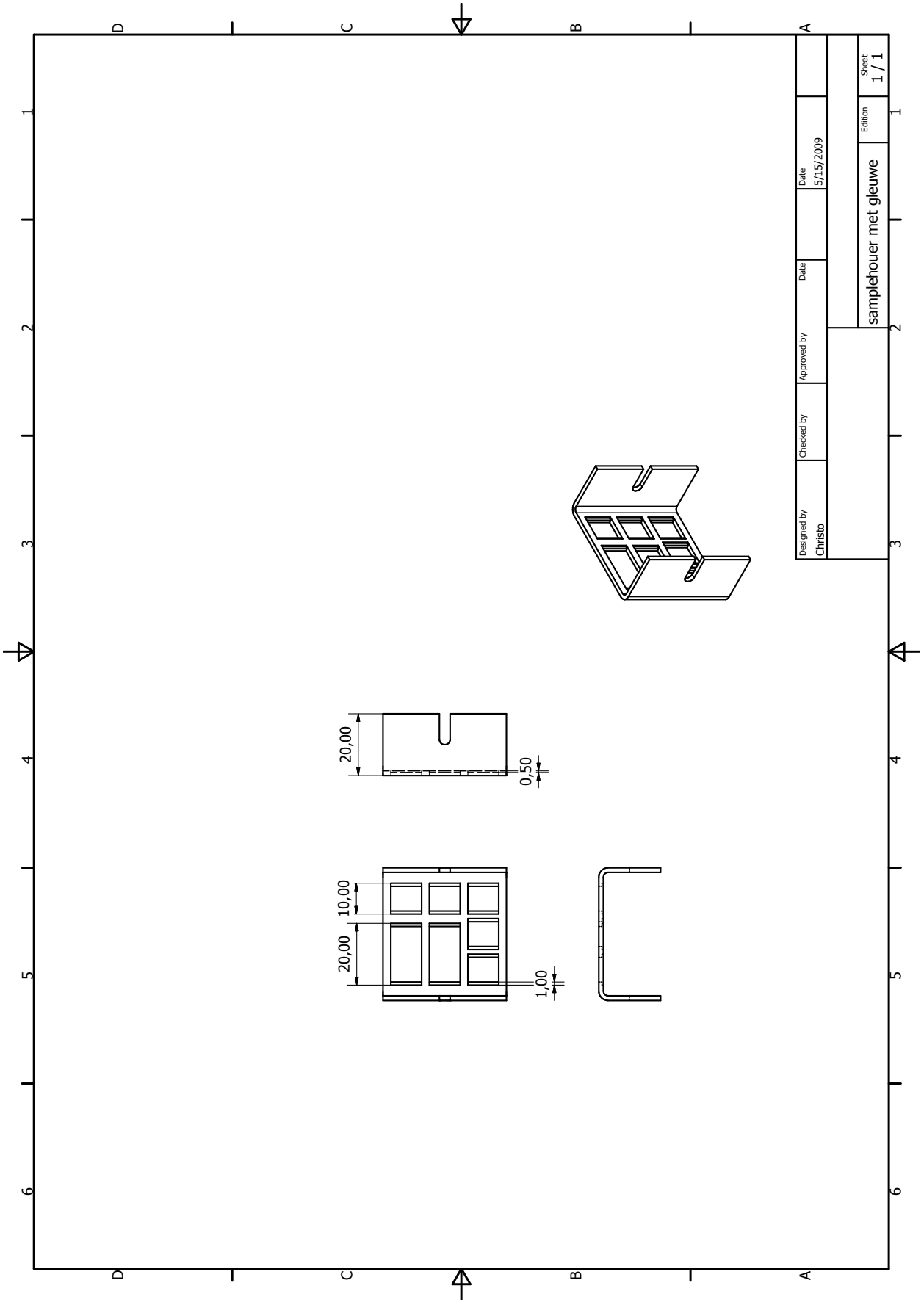
D
C
B
A
1
2
3
4
5
6
Designed by
Christo
Checked by
Approved by
Date
Date
5/15/2009
samplehouer met gleuwe
Edition
Sheet
1 / 1
20,00
0,50
10,00
20,00
1,00

Bibliography

[1] M. Meyyappan, *Carbon Nanotubes: Science and Application*. CRC Press, 2005.

[2] F. Schedin, A. K. Geim, S. V. Morozov, E. W. Hill, P. Blake, M. I. Katsnelson, and K. S. Novoselov, "Detection of individual gas molecules adsorbed on graphene," *Nature Materials*, vol. 6, p. 652, 2007.

[3] J. T. W. Yeow, *Carbon Nanotube Devices*. Wiley-VCH, 2008.

[4] N. Sinha, J. Ma, and J. T. W. Yeow, "Carbon nanotube-based sensors," *Journal of Nanoscience and Nanotechnology*, vol. 6, p. 573, 2006.

[5] A. K. Geim, "Graphene: Status and prospects," *Science*, vol. 324, p. 1530, 2009.

[6] A. K. Geim and K. S. Novoselov, "The rise of graphene," *Nature Materials*, vol. 6, pp. 183–191, 2007.

[7] C. Lee, X. Wei, J. W. Kysar, and J. Hone, "Measurement of the elastic properties and intrinsic strength of monolayer graphene," *Science*, vol. 321, p. 385, 2008.

[8] J. Chen, C. Jang, S. Xiao, M. Ishigami, and M. S. Fuhrer, "Intrinsic and extrinsic performance limits of graphene devices on SiO_2," *Nature Nanotechnology*, vol. 3, p. 206, 2008.

[9] L. Tune, "Physicists show electrons can travel more than 100 times faster in graphene." [Online]. Available: `http://newsdesk.umd.edu/scitech/release.cfm?ArticleID=1621`.

[10] Y. Dan, Y. Lu, N. J. Kybert, Z. Luo, and A. T. C. Johnson, "Intrinsic response of graphene vapor sensors," *Nano Letters*, vol. 9, p. 1472, 2009.

[11] J. D. Fowler, M. J. Allen, V. C. Tung, Y. Yang, R. B. Kaner, and B. H. Weiller, "Practical chemical sensors from chemically derived graphene," *ACS Nano*, vol. 3, p. 301, 2009.

[12] J. Han, *Carbon Nanotubes: Science and Application*. CRC Press, 2005.

[13] A. Modi, N. Koratkar, E. Lass, B. Wei, and P. M. Ajayan, "Miniaturized gas ionization sensors using carbon nanotubes," *Nature*, vol. 424, p. 171, 2003.

[14] S. Ghosh, A. K. Sood, and N. Kumar, "Carbon nanotube flow sensors," *Science*, vol. 299, p. 1042, 2003.

[15] T. Kenny, *Sensor Technology Handbook*. Elsevier, 2005.

[16] F. Yavari, C. Kritzinger, C. Gaire, L. Song, H. Gulapalli, P. M. A. T. Borca-Tasciuc, and N. Koratkar, "Tunable bandgap in graphene by the controlled adsorption of water molecules," *Small*, 2010.

[17] H. C. Schniepp, J. Li, M. J. McAllister, H. Sai, M. Herrera-Alonso, D. H. Adamson, R. K. Prud'homme, R. Car, D. A. Saville, and I. A. Aksay, "Functionalized single graphene sheets derived from splitting graphite oxide," *J. Phys. Chem. B*, vol. 110, p. 8535, 2006.

[18] M. J. McAllister, J. Li, D. H. Adamson, H. C. Schniepp, A. A. Abdala, J. Liu, M. Herrera-Alonso, D. L. Milius, R. Car, R. K. Prud'homme, and I. A. Aksay, "Single sheet functionalized graphene by oxidation and thermal expansion of graphite," *Chem. Mater.*, vol. 19, p. 4396, 2007.

[19] M. S. Silberberg, *Chemistry: The Molecular Nature of Matter and Change*. McGraw Hill, 2003.

[20] M. Ratner and D. Ratner, *Nanotechnology: A Gentle Introduction to the Next Big Idea*. Prentice Hall, 2002.

[21] J. Kahn, "Nanotechnology," *National Geographic*, pp. 98–119, 2006.

[22] C. A. Barbero, "Chemistry and nanotechnology," in *South African Nanoscience and Nanotechnology Summer School 2009*, 2009.

[23] E. L. Wolf, *Nanophysics and Nanotechnology*. Wiley, 2006.

[24] M. Kohler and W. Fritzsche, *Nanotechnology: An Introduction to Nanostructuring Techniques*. Wiley-VCH, 2007.

[25] "IBM celebrates 20th anniversary of moving atoms." [Online]. Available: `http://www.physorg.com/news173344987.html`.

[26] "The project on emerging nanotechnologies." [Online]. Available: `http://www.nanotechproject.org/inventories/consumer/analysis_draft/`.

[27] B. Bhushan and O. Marti, *Springer Handbook of Nanotechnology*. 2006.

[28] M. J. Allen, V. C. Tung, and R. B. Kaner, "Honeycomb carbon: A review of graphene," *Chemical Reviews*, vol. 110, p. 132, 2010.

[29] K. S. Novoselov, A. K. Geim, S. V. Morozov, D. Jiang, Y. Zhang, S. V. Dubonos, I. V. Grigorieva, and A. A. Firsov, "Electric field effect in atomically thin carbon films," *Science*, vol. 306, p. 666, 2004.

[30] C. Soldano, A. Mahmood, and E. Dujardin, "Production, properties and potential of graphene," *Carbon*, vol. 48, p. 2127, 2010.

[31] K. I. Bolotina, K. J. Sikesb, Z. Jianga, M. Klimac, G. Fudenberga, J. Honec, P. Kima, and H. L. Storme, "Ultrahigh electron mobility in suspended graphene," *Solid State Communications*, vol. 146, p. 351, 2008.

[32] A. A. Balandin, S. Ghosh, W. Bao, I. Calizo, D. Teweldebrhan, F. Miao, and C. N. Lau, "Superior thermal conductivity of single-layer graphene," *Nano Letters*, vol. 8, p. 902, 2008.

[33] "Thermal conductivity of metals." [Online]. Available: `http://www.engineeringtoolbox.com/thermal-conductivity-metals-d_858.html`.

[34] K. S. Novoselov, A. K. Geim, S. V. Morozov, D. Jiang, M. I. Katsnelson, I. V. Grigorieva, S. V. Dubonos, and A. A. Firsov, "Two-dimensional gas of massless dirac fermions in graphene," *Nature*, vol. 438, p. 197, 2005.

[35] J. Wood, "Graphene lights up a fundamental truth," *Materials Today*, vol. 11, p. 10, 2008.

[36] T. Mueller, "Detecting light with graphene," *Nature Photonics*, vol. 4, p. 338, 2010.

[37] L. A. Ponomarenko, F. Schedin, M. I. Katsnelson, R. Yang, E. W. Hill, K. S. Novoselov, and A. K. Geim, "Chaotic dirac billiard in graphene quantum dots," *Science*, vol. 320, p. 356, 2008.

[38] K. Bullis, "Tr10: Graphene transistors." [Online]. Available: `http://www.technologyreview.com/read_article.aspx?ch=specialsections&sc=emerging08&id=20242`.

[39] P. Blake, P. D. Brimicombe, R. R. Nair, T. J. Booth, D. Jiang, F. Schedin, L. A. Ponomarenko, S. V. Morozov, H. F. Gleeson, E. W. Hill, A. K. Geim, and K. S. Novoselov, "Graphene-based liquid crystal device," *Nano Letters*, vol. 8, p. 1704, 2008.

[40] X. Wang, L. Zhi, and K. Mullen, "Transparent, conductive graphene electrodes for dye-sensitized solar cells," *Nano Letters*, vol. 8, p. 323, 2008.

[41] T. Mueller, F. Xia, and P. Avouris, "Graphene photodetectors for high-speed optical communications," *Nature Photonics*, vol. 4, p. 297, 2010.

[42] S. Stankovich, D. A. Dikin, G. H. B. Dommett, K. M. Kohlhaas, E. J. Zimney, E. A. Stach, R. D. Piner, S. T. Nguyen, and R. S. Ruoff, "Graphene-based composite materials," *Nature*, vol. 442, p. 282, 2006.

[43] M. A. Rafiee, J. Rafiee, Z. Wang, H. Song, Z. Yu, and N. Koratkar, "Enhanced mechanical properties of nanocomposites at low graphene content," *ACS Nano*, vol. 3, p. 3884, 2009.

[44] D. V. Kosynkin, A. L. Higginbotham, A. Sinitskii, J. R. Lomeda, A. Dimiev, B. K. Price, and J. M. Tour, "Longitudinal unzipping of carbon nanotubes to form graphene nanoribbons," *Nature*, vol. 458, p. 872, 2009.

[45] L. Jiao, L. Zhang, X. Wang, G. Diankov, and H. Dai, "Narrow graphene nanoribbons from carbon nanotubes," *Nature*, vol. 458, p. 877, 2009.

[46] S. Iijima, "Helical microtubules of graphitic carbon," *Nature*, vol. 354, p. 56, 1991.

[47] F. Hennrich, C. Chan, V. Moore, M. Rolandi, and M. O'Connell, *Carbon Nanotubes Properties and Application*. CRC Press, 2006.

[48] M. Monthiouxa and V. L. Kuznetsova, "Who should be given the credit for the discovery of carbon nanotubes?," *Carbon*, vol. 44, p. 1621, 2006.

[49] S. Iijima and T. Ichihashi, "Single-shell nanotubes of 1 nm diameter," *Nature*, vol. 363, p. 605, 1993.

[50] F. Kreupl, *Carbon Nanotube Devices*. Wiley-VCH, 2008.

[51] "Carbon nanotube." [Online]. Available: `http://en.wikipedia.org/wiki/Carbon_nanotube`.

[52] "Carbon nanotubes & buckyballs." [Online]. Available: `http://mrsec.wisc.edu/Edetc/nanoquest/carbon/index.html`.

[53] R. V. B. Q. Wei and P. M. Ajayan, "Reliability and current carrying capacity of carbon nanotubes," *Applied Physics Letter*, vol. 79, p. 1172, 2001.

[54] "Nanotube bike enters tour de france." [Online]. Available: `http://nanotechweb.org/cws/article/tech/22597`.

[55] C. Liu, Y. Y. Fan, M. Liu, H. T. Cong, H. M. Cheng, and M. S. Dresselhaus, "Hydrogen storage in single-walled carbon nanotubes at room temperature," *Science*, vol. 286, p. 1127, 1999.

[56] "Audacious & outrageous: Space elevators." [Online]. Available: `http://science.nasa.gov/science-news/science-at-nasa/2000/ast07sep_1/`.

[57] R. H. Baughman, C. Cui, A. A. Zakhidov, Z. Iqbal, J. N. Barisci, G. M. Spinks, G. G. Wallace, A. Mazzoldi, D. D. Rossi, A. G. Rinzler, O. Jaschinski, S. Roth, and M. Kertesz, "Carbon nanotube actuators," *Science*, vol. 284, p. 1340, 1999.

[58] J. H. Hafner, C. L. Cheung, A. T. Woolley, and C. M. Lieber, "Structural and functional imaging with carbon nanotube AFM probes," *Progress in Biophysics and Molecular Biology*, vol. 77, p. 73, 2001.

[59] S. Li, Z. Yu, S. Yen, W. C. Tang, , and P. J. Burke, "Carbon nanotube transistor operation at 2.6 GHz," *Nano Letters*, vol. 4, p. 753, 2004.

[60] W. A. de Heer, A. Chatelain, and D. Ugarte, "A carbon nanotube field-emission electron source," *Science*, vol. 270, p. 1179, 1995.

[61] J. Kong, N. R. Franklin, C. Zhou, M. G. Chapline, S. Peng, K. Cho, and H. Dai, "Nanotube molecular wires as chemical sensors," *Science*, vol. 287, p. 622, 2000.

[62] S. Chopra, A. Pham, J. Gaillard, A. Parker, and A. M. Rao, "Carbon-nanotube-based resonant-circuit sensor for ammonia," *Applied Physics Letter*, vol. 80, p. 4632, 2002.

[63] J. T. W. Yeow and J. P. M. She, "Carbon nanotube-enhanced capillary condensation for a capacitive humidity sensor," *Nanotechnology*, vol. 17, p. 5441, 2006.

[64] C. Stampfer, T. Helbling, D. Obergfell, B. Schoberle, M. K. Tripp, A. Jungen, S. Roth, V. M. Bright, and C. Hierold, "Fabrication of single-walled carbon-nanotube-based pressure sensors," *Nano Letters*, vol. 6, p. 233, 2006.

[65] M. Endo, M. S. Strano, and P. M. Ajayan, "Potential applications of carbon nanotubes," *Topics in Applied Physics*, vol. 111, p. 13, 2008.

[66] M. Meyyappan, *Sensors, Nanoscience, Biomedical Engineering and Instruments*. 2006.

[67] S. Jewett, *Physics for Scientists and Engineers*. Thomson, 2004.

[68] B. Breton, "The early history and development of the scanning electron microscope." [Online]. Available: `http://www2.eng.cam.ac.uk/~bcb/history.htm`.

[69] A. Nouailhat, *An Introduction to Nanoscience and Nanotechnology*. Wiley, 2006.

[70] "Understanding how the sem works and how to use it on a college level.." [Online]. Available: `http://mse.iastate.edu/microscopy/college.html`.

[71] S. Swapps, "Scanning electron microscopy (SEM)." [Online]. Available: `http://serc.carleton.edu/research_education/geochemsheets/techniques/SEM.html`.

[72] "Scanning electron microscope." [Online]. Available: `http://en.wikipedia.org/wiki/Scanning_electron_microscope`.

[73] "The transmission electron microscope." [Online]. Available: `http://nobelprize.org/educational/physics/microscopes/tem/index.html`.

[74] "Atomic force microscopy." [Online]. Available: `http://www.nanoscience.com/education/afm.html`.

[75] "Atomic force microscopy." [Online]. Available: `http://en.wikipedia.org/wiki/Atomic_force_microscopy`.

[76] J. R. Minkel, "DIY graphene: How to make one-atom-thick carbon layers with sticky tape." [Online]. Available: `http://www.scientificamerican.com/slideshow.cfm?id=diy-graphene-how-to-make-carbon-layers-with-sticky-tape`.

[77] K. V. Emtsev, A. Bostwick, K. Horn, J. Jobst, G. L. Kellogg, L. Ley, J. L. McChesney, T. Ohta, S. A. Reshanov, J. Rhrl, E. Rotenberg, A. K. Schmid, D. Waldmann, H. B. Weber, and T. Seyller, "Towards wafer-size graphene layers by atmospheric pressure graphitization of silicon carbide," *Nature Materials*, vol. 8, p. 203, 2009.

[78] P. Sutter, "Epitaxial graphene: How silicon leaves the scene," *Nature Materials*, vol. 8, p. 171, 2009.

[79] K. S. Kim, Y. Zhao, H. Jang, S. Y. Lee, J. M. Kim, K. S. Kim, J. Ahn, P. Kim, J. Choi, and B. H. Hong, "Large-scale pattern growth of graphene films for stretchable transparent electrodes," *Nature*, vol. 457, p. 706, 2009.

[80] X. Li, W. Cai, J. An, S. Kim, J. Nah, D. Yang, R. Piner, A. Velamakanni, I. Jung, E. Tutuc, S. K. Banerjee, L. Colombo, and R. S. Ruoff, "Large-area synthesis of high-quality and uniform graphene films on copper foils," *Science*, vol. 324, p. 1312, 2009.

[81] J. Rafiee, M. A. Rafiee, Z. Yu, and N. Koratkar, "Superhydrophobic to superhydrophilic wetting control in graphene films," *Advanced Materials*, vol. 22, pp. 1–4, 2010.

[82] L. Song, L. Ci, W. Gao, and P. M. Ajayan, "Transfer printing of graphene using gold film," *ACS Nano*, vol. 3, p. 1353, 2009.

[83] L. Ci, L. Song, D. Jariwala, A. L. Elias, W. Gao, M. Terrones, and P. M. Ajayan, "Graphene shape control by multistage cutting and transfer," *Advanced Materials*, vol. 21, p. 1, 2009.

[84] L. J. V. der Pauw, "A method of measuring specific resistivity and hall effects of disks of arbitrary shapes," *Philips Research Reports*, vol. 13, 1958.

[85] A. Wexler, *Humidity and moisture: measurement and control in science and industry.* 1963.

[86] "HIH series humidity sensors phychrometrics & moisture.." [Online]. Available: `http://content.honeywell.com/sensing/prodinfo/humiditymoisture/lit.htm`, July 2010.

[87] "Relative humidity." [Online]. Available: `http://ww2010.atmos.uiuc.edu/%28Gh%29/guides/mtr/cld/dvlp/rh.rxml`.

[88] "Relative humidity." [Online]. Available: `http://hyperphysics.phy-astr.gsu.edu/HBASE/Kinetic/relhum.html`.

[89] A. Buchsteiner, A. Lerf, and J. Pieper, "Water dynamics in graphite oxide investigated with neutron scattering," *J. Phys. Chem. B*, vol. 110, p. 22328, 2006.

[90] S. Park, J. An, J. W. Suk, and R. Ruoff, "Graphene-based actuators," *Small*, vol. 6, p. 210, 2010.

[91] W. D. Callister, *Materials Science and Engineering An Introduction.* John Wiley & Sons: New York, 1997.

[92] J. D. Livingston, *Electronic Properties of Engineering Materials.* John Wiley & Sons: New York, 1999.

[93] X. Dong, Y. Shi, Y. Zhao, D. Chen, J. Ye, Y. Yao, F. Gao, Z. Ni, T. Yu, Z. Shen, Y. Huang, P. Chen, and L. Li, "Symmetry breaking of graphene monolayers by molecular decoration," *Physical Review Letters*, vol. 102, p. 135501, 2009.

[94] T. Ohta, A. Bostwick, T. Seyller, K. Horn, and E. Rotenberg, "Controlling the electronic structure of bilayer graphene," *Science*, vol. 313, p. 951, 2006.

[95] Y. Zhang, T. Tang, C. Girit, Z. Hao, M. C. Martin, A. Zettl1, M. F. Crommie, Y. R. Shen, and F. Wang, "Direct observation of a widely tunable bandgap in bilayer graphene," *Nature*, vol. 459, p. 820, 2009.

[96] S. Y. Zhou, D. A. Siegel, A. V. Fedorov, and A. Lanzara, "Metal to insulator transition in epitaxial graphene induced by molecular doping," *Physical Review Letters*, vol. 101, p. 086402, 2008.

[97] J. Berashevich and T. Chakraborty, "Tunable band gap and magnetic ordering by adsorption of molecules on graphene," *Physical Review B*, vol. 80, p. 033404, 2009.

[98] "Humidity sensors theory and behavior." [Online]. Available: `http://content.honeywell.com/sensing/prodinfo/humiditymoisture/lit.htm`.

[99] J. C. N. Hopwood, "Greenhouse gases and society." [Online]. Available: `http://www.umich.edu/~gs265/society/greenhouse.htm`.

[100] B. Drafts, "Acoustic wave technology sensors." [Online]. Available: `http://www.sensorsmag.com/sensors/acoustic-ultrasound/acoustic-wave-technology-sensors-936`, October 2001.

[101] A. A. Oliner, *Topics in Applied Physics: Acoustic Surface Waves*. 1978.

[102] *COMSOL Multiphysics Structural Mechanics Module User Guide*. Version 3.5a.

[103] *COMSOL Multiphysics Structural Mechanics Module Model Library*. Version 3.5a.

[104] R. Krishnan, H. B. Nemade, and R. Paily, "Simulation of one-port saw resonator using comsol multiphysics," in *Excerpt from the Proceedings of the COMSOL Users Conference 2006 Bangalore*, 2006.

[105] W. P. Jakubik, M. Urbanczyk, E. Maciak, and T. Pustelny, "Hydrogen detection in surface acoustic wave gas sensor based on interaction speed," *Sensors*, vol. 3, p. 1514, 2004.

[106] "Introduction to pH." [Online]. Available: `http://www.omega.com/techref/ph.html`, February 2010.

[107] "Helping hydrogen: Student inventor tackles challenge of hydrogen storage." [Online]. Available: `http://news.rpi.edu/update.do?artcenterkey=2690`, March 2010.

[108] U. D. of Energy, "Hydrogen production." [Online]. Available: `http://www1.eere.energy.gov/hydrogenandfuelcells/production/natural_gas.html`.

[109] S. Kim, N. Koratkar, T. Karabacak, and T. Lu, "Water electrolysis activated by Ru nanorod array electrodes," *Applied Physics Letter*, vol. 88, p. 263106, 2006.

[110] D. Mann, *Carbon Nanotubes Properties and Application.* CRC Press, 2006.

[111] L. Delzeit, C. Nguyn, B. Chen, R. Stevens, A. Cassell, J. Han, and M. Meyyappan, "Multiwalled carbon nanotube by chemical vapor deposition using multilayered metal catalysts," *Physical Chemistry B*, vol. 106, p. 5629, 2002.

[112] L. Delzeit, C. Nguyn, B. Chen, R. Stevens, A. Cassell, J. Han, and M. Meyyappan, "Multilayered metal catalyst for controlling the density of single-walled carbon nanotube growth," *Chemical Physics Letters 348*, vol. 348, p. 368, 2001.

[113] J. Maultzsch and C. Thomsen, *Carbon Nanotube Devices.* Wiley-VCH, 2008.

[114] R. B. Sadeghian and M. Kahrizi, "Finite element modeling of the field enhancement phenomenon in nanoscale field emitters and field ionizers," in *Excerpt from the Proceedings of the COMSOL Users Conference 2005 Boston*, 2005.

[115] R. B. Sadeghian and M. Kahrizi, "A novel miniature gas ionization sensor based on freestanding gold nanowires," *Sensors and Actuators*, vol. 137, p. 248, 2007.

[116] R. B. Sadeghian and M. Kahrizi, "A novel gas sensor based on tunneling-field-ionization on whisker-covered gold nanowires," *Sensors*, vol. 8, p. 161, 2008.